**Georgia Institute of Technology**

# PERMEABILITY OF IMPACTED COATED COMPOSITE LAMINATES
## Final Report

## Dr. W. S. Johnson
## Benjamin C. Findley

**Georgia Institute of Technology**
**Atlanta, GA 30332-0245**

**August 2002**

# PERMEABILTIY OF IMPACTED COATED COMPOSITE LAMINATES

# ACKNOWLEDGEMENTS

# TABLE OF CONTENTS

vi

# LIST OF TABLES

# LIST OF FIGURES

# LIST OF SYMBOLS AND ABBREVIATIONS

| | |
|---|---|
| 8250 | Dynatup 8250 impact test machine |
| 8552 | epoxy matrix material made by Hexcel |
| 2% nanocomposite | GRC polyimide with 2% Bentolite clay |
| 5% nanocomposite | GRC polyimide with 5% Bentolite clay |
| $[X/Y]_4$ | Symbol for lay-up of composite |
| " | inch, unit of length |
| ' | foot, unit of length |
| @ | at |
| $ | Dollars |
| o | degree symbol |
| °C | degree Celsius, unit of temperature |
| °F | degree Fahrenheit, unit of temperature |
| ASTM | American Society for Testing and Materials |
| Bentolite | Bentonite clay made by Southern Clay Products |
| CAD | computer aided design |
| Centurion | water based polyurethane made by Sherwin Williams |
| CFRP | carbon fiber reinforced plastics |
| cm | centimeter, unit of length |

| | |
|---|---|
| Corothane I Aliphatic Finish | polyurethane coating made by Sherwin Williams |
| Corothane I MIO-Aluminum | polyurethane coating made by Sherwin Williams |
| CTE | coefficient of thermal expansion |
| DC-XA | Delta Clipper Advanced, prototype RLV |
| Ea | absorbed energy |
| EB | electron beam cured composite |
| EX 1552 | epoxy matrix made by Bryte Technologies |
| ft | feet, unit of length |
| ft*lb | foot-pounds, unit of energy |
| g | gravity, 9.81 m/s or 32.2 ft/s |
| GRC | NASA GRC |
| Gpa | giga-Pascal, unit of strength |
| IE | impact energy |
| IM7 | carbon fiber made by Hexcel |
| in | inch, unit of length |
| in/sec-psi | inch per second-pound per squre inch, unit of rate of permeation |
| IPN | interpenetrating network |
| J | Joule, unit of energy |
| K | Kelvin, unit of temperature (0K = -273 °C) |
| kPa | kilo-Pascal, unit of pressure |
| ksi | kips per square inch, unit of strength |

| | |
|---|---|
| lb | pound, unit of force |
| $LH_2$ | liquid hydrogen |
| $LHe_2$ | liquid helium |
| $LN_2$ | liquid nitrogen |
| $LO_2$ | liquid oxygen |
| m | meter, unit of length |
| m/s | meters per second, unit of velocity |
| min | minute |
| MPa | mega-Pascal, unit of pressure ($10^6$ Pa) |
| N | Newton, unit of force |
| NASA | National Aeronautics and Space Administration |
| NASA GRC | NASA Glenn Research Center |
| NASA LaRC | NASA Langley Research Center |
| NASA MSFC | NASA Marshall Space Flight Center |
| nm | nanometer, unit of length |
| Pa | Pascal, unit of pressure |
| PETI-5 | Themoplastic matrix material made by Cytec |
| Poly-Lon 1900 | polyurethane made by Sherwin Williams |
| psi | pounds per square inch, unit of pressure or strength |
| R7K15 | Sherwin Williams proprietary solvent |
| RLV | reusable launch vehicle |

| | |
|---|---|
| SCC/sec-in$^2$ | standard cubic centimeter per second-inch squared, unit of permeability |
| $T_g$ | glass transition temperature |
| Thermaflex IIC | thermoplastic made by Avtec Industries |
| Thermashield | thermoplastic made by Avtec Industries |
| UV | ultraviolet radiation |
| V | velocity at impact |
| $V_r$ | rebound velocity |
| VOC | volatile organic compounds |
| $W_{flag}$ | width between leading edges on the velocity flag of the Dynatup 8250 |
| X-33 | prototype RLV |

# SUMMARY

Composite materials are being considered for use on future generations of Reusable Launch Vehicles (RLVs) for both fuel tanks and fuel feedlines. Through the use of composite materials NASA can reduce the overall weight of the vehicle dramatically. This weight savings can then be translated into an increase in the weight of payload sent into orbit, reducing the cost per pound of payload. It is estimated that by switching to composite materials for fuel tanks the weight of the tanks can be reduced by 40 percent, which translates to a total vehicle weight savings of 14 percent.[2]

In this research, carbon/epoxy composites were studied for fuel feedline applications. There are concerns about using composite materials for feedlines and fuel tanks because these materials are extremely vulnerable to impact in the form of inadvertent bumping or dropped tools both during installation and maintenance. Additionally, it has been found that some of the sample feedlines constructed have had leaks, and thus there may be a need to seal preexisting leaks in the composite prior to usage.

Composite materials dissipate impact energy in several different ways. First, microcracking of the matrix material occurs. Next, delaminations begin to form between fiber layers of different orientations. Lastly, fibers begin to break starting at the back face of the material. [8, 11, 17, 18] There does not need to be any visible damage in the composite for fuel to permeate, provided that sufficient microcracking has occurred.[4]

In prior work done at NASA MSFC, it was found that impacts with very little impact energy could cause sufficient damage in the composite materials for fuel permeation to become a problem. To simulate impacts caused by bumping and dropped tools, a drop weight type impact test machine was used with a ½" (1.27 cm) hemispherical tup. Using this device it was found that impacts with as little as 0.79 ft*lb (1.07 J) could produce enough microcracking in woven carbon fiber/epoxy matrix composites for gaseous helium to permeate through the material.[4]

In order to improve the composite's ability to withstand low-energy impact events, and also to salvage any initially leaking feedlines, it was decided that coatings should be considered. This research centers on the application of commercially available coatings, as well as several coatings supplied by NASA LaRC and GRC, to improve the impact resistance and reduce the permeability of the composite. In particular three different polyurethane coatings, two thermoplastic, and several polyimide nanocomposites were studied.

For this research many four-inch by four-inch IM7/EX 1552 specimens were tested in leakage, impact and permeability. All of the specimens received were tested for leakage using a device that was built based on a design used at NASA MSFC. The specimens were then divided according to the number of leaks present in them so that coatings sealed preexisting leaks and improved impact resistance, and also to determine how much improvement occurred in the impact resistance of initially impermeable specimens.

Because keeping the weight of the vehicle down is the impetus for using composite feedlines and fuel tanks, the weight of the coatings is critical. It is desired to apply the coatings as thinly and uniformly as possible.

After coating, the specimens were impacted using a Dynatup 8250 drop weight test machine. The impact energy was adjusted until the critical value, energy just before a specimen will begin to leak, was found (from here on referred to as the critical impact energy). All of the specimens that were impacted and found to leak were then tested to determine the rate of gaseous permeability through the impact damage. The permeability device used was based upon a similar device at NASA MSFC, which was derived from the ASTM standard.[60, 62]

Each of the coatings was applied to initially impermeable specimens as well as initially leaking specimens so that the critical impact energy could be found for each condition. This was necessary to show that the sealed initially leaking specimens performed just as well as the initially impermeable coated specimens. The critical impact energies for the coated specimens were then compared to the critical impact energy found for the initially impermeable uncoated specimens. As was suspected, tremendous improvement could be achieved in the impact resistance of the specimen through the use of coatings. This testing was all performed at room temperature, and the coatings next had to be tested in thermal cycling due to the wide temperature ranges that these materials will experience.

One of the largest challenges confronting the use of coatings on composite parts meant for cryogenic use is that these coatings tend to delaminate due to the large thermal

stresses, which result from the mismatch in coefficients of thermal expansion of the composite constituents and the coating. During a typical launch to landing cycle, the composite fuel tanks and feedlines will experience temperatures ranging from 20K to 394K (-423 °F to 250°F).[43] It was therefore necessary to perform thermal cycling tests upon all of the coatings considered. McManus et al. found that while it was necessary to cool composites to below 60K to initiate cracking of the composite, coatings suffered damage above 77K and thus liquid nitrogen could be used for this thermal cycling.[24]

In addition to thermal cycling, the effects of aging on the coatings were also considered. There was concern that the coatings would become more brittle with time. Aged specimens were impacted at the critical impact energies and then tested for leakage to determine what effect, in any, age had on the coated specimens. From this work it was determined that aging is not nearly as significant as thermal cycling of the coated composite.

# CHAPTER I

## INTRODUCTION AND RESEARCH OBJECTIVES

Composite materials are prevalent in a wide variety of structures, especially those in the aerospace, marine, and civil infrastructure industries. While the motivations for the use of composite materials may vary some, generally the weight savings provided by using composites over more traditional metal materials is involved.

The use of composite materials for fuel feedlines and fuel tanks was deemed necessary in order to achieve the goals set forth by NASA for the next two generations of reusable launch vehicles (RLV's), to cut the cost per pound of payload down from $10,000 currently to $1,000 for the second generation, and to $100 per pound for the third generation.[1] The simplest way to achieve this cost savings is to reduce the overall weight of the vehicle, thus enabling the vehicle to carry more payload into space. In addition, simply by switching to composite fuel tanks the weight of the vehicle can be reduced by 14 percent.[2]

The use of composites for fuel tanks and fuel feedlines is not a new concept, but applying these young technologies at cryogenic temperatures had not been attempted until the DC-XA project.[3] There are numerous differences between the ways that composite materials behave at these temperatures compared to the traditional metal materials, most of which are due to the directional and heterogeneous nature of composites. At cryogenic temperatures, microcracking in the matrix material of

composites may occur due to the thermal mismatches between the fibers and the matrix. This microcracking can allow for potential leak paths to form through the thickness of the material.

Beyond the concerns regarding microcracking, NASA is extremely concerned that during installation and maintenance of the composite feedlines and fuel tanks someone may bump the lines or drop a tool leading to a low-energy impact event. The energy from impact events is dissipated within composite materials through the formation of several different modes of damage: microcracking, delaminations, and fiber breakage. From work done by Dr. Nettles, NASA MSFC, it has been found that impacts with as little energy as 0.79 ft*lb (1.27 J) could cause leaks to form in a composite feedline (made from similar materials to those considered in this study).[4] The challenges presented by low-energy impacts are especially complex when one considers that impacts that leave no visible damage on the surface of the material may cause extensive damage through the thickness of the material.

NASA determined that the critical leak rates for the feedlines are extremely low, and thus virtually any leakage is unacceptable. Thus, for composite materials to be viable for use as fuel feedlines and fuel tanks they had to be toughened to resist impact damage and subsequent fuel leakage. To achieve this toughening, it was decided that a coating needed to be applied to the exterior of the feedlines.

In addition to having concerns regarding impact damage, NASA found that some of the sample feedlines that had been made for previous research were actually leaking prior to any impact events whatsoever. Thus it is also necessary to try and seal

preexisting leaks in order to ensure that the feedlines are in fact impermeable prior to use. Furthermore, it is important that the sealed feedlines perform as well in impact events as feedlines that were impermeable prior to coating.

There are two distinct types of coatings that one should consider when trying to improve the impact resistance of the composite feedlines: low-density coatings (foams) that absorb the impact energy such that the composite sustains no damage, and thinner denser coatings that remain intact even if the composite substrate suffers cracking.[5] Because the first type of coating would make the fuel lines much thicker and would not be as effective in sealing preexisting leaks it was eliminated from consideration.

The objective of this research was to determine how effectively coatings could be used to improve the impact resistance of composite fuel feedlines. Also the effectiveness of sealing preexisting leaks with the same coatings was determined.

The approach taken in this research was to study a variety of coating materials in an effort to find what type of coating best meets the needs outlined above. Included in this effort were several commercially available polyurethane coatings, two thermoplastic coatings, and some coatings provided by NASA LaRC and NASA GRC, who are both developing some materials that may be ideally suited for this research. Each of the coatings tested was applied to both a set of specimens with preexisting leaks and a set of initially impermeable specimens. The specimens with preexisting leaks were used to determine how effectively each coating sealed leaks and then subsequently to find the critical impact energy at which sufficient damage occurred for leakage to initiate. The impermeable coated specimens were used to find the critical impact energy in the same

way as the specimens with preexisting leaks. A comparison of the effectiveness of the sealed specimens and the coated initially impermeable specimens was then made.

The balance of this thesis is divided into six other chapters. Chapter II provides some background and historical information regarding the basics of this research. A brief history of impact testing, the mechanics of impact in composite materials, the basics of permeability as related to this research, and prior research into composite fuel tanks and feedlines. Chapter III discusses the specifics of the materials that were used for the specimens in this project. Chapter IV outlines both the methodology and the equipment used for all of the testing in this project. The methods used for the application of coatings are also described in this particular chapter, as are the methods used for thermal cycling and aging of specimens. Chapter V presents the data from the testing performed along with thorough analysis. In Chapter VI the conclusions drawn from the research are presented and Chapter VII presents the lessons learned and the recommendations for future research in this field.

# CHAPTER II

## BACKGROUND AND LITERATURE REVIEW

One of the original applications of composite materials was in the aerospace field because they have tremendous strength to weight ratios. With NASA set to produce the next two generations of reusable launch vehicles (RLVs), second generation by 2010 and third by 2025[1], weight savings is a driving force in the design and thus they are looking to composites to achieve much of this weight savings. For the second generation RLV, NASA wants to reduce the cost per pound of payload from $10,000 (current cost) to $1,000, and by the third generation reduce this cost to $100. Along with the composite fuel tanks NASA plans to make the fuel feedlines from composites as well.

As mentioned in Chapter 1, RLV feedlines are vulnerable to impacts from dropped tools and inadvertent bumping during installation and maintenance. Composites dissipate impact energy through the formation of internal damage, which could lead to fuel leakage. To remedy these problems, NASA would like to explore the usefulness of applying a coating to the composite that can improve the material's impact resistance and prevent fuel leakage.

There has been extensive research already conducted on the mechanics of composites in impact events and also some research done on the permeability of composites, it is this work that will be discussed in this chapter.

## 2.1. Impact Testing

Composites react very differently to impact than metals do. Metals dissipate impact energy through elastic and plastic deformations. While plastic deformation does leave permanent deformation, metals with plastic deformations frequently can still carry significant loads and these materials generally remain free from cracking. Composites on the other hand may suffer permanent damage that dramatically reduces their ability to carry load and also can cause cracking that may link through the entire thickness of the material.

Impact events are generally broken down into two classifications, low-velocity impact (up to around 20 m/s, 65.6 ft/s) and high-velocity impacts (ballistic impacts).[6] Low-velocity impacts model such events as dropped tools, while high-velocity impacts model events such as runway debris or small arms fire. There are many different impact tests to model these two scenarios. High-velocity impacts are generally modeled using a Split Hopkinson-bar, a Gas gun impact, or a ballistic projectile. Low-velocity impacts are generally modeled by a pendulum test (Charpy or Izod), drop-weight impact, or hydraulic impact.

The Split Hopkinson-Bar provides a dynamic high strain-rate impact test. In these tests a specimen is adhered between two bars. The input bar is then struck such that the impact of the bar can cause strain-rates as high as 1000/second. There are several different types of Split Hopkinson bar tests including punch loaded, compression bar, tensile bar, and the shear test.
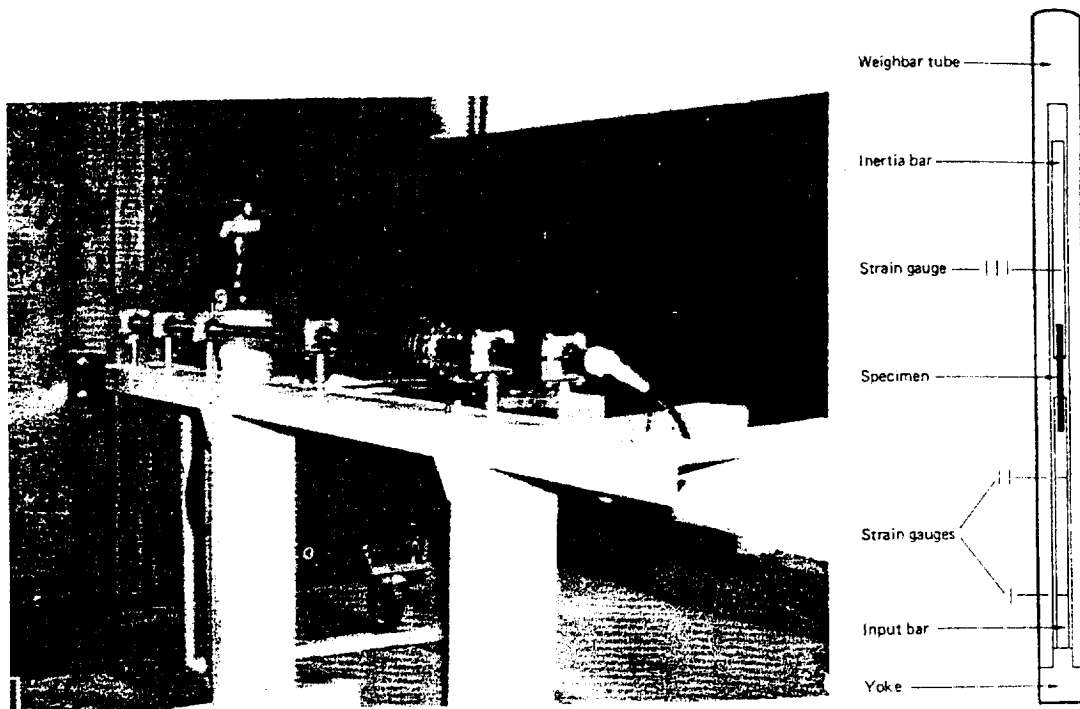
Figure 2.1. A Split-Hopkinson Bar set up for tension.[6]

Ballistic impacts and gas gun impacts are very similar. In both cases, a small projectile is shot at a specimen at high velocity. The main difference being the method in which the projectile is propelled. Figure 2.2 shows a schematic of a gas gun impactor.[7]
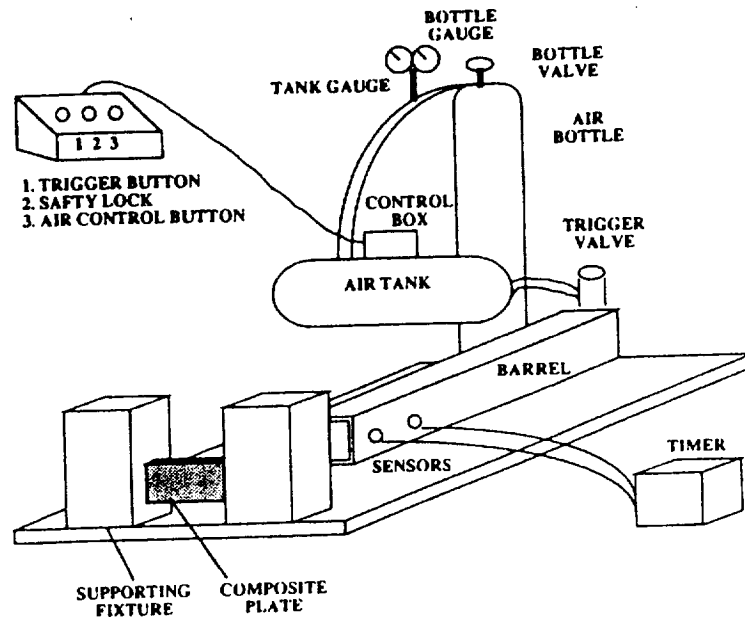
Figure 2.2. Gas gun impact test machine.[7]

Pendulum impacts are modeled using either the Izod or Charpy test set-up. While these tests work well for metals and isotropic materials, they are not very useful for composites because one can only test continuous fiber composites. Additionally, both these impacts feature a swinging arm striking a short beam specimen, which is very dissimilar to the impacts that are common in engineered components. The tests also show a great deal of geometric variation, and are therefore not very suitable for describing a composite material's reaction to impact.

Hydraulic impacts are a good measure of a materials reaction to a tensile impact (dynamic tensile loading). The specimens generally tested in this manner include dog-bone and double cantilever beams. The main advantage of this method is that one can

easily get the strain history of the specimen. Again this setup is not particularly realistic because it does not address the contact effects in impacts.

Drop-weight impact machines model impacts that are very similar to those caused by dropped tools. In these tests an instrumented impactor of known weight is dropped on the specimen from a predetermined height. Generally this type of impact does not destroy the specimen, but inflicts some damage and then the impactor rebounds (allowing the rebound energy to be determined and subsequently the energy absorbed by the specimen).

Drop-weight testing allows one to test specimens very similar to engineered components, and the test also allows for a wide variety of impact tip geometry (generally a hemispherical tip is used). This is extremely important because impact of composites is very dependent upon not only the laminate and its constituents, but also the nature of the impact event itself. One simply cannot compare two different impact scenarios and expect the results to be the same unless the entire process is similar.[8] The vast majority of the testing that has been done has used this test method and it is the test method used for this research. Thus, it is the method that will be discussed further.

## 2.2. Impact Mechanics

In toughened matrix composites (typically epoxy), energy from low-velocity impacts on composites is dissipated in two ways: generation of frictional heat, and creation of damage within the composite.[9] Low-velocity impacts on composites cause

several different damage modes including: matrix cracking, delamination, indentation, and fiber/matrix debonding.[10]

The first mode of damage that occurs in composites due to impact events is microcracking of the matrix material.[11] This microcracking is a result of the different toughness of fibers and matrix materials respectively. Typically, for polymer matrix composites, the matrix material will be far more ductile than the fibers, and thus in an impact the bond with the fibers restricts the matrix from deforming to its full capability. As a result, cracks form perpendicular to the fibers.[12] Matrix microcracking is typically a result of shear stresses in the interior of the composite and tensile stresses on the face opposite to the impact. De Freitas et al. note that microcracking will occur after impacts with insufficient energy to leave visible damage.[10] The matrix cracking is most dense immediately around the impact location and drops off quickly the further away one looks from the impact site.[13] The exception to this is that the region grows in radius in each subsequent ply away from the contact surface.

Delaminations occur in composite specimens only after microcracking has taken place.[14] It is theorized that delaminations occur when microcracks in two plies of different orientation overlap. At these locations there are discontinuities that make transferring the shear stresses impossible, which leads to the formation of the delamination. Additionally, Papanicolaou et al. theorize that the difference in bending stiffness of plies with different orientations leads to some delaminations.[15] One can tell that delamination has occurred by looking at the load vs. time plot for an impact event, the first delamination occurs when the first vertical drop appears on the plot (typically at

about half of the maximum load).[13]  Two modes of delamination were observed by Xu, opening dominated "delamination buckling" (inter-layer cracking), and "shear delaminations" (shear dominated inter-layer cracks, generally occurs in materials subjected to out of plane impacts).[16]

Delaminations always have a two lobed shape, with the major axis following the orientation of the fibers on the bottom layer of the delamination (impact location is always the top side).[17]  When the mismatch angle between the two plies is greater than 30°, damage size is virtually independent of the mismatch angle, yet when it is smaller than 20° damage is long and narrow.  In fact, frequently when the mismatch angle is smaller than 20° matrix cracks act as borders along each side of the delamination.[18]  As was the case with the microcracks, the sizes of the delaminations grow towards the back face of the specimen (away from contact with impactor).

Much of the energy that is absorbed by composites during impact events is dissipated through the formation of delaminations.  These delaminations are of particular importance because they seriously deteriorate a composites compressive strength and they also provide more paths for permeation.

Fiber rupture is a continuation of the damage following microcracking of the matrix and the delaminations between the plies in composites with toughened matrices (typically epoxy).  After progressive delaminations high shear stresses ahead of the crack tip cause more delaminations, which in turn blunts the crack tip reducing the stress concentration.  The specimen continues to carry load until the fibers in the next layer begin to fail in tension.  This pattern continues until the entire composite laminate has

failed.[19] Fiber fracture also occurs at the back face of composites during impact. In woven composites fiber fracture occurs immediately below the impact site and may be due to the perturbation caused by the overlapping tows and resultant stress concentrations.[13]

Impacts with sufficient energy may cause indentation or crushing of the matrix material. This is evident when a dent is left in the surface of the composite. Impacts that cause indentation frequently cause shear stress waves with enough energy to actually cause some cracking of the matrix material on the surface of the composite immediately around the impact site.[20]

With stiff fibers in a more ductile matrix, fiber pullout becomes a significant source of energy dissipation, and subsequently damage. In the case of brittle fiber reinforced matrix composites, much of the toughness actually comes from matrix cracks getting diverted along the fiber/matrix interface.[12] According to Beaumont, this is particularly true of carbon fiber composites.[6] Some have tried to improve the damage resistance of composites by coating the fibers with a tougher sizing to improve the bonding with the matrix material. These efforts actually reduced the impact resistance of the system by eliminating the energy dissipation from fiber/matrix debonding, resulting in a more brittle failure than would otherwise occur.[19]

In composites with brittle fibers, toughening the matrix material improves the impact resistance. In fact, toughened epoxy matrices have improved the interlaminar fracture toughness of carbon fiber reinforced plastics (CFRP) by as much as 8 times.[21] This improvement is not as significant as one might have expected though, since

toughening the matrix alone yielded a 20-fold improvement over the un-toughened matrix material. Composites made with these toughened matrices end up with much smaller damage zones after impact, but only if the fibers are brittle. This occurs because brittle fiber composites absorb most of their impact energy in the formation of delaminations, whereas composites with tougher fibers, e.g. glass fibers, absorb the energy in ductile deformation of the fibers.[9] Toughening of thermoset polymers can be achieved in one of two ways. One can add a rubbery phase to the polymer[22], or one can add some thermoplastic material to yield an interpenetrating network (IPN). IPNs do exhibit improved fracture toughness, but the resultant prepreg has decreased handleabiltiy.[12] One of the properties that tougher thermoset polymers have is that they are lightly cross-linked. Reducing the cross linking of a polymer will improve its ductility, but this also reduces its strength and makes the polymer more permeable.

Increasing the toughness of the fibers will also increase the toughness of the composite. Fibers with greater ductility can deform more and thus resist fracture more than brittle fibers, which increases the impact resistance of the composite. Increasing the toughness of the fiber also makes the composite more rate-sensitive though. Ductile fibers do not have sufficient time to deform fully in high-velocity impacts and thus fail prematurely; brittle fibers on the other hand show little variation based on loading rate.[9]

## 2.3 Permeability Research

In terms of this project, the term permeability is being used rather loosely. When speaking of composites with impact damage, or other damage, it would actually be more

13

accurate to say that the gaseous permeation is occurring. The term permeability implies that there is diffusion through a porous material, whereas in reality there are a few distinct paths through which the permeants may escape. Permeability is an important consideration of this project because concentrations of hydrogen of 4% in air are flammable, and concentrations 18.3% or higher are explosive. For the National Aerospace Plane project, the acceptable hydrogen permeability rate was between $10^{-4}$ and $10^{-3}$ SCC/sec-in$^2$ (standard cubic centimeter per second per square inch) which helps to illustrate just how important eliminating hydrogen leakage is.[23]

## 2.3.1 Permeation

In work done by Kessler et al. it was found that carbon/epoxy composites are very vulnerable to microcracking caused by thermal cycling. At temperatures below 60K (-351 °F) cracking of the matrix material initiates, and after only a few cycles between 60K and 400K (261 °F) the maximum microcracking density is reached (generally on the order of 5 cycles).[24] Cracks that form due to thermal cycling grow parallel to the fibers because the matrix has a much greater coefficient of thermal expansion than the fibers. It was found that laminates with more variation in the orientation of the fibers had greater permeations than did those with fewer fiber orientations because the cracks had more overlap, and thus created more complete paths through the material. Figure 2.3 is a good example of how cracks in plies of different orientations create leak paths through composite materials.
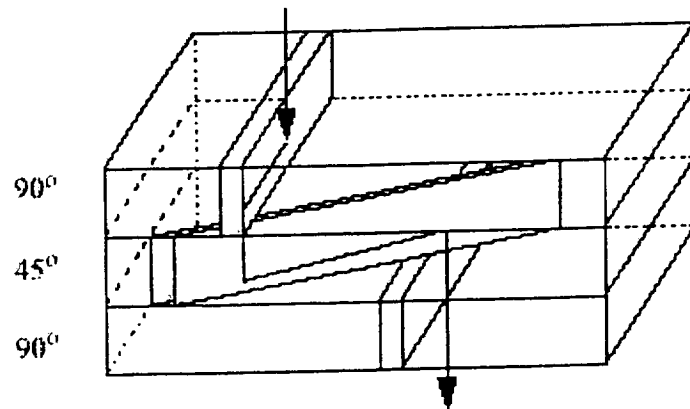
Figure 2.3. Cracks in a laminate such that leakage occurs.[24]

Composites become far more brittle at cryogenic temperatures. In particular polymeric matrix materials become quite brittle, meaning that much lower loads are required to initiate cracking than at room temperature. Kumazawa et al. found this not only reduced the mechanical performance of the composites but also more importantly led to paths large enough for gaseous helium to permeate through.[25] This is of particular concern because the feedlines that are to be used on future RLVs will be under pressure (albeit low, typically around 30 psi, 0.21 MPa).

Polymeric materials tend to absorb moisture from their environments in a non-Fickian manner. Fick's Law describes permeability in the true sense of the word (uniform diffusion across a surface) and with polymeric composites moisture is absorbed into cracks and flaws. This is significant should cracks form as a result of thermal cycling or impact events. In turn this moisture accumulation changes the residual stresses present in the composite and can lead to further generation of microcracking.[26]

Furthermore, should moisture accumulate in the fiber/matrix interface serious damage could occur should the moisture freeze or boil.

Most of the testing that has been done regarding permeability of polymer matrix composites has been done on test coupons as opposed to sample feedlines or fuel tanks. While these tests present a facsimile of what will happen with composite feedlines and fuel tanks, the test coupons lack the geometric complexity of the actual parts. Because of the complexities of the feedlines and fuel tanks these production parts may be more vulnerable to leakage than the test coupons indicate.[27]

## 2.3.2 Permeability of Coatings

To prevent fuel leakage through the feedlines and fuel tanks it is important to find coatings that are highly impermeable as well as impact resistant. Highly cohesive polymers are excellent in resisting gaseous permeability. Crystalline polymers are also highly impermeable. In crystalline polymers, the permeability is proportional to the amorphous volume fraction. Permeability through polymeric materials is usually a result of activated diffusion, and flaws such as pinholes and cracks. Assuming that there are no flaws in the coating permeability requires four steps: [28]

1. Absorption of permeant onto the surface of the polymer

2. Solution of gas/vapor into polymer matrix

3. Diffusion through the wall along a concentration gradient

4. Desorption from the other surface

Thus it can be seen that increasing the thickness of the coating reduces the permeability significantly as long as there are no flaws. Coatings that are able to penetrate the substrate and fill/seal the pores are further reduce the permeability.[29] To be a good barrier, a material should be slightly polar, have a high chain stiffness, be inert to the permeant, have close chain-to-chain packing with some bonding between chains (cross-linking), and have a high glass transition temperature ($T_g$). Polyurethane materials can have a high degree of cross-linking, particularly those that cure with the aid of a cross-linking agent.[30] Additionally, the inclusion of inert mineral fillers can reduce the permeability of polymeric materials.[31]

Nanocomposites are simply polymers with nanoscale reinforcement distributed within them. The most studied type of nanocomposite are those reinforced by the addition of silica particles (generally some type of clay). The term nanocomposite refers to the size of the reinforcement in the polymer. A typical clay platelet will be on the order of 1 nm in thickness and 100 to 1000 nm ($3.94*10^{-6}$-$3.94*10^{-5}$ in) in width.[32] Nanocomposites make excellent permeability barriers because of the highly impermeable clay particles distributed evenly throughout the material. Thus for a gas to permeate through a nanocomposite it must navigate a much longer and difficult path through the material than a traditional polymer coating, as is illustrated in Figure 2.4.
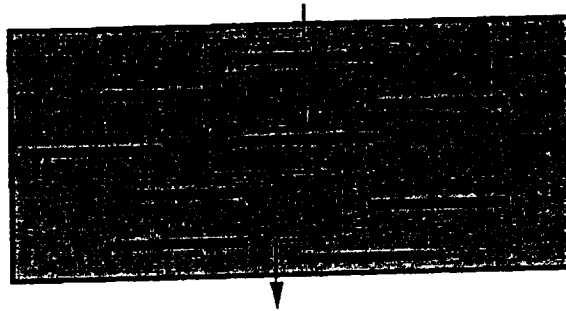
Figure 2.4. Illustration of the tortuosity of leak path through a nanocomposite.[33]

In addition to reducing the permeability of the polymer material (ten-fold reduction for some polyimides), the addition of the silicas improves many of the materials mechanical properties. For instance it was found that loading Nylon-6 with 4.2% clay, by weight, the modulus doubled, the strength increased more than 50%, and the heat distortion temperature increased by 80 °C (176 °F).[33] The best part is that because so little clay must be added to the polymer to achieve these benefits the difference in weight is minimal. As well as improving the mechanical properties, the addition of clay particles to the polymer matrix improves the materials resistance to the corrosive liquid oxygen and hydrogen environments (and also to atomic oxygen, a concern in low earth orbits). It has been found that polymeric coatings applied to composites tend to delaminate at cryogenic temperatures due to the mismatches of the CTE (coefficients of thermal expansion).[34] With nanocomposites the CTE can be adjusted to minimize the difference, thus preventing delamination of the coating.

In the case of a coating with flaws or damage the permeability rises dramatically. Three distinct types of damage can occur that increase the permeability of a material.

Firstly, there can be internal damage in the material such that two distinct phases of material exist (essentially the creation of voids) with each having reduced thickness. Secondly, there can be surface damage, which simply reduces the effective thickness of the material. Lastly, there can be through damage.[35] The three types of damage are illustrated in Figure 2.5.
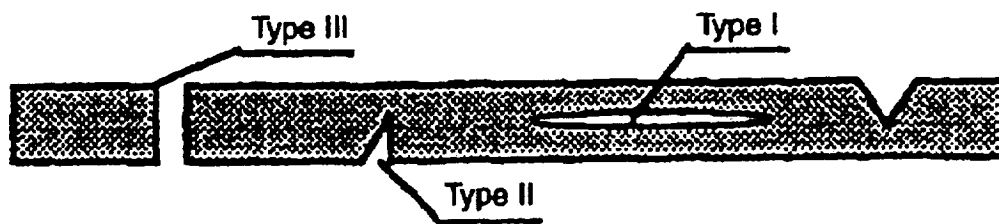


Figure 2.5. Types of damage that increase the permeability of a material.[35]

The importance of coating materials remaining crack free is magnified by the fact that it has been found that polymers are not diffusive at cryogenic temperatures.[36] Fuel leakage at cryogenic temperatures will therefore require a path through the coating and composite substrate. At room temperatures however, composite cryostats have been found to loose pressure due to diffusion. It was determined that in order to prevent hydrogen permeation there needed to be at least 0.04 in thick of matrix (or polymer) material.[37]

## 2.4 Woven Laminates – Effects on Impact and Permeability

Woven composites behave differently in terms of both their impact resistance and their permeability (this term shall be used through the remainder of this thesis in place of permeation).

19

## 2.4.1 Effects of Woven Composites on Impact

Compared to unidirectional laminates, woven laminates are much more resistant to impact. There is conflicting evidence regarding any improvement in the level of impact at which damage initiates compared to unidirectional laminates, but evidence shows that woven composites have smaller damage areas for given loads. Briscoe et al. showed that the weaving process caused fiber bridging which enhances the toughness of a composite by physically blocking crack growth.[13] In particular, woven composites limit the splitting along the fiber direction on the backside that normally occurs with unidirectional laminates.[12] Additionally, the interlaminar and intralaminar fracture toughness of woven composites is increased over unidirectional composites.[21]

If a composite endures both an impact and then compression, woven composites present definite advantages due to the smaller delamination areas (less buckling due to shorter unsupported fiber lengths). In tension however, woven composites are weaker than unidirectional composites even though the woven material has a smaller region of damage, due in large part to the perturbation of the fibers.[38]

To further reduce the damage that occurs in impact events, woven composites can be made 3D. Meaning that there are also fibers woven in the z-axis that bind the system together. Three dimensional weaves have been found to limit the size of delaminations more than just 2D weaves, because the 3D stitching binds the plies together preventing one ply from delaminating and then sliding away from another.[12]

Work done by Hosur et al. is worth noting simply because it suggests that the weave chosen may have a large role in the size of the damage region formed by impact. From some C-scanning of both plain weave and satin weave graphite/epoxy composite specimens impacted with the same set of energies the satin weave consistently suffered much less damage. The damage in these two figures is appears as a black region that the authors circled. These two figures are recreated below as Figure 2.6.

(a) 5 J        (b) 7.5 J        (c) 10 J

(d) 15 J        (e) 20 J        (f) 25 J
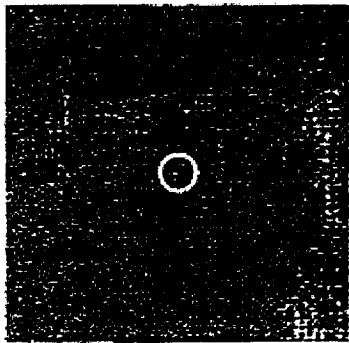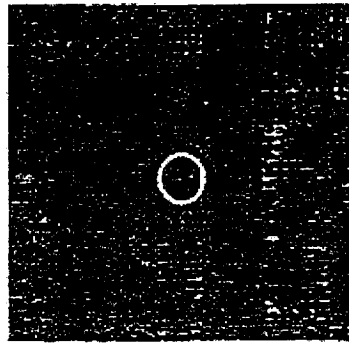
(g) 30 J        (h) 35 J        (i) 40 J

(a) 5 J        (b) 7.5 J        (c) 10 J
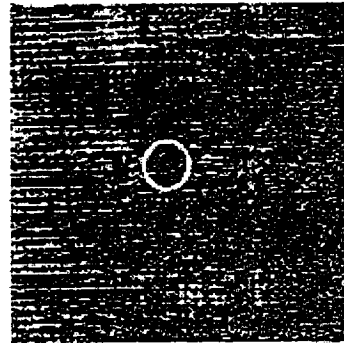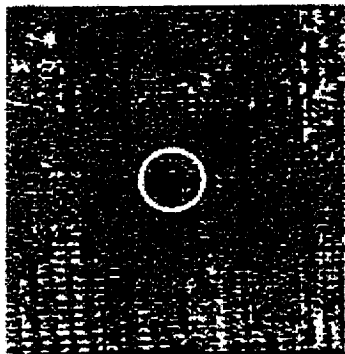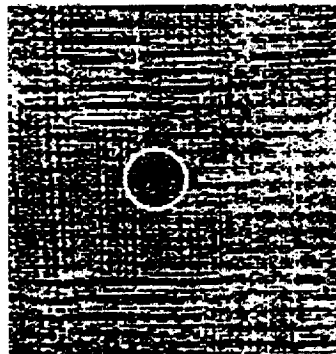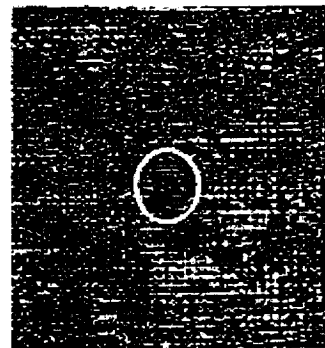
(d) 15 J        (e) 20 J        (f) 25 J
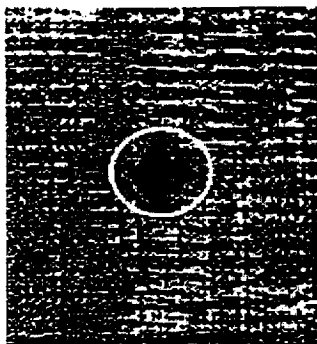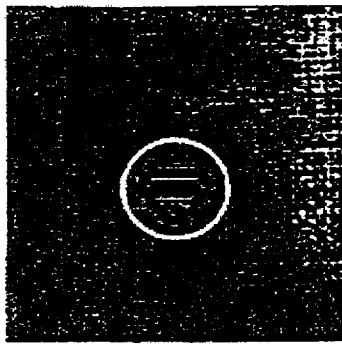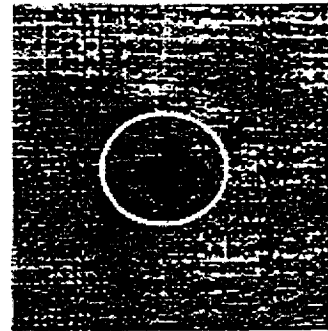
(g) 30 J        (h) 35 J        (i) 40 J
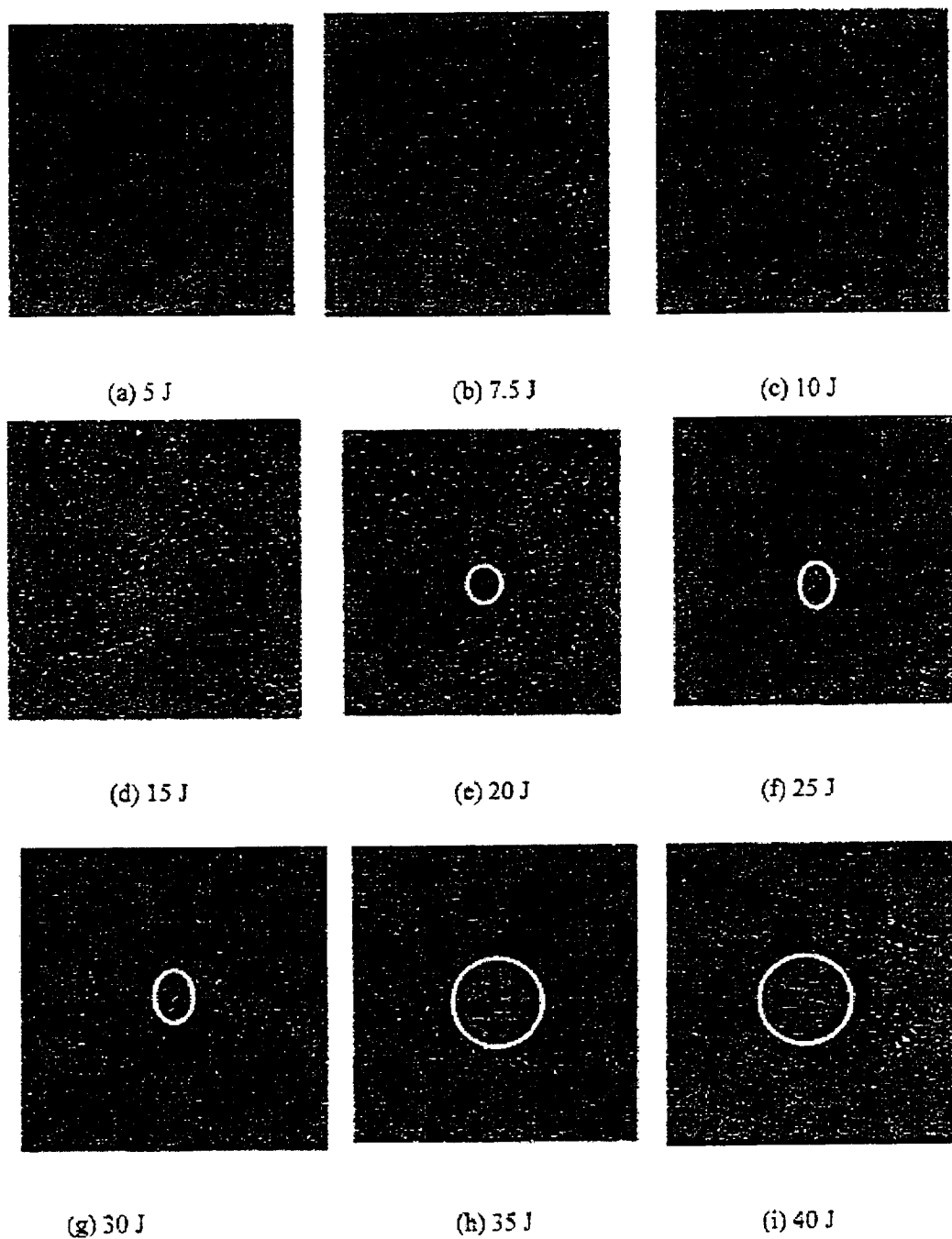
Figure 2.6. C-scans of plain weave graphite/epoxy specimens (first page) compared to satin weave specimens.[39]

### 2.4.2 Implications of Woven Composites on Permeability

A great deal of microcracking can be caused by thermal cycling of composites, to this end woven composites are much less susceptible to residual thermal stresses compared to unidirectional composites.[21] Despite being less vulnerable to thermal stresses, woven composites have pores between the warp and weft tows. It is common for these pores to align in which case if there is not proper matrix wetting leak paths may exist prior to the application of any external stresses, which will increase the composite's permeability significantly.[40]

### 2.5 Composite Fuel Tank and Feedline Research

Some research has already been done specifically looking at difficulties associated with making cryogenic fuel tanks and feedlines from composite materials for the next two generations of RLVs. In particular, a great deal of work was done on both composite fuel tanks and fuel feedlines for both the X-33 and the Delta Clipper (DC-XA) projects. Going into these projects no one had attempted to make composite cryogenic fuel tanks and thus there were great concerns regarding the viability of this technology.

The DC-XA was an adaptation of a previous vehicle that McDonnell-Douglas had made using metal fuel tanks. When it was decided that composites were the way to go due to the tremendous weight savings an effort was made to prove the viability of this technology with several test flights, the first of which took place May 20, 1996.[3] This first test flight lasted one minute with a maximum altitude of 800 ft. The fuel tank that

was used in the DC-XA weighed in at 2020 lb (8985 N), a savings of 1200 lb (5338 N) over the metal tanks originally used. The vehicle was unfortunately destroyed at the end of the fourth flight, when the tanks ruptured after part of the landing gear failed to deploy and the vehicle collapsed, rupturing the tanks. Prior to the accident though, the vehicle made four successful test flights, the longest lasting 142 seconds reaching an altitude of 10,300 ft (3139m).

To go along with the composite $LH_2$ and $LO_2$ fuel tanks, the DC-XA had composite fuel feedlines. The feedlines that were designed for the DC-XA had to demonstrate:[41]

> ➤ Acceptable hydrogen permeability levels for flight hardware

> ➤ Composite-to-composite adhesive joints

> ➤ Composite-to-metallic adhesive joints

> ➤ Composite-to-composite flange interface

> ➤ Composite elbows (90° bends in tubes)

> ➤ Composite valves for $LH_2$

The feedlines tested by Nettles at NASA MSFC were made from materials very similar to the ones considered in this thesis. The feedlines were developed by McDonnell-Douglas and consisted of IM7/8552 eight harness weave prepregs layed up in a [0/90/±45/±45/90/0] orientation. Some splice material was also necessary for the feedlines, and this was made of unidirectional tape layed-up as [60/-60/0]$_s$. The final result is pictured below in Figure 2.7.

IM7/8552

Adhesive Bonds
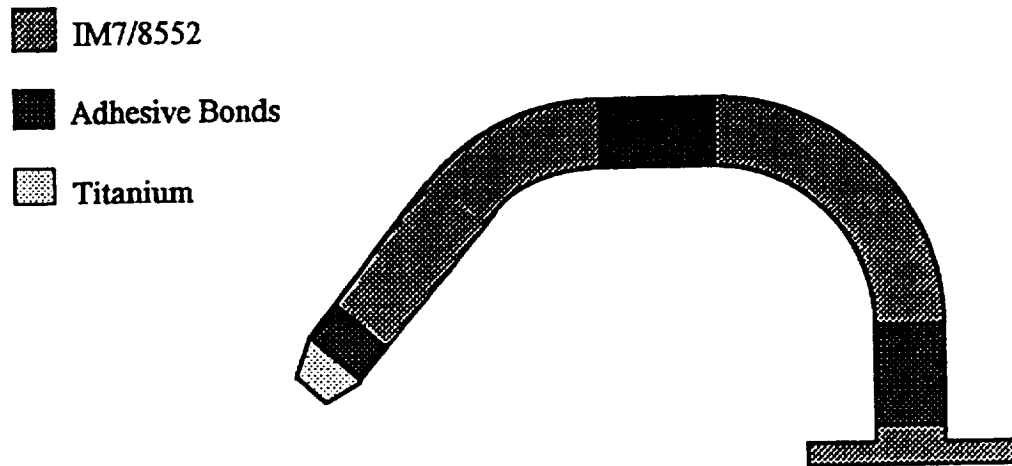
Titanium

Figure 2.7. Sample LH$_2$ feedline.[41]

Flat panel specimens were also made, and these specimens were tested for permeability. Additionally, some specimens were made of the composite bonded to titanium washers to measure the permeability of the bondlines. Dr. Nettles found that the composite material itself was virtually impermeable to nitrogen gas (used in his research due to similar molecular size to hydrogen) with permeabilities on the order of $10^{-6}$ in$^3$/sec-psi ($2.38*10^{-6}$ cm$^3$/sec-kPa). The bondline specimens had permeabilities ranging from $5*10^{-6}$ to $6*10^{-3}$ in$^3$/sec-psi ($1.19*10^{-5}$ to $1.43*10^{-2}$ cm$^3$/sec-kPa). After thermal cycling of these specimens the permeability change was extremely small, cycled from 77K (-321 °F) to 100 °C (212 °F), and it was determined that as long as the composites were properly processed they would not be the cause of any appreciable leakage. It appears that there is some difficulty properly processing composite feedlines though, since Dr. Nettles has had several in subsequent work that had leaks.[40]

26

Some concern existed that during installation and maintenance of these composite feedlines someone might accidentally cause a low energy impact event. Because it is known that composites suffer matrix cracking prior to the loss of any mechanical properties it was necessary to assess the impact resistance of the material. The impact testing performed used a drop-weight impact machine with a variety of different tips, a sharpened bolt, a hemispherical tip, and a blunt tip. After impact the sample feedlines were pressurized to 60 psi (413.8 kPa), twice the normal expected operating pressure.

Dr. Nettles found that the specimens impacted with the sharpened bolt tended to have complete punctures, but that when the impactor did not completely penetrate the composite there was not always sufficient matrix cracking for permeation to occur. The blunt impactor and the hemispherical tip impactors, however, did not penetrate the composite but instead inflicted much more damage to the matrix. In fact, it was found that the surface damage could not be used as a reliable measure of the permeability of the composite material. Also, it was found that composite feedlines could leak after impacts that caused no fiber breakage whatsoever. Impacts with the blunt tip with as little energy as 0.61 ft*lb (0.83 J) were found to be sufficient to initiate leakage in some specimens, with impacts of 0.79 ft*lb (1.07 J) causing leakage in all cases.[4]

The X-33 demonstration vehicle was also to have composite fuel tanks. One of the tanks designed for this vehicle were filament wound graphite/epoxy with a titanium lining and were to have a service pressure of 3200 psi (22.1 Mpa), and during proof testing of these tanks they were taken to 6400 psi (44.1 Mpa) with $LH_2$ and no leaks were found.[42] Even after 50 life cycles, the tanks were filled with $LHe_2$ to 3200 psi and held at

this pressure for 4 hours in a LH$_2$ bath (-423 °F, 20K) and then the pressure was bled off rapidly to simulate takeoff, the tanks were found to have only negligible degradation. Typically, cryogenic fuel tanks will be at much lower pressures than these, on average 30 to 40 psi (.21 to 0.28 Mpa) for large vehicles and 75 psi (0.52 Mpa) for smaller vehicles.[43]

In the end the tanks that were chosen for the X-33 were carbon fiber honeycomb core sandwich panel tanks. These tanks did not survive all of their proof testing. Eventually they failed due to a build up of pressure in the honeycomb core of the sandwich structure that made up the tank walls, which led to debonding of the facesheets. Hydrogen had leaked into the core through microcracks that formed in the interior facesheet.[23]

Another concern confronting those who wish to design composite feedlines and tanks for future RLVs is that some of the structures will be very large. It is estimated that to maximize launch vehicle performance some tanks will need to be 16 to 40 ft (4.9 to 12.2 m) in diameter. At this time, no autoclaves exist that can handle such tanks.[44] Thus these structures would have to be made using Electron Beam (EB) cured composites. These materials are far more brittle than traditional cured epoxies, and are therefore more vulnerable to cracking. Also, many of the EB composite feedlines that NASA made were found to be permeable prior to any impact events whatsoever.[40]

# CHAPTER III

# MATERIALS

The materials used in this research are to model the fuel lines that NASA proposes to use for future fuel feedlines in RLVs. The materials that were studied here are similar to those studied previously by Nettles.[41] These materials are similar to those chosen by McDonnell-Douglas for the X-33 prototype vehicle. In addition to the composite materials that were used to model the feedlines a variety of coating materials were chosen for study as part of this project. These materials will be discussed in this section as well.

## 3.1 Composite Constituents

The composite feedlines were made up of carbon fibers in an epoxy matrix. Each of these two materials will be discussed independently and then the method used for the lay-up and processing will be discussed.

### 3.1.1 Fibers

The composite feedlines that were made for previous research done by Nettles and for the research described in this document used IM7 carbon fibers made by the Hexcel Corporation. The fibers are available in both 6,000 and 12,000 filament count

tows, and it is not known which was used for this composite. IM7 fibers are PAN based fibers. The general properties for the IM7 fibers are presented in Table 3.1.

Table 3.1 Properties of Hexcel IM7 Fibers.[45, 46]

| Fiber Type | Tensile Strength, MPa (ksi) | Tensile Modulus, MPa (Msi) | Ultimate Elongation (%) | Carbon Content (%) | Density, $N/cm^3$ $(lb/in^3)$ |
|---|---|---|---|---|---|
| IM7 (5000) 6K | 5170 (750) | 275900 (40.0) | 1.87 | 94.0 | 0.0176 (0.0643) |
| IM7 (5000) 12K | 5520 (800) | 275900 (40.0) | 2.00 | 94.0 | 0.0176 (0.0643) |
| IM7 (6000) 12K | 5760 (835) | 289700 (42.0) | 1.99 | 94.0 | 0.0177 (0.0646) |

### 3.1.2 Matrix

The matrix material used for the feedlines studied by Nettles was Hexcel 8552 epoxy, however this matrix material was not used for the specimens provided for this research.[41] The matrix used here was EX 1552, which is supposed to be very similar to Hexcel's 8552. Both are toughened epoxy materials. EX 1552 is a product of Bryte Technologies, Inc. Mechanical properties of EX 1552 can be found below in Table 3.2.

Table 3.2. Properties of EX 1552 Toughened Epoxy.[47]

| Density, $N/cm^3$ $(lb/in^3)$ | 0.0144 (0.0526) |
|---|---|
| $T_g$, °C (°F) | 202 (396) |
| CTE, ppm/°C (ppm/°F) | 50.94 (28.3) |
| Tensile Strength, MPa (ksi) | 66.2 (9.6) |
| Modulus, MPa (Msi) | 4000 (0.58) |
| Poisson's Ratio | 0.48 |
| Flexural Strength, MPa (ksi) | 155.9 (22.6) |
| Flexural Strain (%) | 5.5 |
| Compressive Strength, MPa (ksi) | 147.6 (21.4) |
| Thermal Conductivity, N/(°C*s) [lb/(°F*s)] | 0.171 (0.0688) |

### 3.1.3 Lay-Up and Processing

The composite was formed from 2D 5-harness woven 3.5' by 3.5' (1.07 m by 1.07 m) prepreg with a [0/90]₄ lay-up. The panels were made in sheets and cured at 350 °F (177°C), ramped up at 3 °F/min, held at 350 °F for two hours, and then cooled at 5 °F/min (2.8 °C). A pressure of 80 psi (0.55 MPa) was maintained throughout the curing process.[48]

All of the specimens were made at NASA MSFC in large panels that were cut into 4" by 4" (10 cm by 10 cm) specimens prior to shipping. The first specimens that were received (all from the same sheet of material) made from this material all had some unique surface flaws as shown in Figure 3.1. These flaws appear to be due to gas becoming trapped between the composite and the tool surface during autoclaving. The flaws appear in a thicker resin rich area that appeared consistent across all of the specimens received from this panel. Subsequent specimens were thinner than this initial batch of specimens and appeared to have a release ply used on both sides. The thickness of the specimens received varied from just under a millimeter to just more that a millimeter and a half. Each batch of specimens received was at least slightly different than the others received, and from some C-scanning done by Erik Weiser, NASA Langley Research Center (NASA LaRC), it is evident that there is a great deal of variation within single panels. Figure 3.2 shows some of the C-scan images received from NASA LaRC. All of the C-scanning was done on specimens from the first batch

received.   The different shades of gray visible in the C-scan images indicate the variability in the material received.   The lighter color areas represent voids in the composite, or simply regions that were poorly cured.
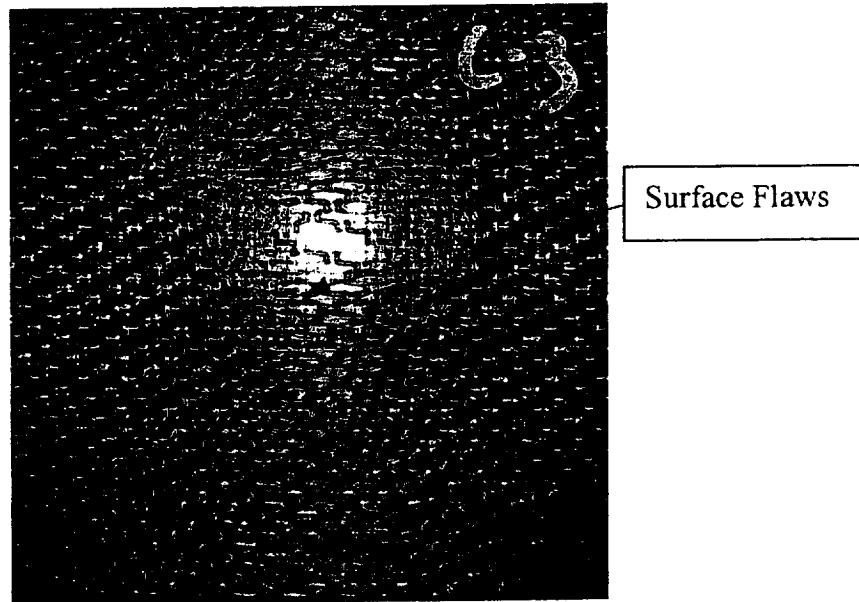


Figure 3.1. Typical specimen from the first batch received showing surface flaws.

Ch:1 G:1: Peak
EW-A1.CS1          312        ZFSH
Inches
                                    100

4                                   80

                                    60

2                                   40

0                                   20

                                    0
0        2        4      Inches
Page 1 of 2
4X4 WOVEN FABRIC P-E A10

EW-A1.CS1   Ch:1 G:1: Pea

| 2.59In² | 15.61% | 103439pts | |
| 2.56In² | 15.46% | 102427pts | |
| 4.93In² | 29.79% | 197359pts | |
| 4.97In² | 29.98% | 198644pts | |
| 1.52In² | 9.16% | 60702pts | |

Ch:1 G:1: Peak
EW-C10.CS1         38%        ZFSH
Inches
                                    100

4                                   80

                                    60

2                                   40

0                                   20

                                    0
0        2        4      Inches
Page 1 of 4
4X4 WOVEN FABRIC P-E C10
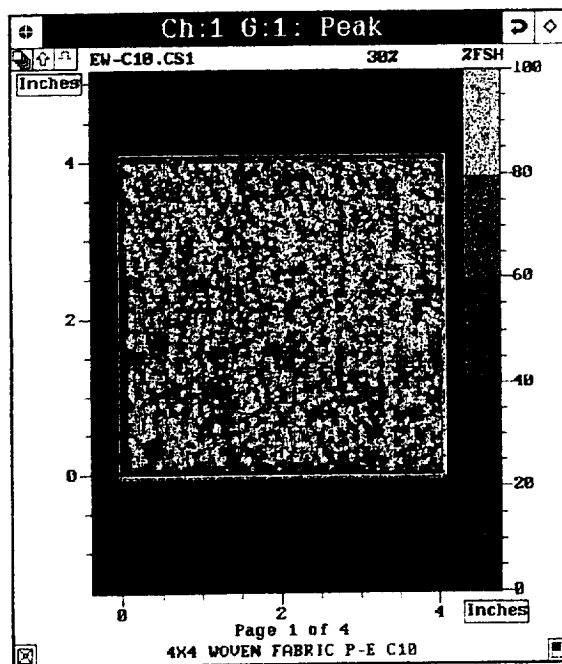
EW-C10.CS1   Ch:1 G:1: Pe

| 4.11In² | 24.83% | 164294pts | |
| 4.79In² | 28.96% | 191674pts | |
| 5.03In² | 30.42% | 201338pts | |
| 2.05In² | 12.37% | 81857pts | |
| 0.56In² | 3.41% | 22599pts | |

Figure 3.2. C-scan images of two specimens from the first batch received from NASA MSFC.

33

### 3.1.4 Composite Properties

The composite specimens received were tested to find their tensile properties. All of the testing was done according to the ASTM standard.[49] The tensile modulus and the ultimate tensile strength for the composites received are presented below in Table 3.3. Specimens S1, S3, and S4 were all from the first batch of specimens received while S2 was from a different batch (and was around 2/3 as thick as the other specimens).

Table 3.3. Tensile properties of the IM7/EX 1552 composite.

| Specimen | Ultimate Tensile Stress, MPa (ksi) | Modulus, MPa (Msi) |
|---|---|---|
| S1 | 771 (111.8) | 30344 (4.40) |
| S2 | 950 (137.8) | 29723 (4.31) |
| S3 | 808 (117.2) | 26551 (3.85) |
| S4 | 737 (106.9) | 25448 (3.69) |

### 3.2 Coatings

Eleven different coating materials were considered for this research. Of these 11, two were to be liquid crystal coatings supplied by Erik Weiser of NASA Langley Research Center. Unfortunately, due to the redirect in funding for the Second Generation RLV project, the funding needed to supply these coatings was no longer available. Still, this leaves 9 coatings that were studied to see if they could improve the impact resistance of composites for use as fuel feedlines. The nine remaining coating materials included

four polyurethane materials, two thermoplastic coatings (commercially used in the fire proofing industry), and a polyimide and two polyimide nanocomposites coatings supplied by Sandi Campbell of NASA Glen Research Center (NASA GRC).

### 3.2.1 Polyurethane Coatings

Four different commercially available polyurethane materials were selected for testing as part of this project, Centurion Water Based Urethane, Corothane I Aliphatic Finish, Corothane I MIO-Aluminum, and Poly-Lon 1900 (all are Sherwin Williams products).

The Centurion Water Based Urethane is a polyester based urethane enamel. This coating system is a two-part system and is low in VOCs.[50]

Corothane I Aliphatic Finish is a single component moisture curing urethane. Aliphatic urethanes consist of a long main chain with bonded carbon atoms. Unlike other polyurethane's, aliphatic urethanes do not break down when exposed to UV radiation. This particular coating exhibits outstanding adhesion to most surfaces, as well as being resistant to most chemicals.[51]

Corothane I MIO-Aluminum is also a single component moisture curing polyurethane. This coating however is loaded with both aluminum and micaceous iron oxide particles. According to the product data sheet for this coating it too features outstanding adhesion to most materials, and is chemical resistant.[52]

The last of the polyurethane materials considered was Poly-Lon 1900. This coating is a two-component, high solids, polyester-aliphatic urethane. Poly-Lon 1900 was designed to withstand impact events and chemical attack.[53]

The technical product information available for these coatings is presented below in Table 3.4. The direct impact resistance data presented was performed according to ASTM D2794, which requires a 24-gage (0.025", 0.0635 cm, thick) steel plate be used as a substrate for the coating.[54] The flexibility data presented in the table was determined according to the ASTM mandrel standard.[55] Again, in this standard the coating is applied to a thin steel substrate (22-gage, 1/32 in, 0.079 cm, thick), which is then bent around a conical mandrel.

Table 3.4. Mechanical properties of the polyurethane coatings tested.

| Coating | Direct Impact Resistance, J (in*lb) | Flexibility, mandrel diameter, cm (in) |
|---|---|---|
| Centurion | >217 (>160) | 5/16 (1/8) |
| Corothane I Aliphatic Finish | 217 (160) | 5/16 (1/8) |
| Corothane I MIO-Aluminum | 108 (80) | 5/16 (1/8) |
| Poly-Lon 1900 | 136 (100) | 5/8 (1/4) |

### 3.2.2 Thermoplastic Coatings

Two thermoplastic coatings were considered in this research, Thermaflex II-C and Thermashield. Both of these coatings are claimed to have outstanding impact resistance, and low permeability's.[56] These materials are commercially marketed in the fireproofing industry, but due to their mechanical properties both were considered for this research.

36

Thermaflex II-C has excellent adhesion to composite laminates.[57] Thermaflex II-C is a water-based that contains no VOCs, while Thermashield is a solvent-based thermoplastic material.

### 3.2.3 Polyimide Nanocomposites

NASA Glenn Research Center is supplying three different coating materials as part of this project. Two of the materials are polyimide nanocomposites while the third coating is simply the neat polyimide resin. The nanocomposites are made by adding either 2% or 5% by weight Bentolite H from Southern Clay Products to the neat polyimide resin. Bentolite H is a white bentonite produced from colloidal aluminum silicate.[58]

The resin was made by converting a Bisphenol-A dianhydride (BPADA) to a diacid ester (BPADE) by refluxing overnight in methanol. The amount of BPADA/MeOH was calculated to yield a 50 %wt solution of BPADE. In order to coat four of the test specimens 2.65g of BPADE and 2,2-bis(4-aminophenoxyphenyl)propane (BAPP), 1.85g, were mixed in a 50:50 mixture of methanol and acetone, which was then reduced by evaporating much of the solvent. This process yields 4.5g of polyimide.

The nanocomposites were made the same way except that either 2 %wt or 5 %wt Bentolite H clay was added to the BPADE-BAPP solution. Prior to being mixed into the polyimide solution though the clay had to undergo ion exchange in order to get a proper dispersion throughout the resin.[59] Table 3.5 shows some material properties for both the

neat polyimide resin and the 2% nanocomposite, there is no 5% nanocomposite data available.

Table 3.5. Material properties of the neat polyimide and 2% nanocomposite coatings.

| Coating | Ultimate Tensile Strength, MPa (ksi) | Modulus, GPa (ksi) | Permeability [(mol/m/s/Pa)*10^-15] |
|---|---|---|---|
| Neat Polyimide | 84.8 (12.3) | 325.5 (472) | 2.85 |
| 2% Nanocomposite | 91.7 (13.3) | 322.1 (467) | 2.45 |

# CHAPTER IV

# EXPERIMENTAL EQUIPMENT AND TECHNIQUES

This research was divided into several different unique phases. Specimens were all checked for leaks and coated. As the thesis title would suggest the vast majority of the specimens were impacted, and permeability tested. It is also important to determine the effects of cycling the coated composite from cryogenic temperatures up to the elevated temperatures that the composite feedlines would encounter during reentry. Finally, many polymers continue to embrittle over time. Thus an effort was made to determine the effects of aging on the coatings. In this chapter both the experimental methods used in the testing will be described as will the equipment that was used, and in some cases constructed.

## 4.1 Leak Detection Testing

### 4.1.1 Leak Detection Equipment

The leak detection apparatus that was constructed in house was based on the equipment that was used for some prior research at NASA MSFC.[60] As the name of the equipment would suggest, the leak detection apparatus was intended only to provide a quick method of determining whether or not a specimen was leaking and would therefore need to tested to quantify the rate of permeation.

In order to accurately determine whether or not a specimen was leaking it was important to devise a method by which a gas could be applied at pressure to one side of a specimen such that the only escape route was through the composite. Then it is necessary to make any leaks that do exist clearly visible. The leak detection apparatus used at NASA MSFC accomplished these goals by creating a two-plate system. The bottom plate had a chamber created in it that could be connected to a gas line one side and would be flush with the specimen on the other. The top plate simply had a hole through its thickness in the exact size and shape of the chamber in the bottom plate. This hole in the top plate could then be filled with a liquid solution that would make any leaks visible as a stream of bubbles. Because it would be very difficult to obtain a seal against the composite using just the two aluminum plates, neoprene gaskets were designed to be sandwiched between the plates and the specimen. The plates were clamped against the specimen by tightening a series of eight bolts that were spaced evenly around the periphery of the plates. A diagram of the NASA MSFC leak detection apparatus can be seen in Figure 4.1.

Leak Detection
Solution

Specimen

Neoprene
Gaskets

Helium Gas
in at Pressure
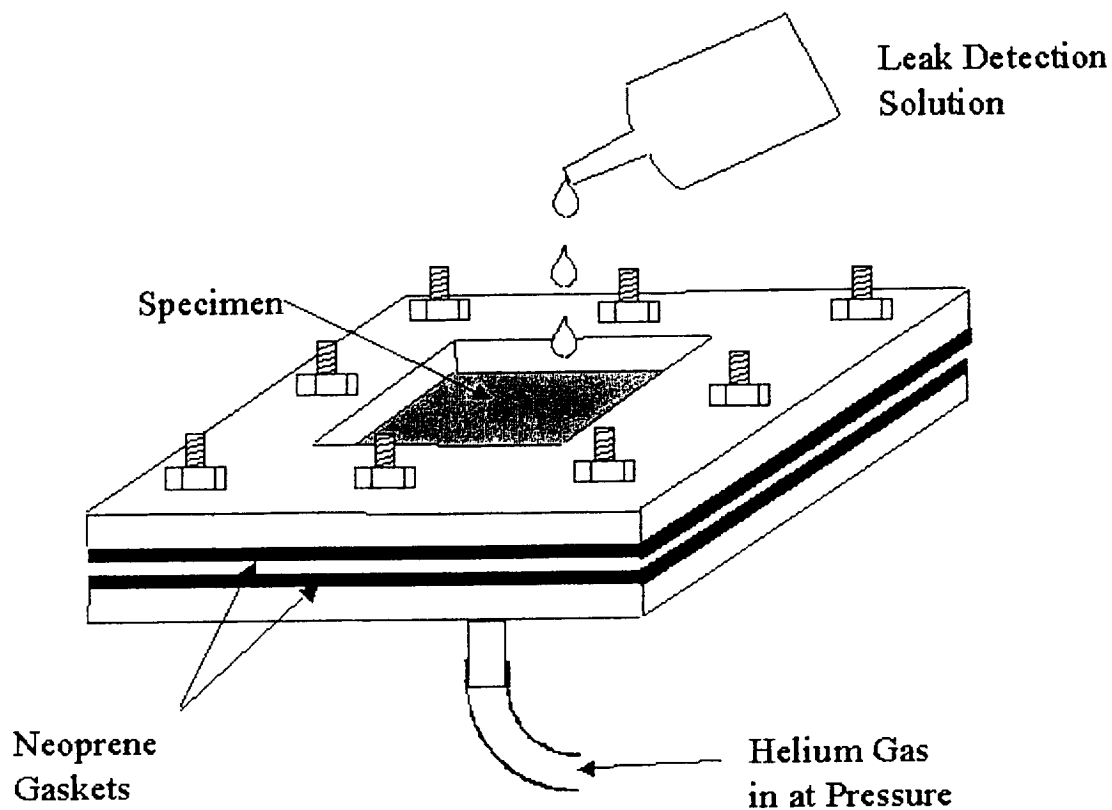
Figure 4.1. NASA MSFC leak detection apparatus. [60]

As shown in the figure, the NASA MSFC apparatus has a square opening in the

top plate and a corresponding square opening in the bottom chamber. Also, it should be

noted that the sides of this apparatus are 5" (12.7 cm) long. The version that was

designed for this research is slightly different. Due to the size of the pneumatic clamp on

the impact test machine used, the specimens that were tested in this research are larger

than those tested at NASA MSFC. Thus, the leak detection apparatus constructed here at

Georgia Tech has sides 6" (15.25 cm) long. Also, it was decided that both a circular

chamber in the bottom plate and a circular hole in the top plate made more sense than the

square holes used by MSFC because the damage caused by impacts would radiate outwards from the impact location (in the center of the test specimens) and because maintaining a proper seal in corners can be difficult. The leak detection apparatus that was constructed for this project was made from a one inch thick piece of 6061 aluminum. Figure 4.2 shows a multi-view of the plates of the leak detection apparatus that was used for this research.
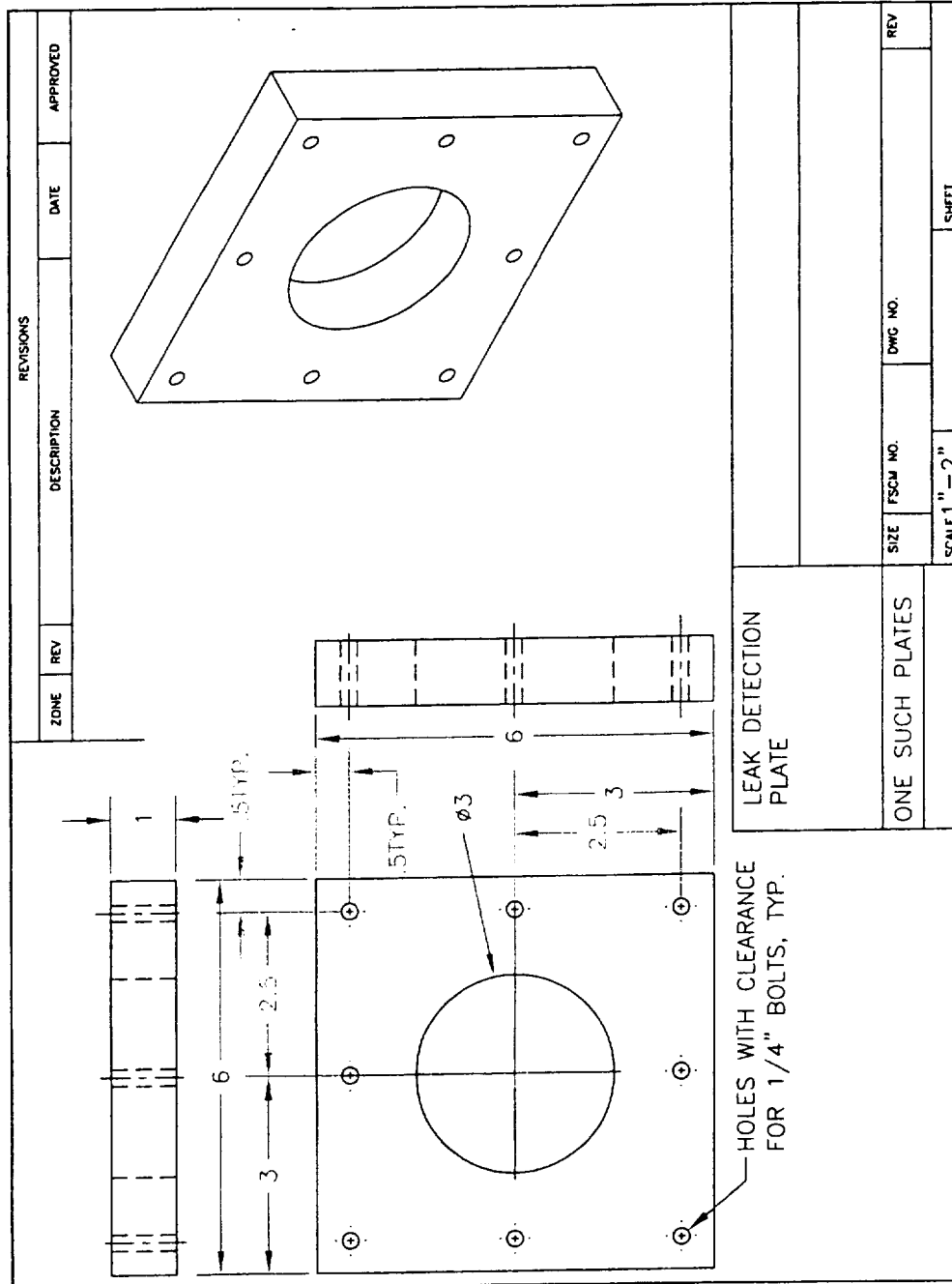
(a)
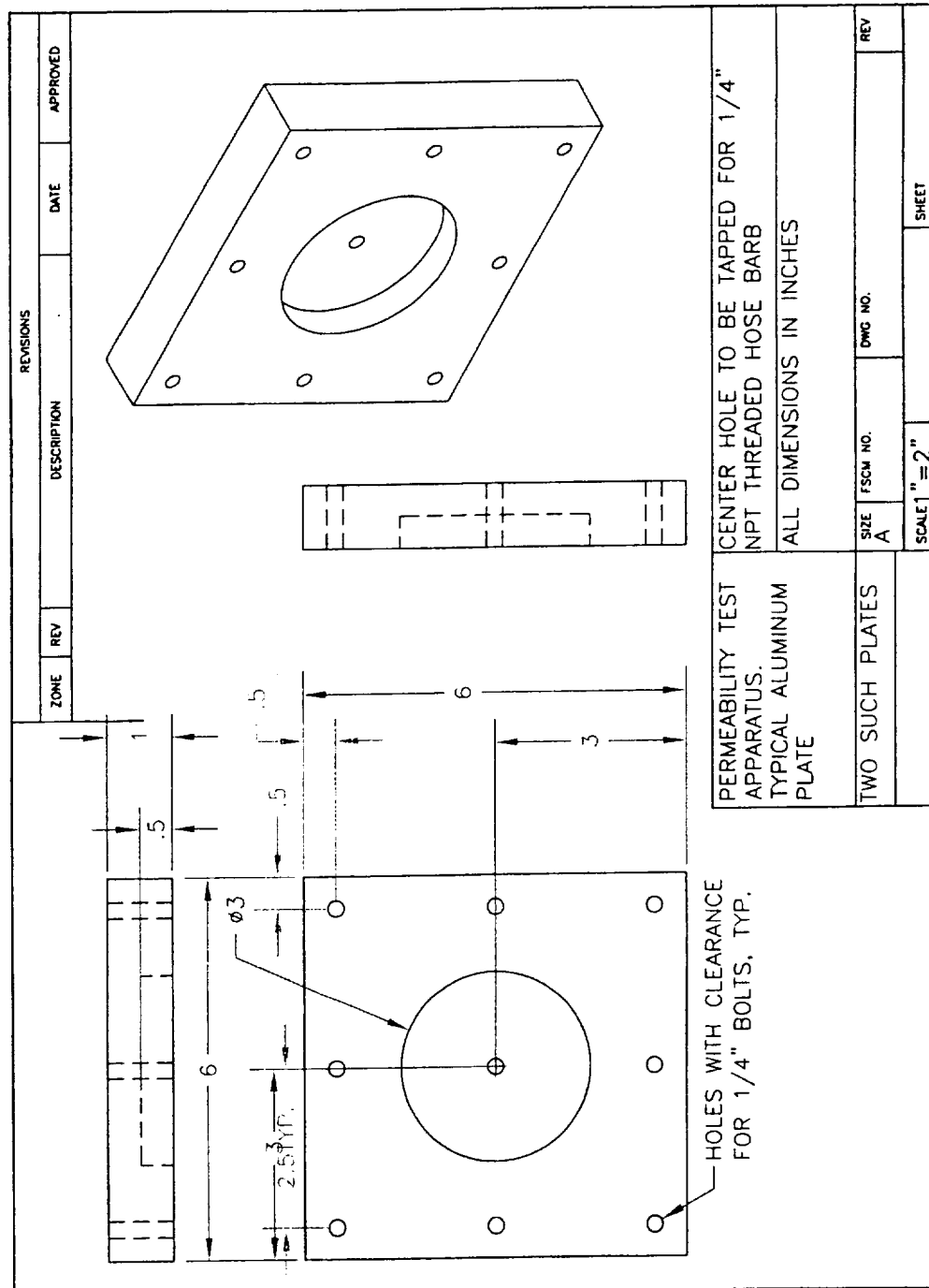
(b)

Figure 4.2. Multi-views of the leak detection apparatus plates: (a) top plate, (b) bottom

plate.

## 4.1.2 Leak Detection Test Procedure

As mentioned earlier every specimen that was received had to be leak tested and the test procedure used is outlined here. The bottom plate of the test apparatus is clamped in a bench vice. To ensure that there are no leaks between the specimens and the gaskets some vacuum grease is applied around the openings on both the top and bottom plate gaskets on the side will contact the specimen. Next the specimen is centered over the hole in both the bottom gasket and the bottom plate. The top plate and gasket are then placed on top of the specimen so that the bolt holes line up with both plates. Then the bolts were tightened as tightly as could be done by hand. A solution of around 3 ounces of water and a drop of liquid dish washing detergent was then mixed and poured into the hole in the top plate (from here on this will be called leak detection solution). Next helium gas was applied to the chamber in the bottom plate, building the pressure up slowly to 30 psi (207 kPa), the expected pressure in the feedlines. The number of leaks was then determined and the pressure at which the last leak appeared in the specimen was recorded. After testing the leak detection solution was drained, the specimen removed from the apparatus, and the excess vacuum grease was wiped away with a paper towel.

## 4.2 Coating Application

### 4.2.1 Specimen Preparation

Because every specimen was leak tested, they all had a residual coat of vacuum grease that had to be removed. This was accomplished by spraying the specimens with acetone and wiping them down. Both sides of the specimens were degreased, even though the coating was only to be applied to the side with flaws (side with the surface flaws in the case of the first batch of specimens received, and the side with more flaws for all other specimens). After degreasing the specimens that were to be coated by NASA GRC were sent off to them so that they could do whatever surface preparations were necessary for their coatings.

The specimens that were coated at Georgia Tech with polyurethane or thermoplastics underwent a couple more steps of surface preparation. Following the degreasing, the side that was to be coated was sanded with a 320-grit paper to roughen the surface and improve the mechanical bonding between the coating and the composite. After sanding the specimens were cleaned with acetone again to remove all of the dust from the sanding.

Prior to coating or being sent to NASA GRC, all of the specimens were marked with the specimen identification number and also two points where thickness measurements were taken. Each specimen was then weighed so that the weight added by the coating could be determined.

## 4.2.2 Procedure for Determining the Thickness of the Coatings

The thickness of the coatings is extremely important for this research, so it was important to devise a method to accurately assess this data. The thickness measurements were taken at two points on each of the specimens so that the average thickness could be determined. All thickness measurements were done using a handheld micrometer according to the relevant ASTM standard.[61] Thickness measurements were taken both prior to and following coating application (being careful not to indent the coating when measuring the coated specimen), so that the thickness of the coating could be found.

## 4.2.3 Procedure for Coatings Applied at Georgia Tech

All of the coatings applied at Georgia Tech were applied in a similar fashion. In all cases paintbrushes were used to apply the coatings. While it is acknowledged that coatings are far more likely to be sprayed onto the actual feedlines and fuel tanks due to their sizes it was not economically feasible, for this research, to purchase a professional quality sprayer and air compressor. Furthermore, from preliminary work done coating some panels with a brush it was determined that a relatively uniform coating could be applied without too much difficulty. In all cases, the coating manufacturers directions for coating application via brush were followed. Finally, before any of the test specimens were coated, several practice specimens would be coated to ensure that the application procedure was mastered.

Centurion Water Based Urethane is a two-part system, that has to be mixed at a ratio of 3 parts component A with 1 part component B (the hardener) and this mixture then has to be reduced with water 10 percent.[50] Despite following this procedure, the coating never mixed properly and it was impossible to achieve a uniform coating or to even avoid having some visible pinholes. Figure 4.3 shows a typical practice specimen. Thus this coating had to be eliminated from consideration.
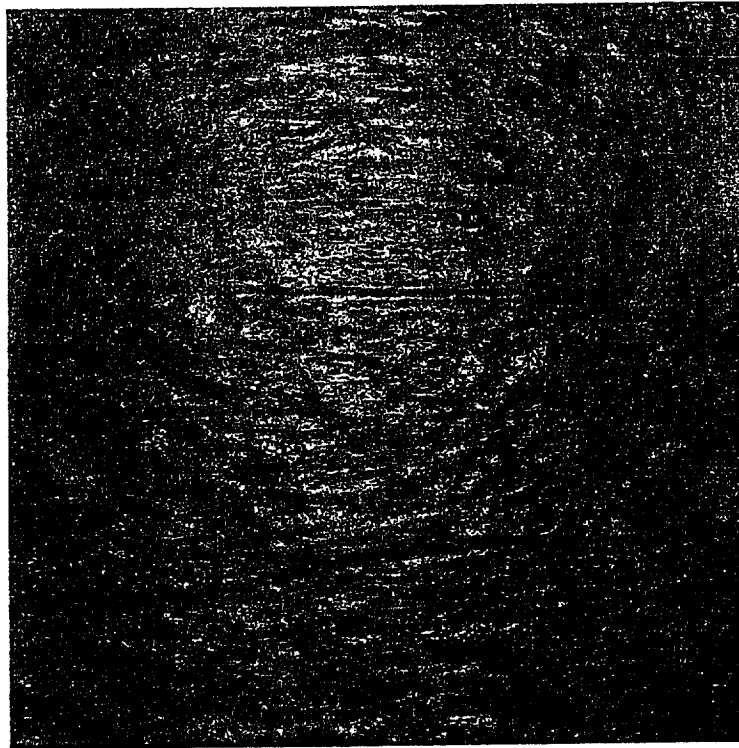


Figure 4.3. Typical specimen coated with Centurion Water Based Urethane.

Corothane I Aliphatic Finish is a single component urethane. When applying this coating to the practice specimens it became clear that a single coat would not provide adequate coverage, as can be seen in Figure 4.4. It is theorized that some of the regions

that appear uncoated after the first application occurred due to the coating being too viscous to fill in locations where small air bubbles (initially trapped in the voids in the composite surface) escaped. Thus it was decided that in accordance with the application instructions the coating would be reduced by the maximum allowable 10% with reducer R7K15 (a Sherwin Williams proprietary solvent).[51] Specimens coated with this mixture had much better coverage after the first coat and a smoother more uniform coating after the second coating. Thus all of the specimens with this coating were coated in this manner. Figure 4.5 shows a typical specimen after two coats of Corothane I Aliphatic Finish.
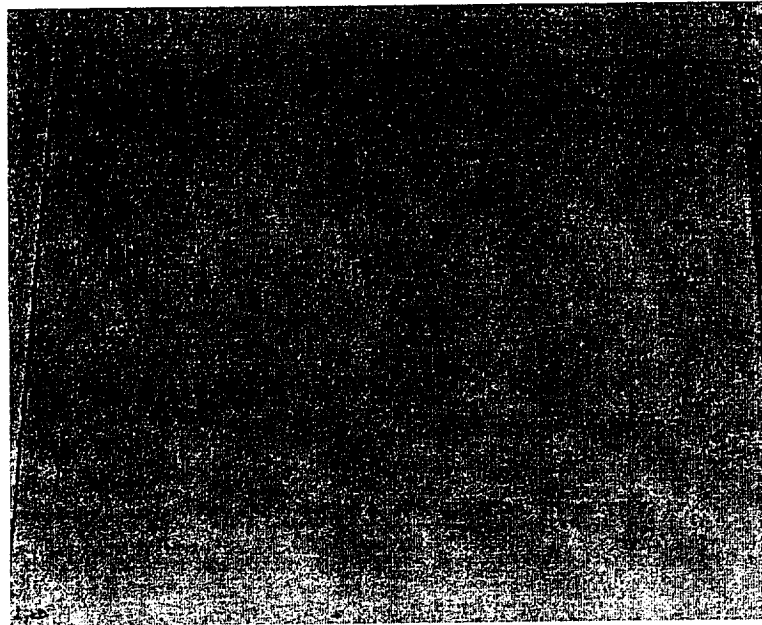


Figure 4.4. A composite specimen after a single coating of Corothane I Aliphatic Finish.
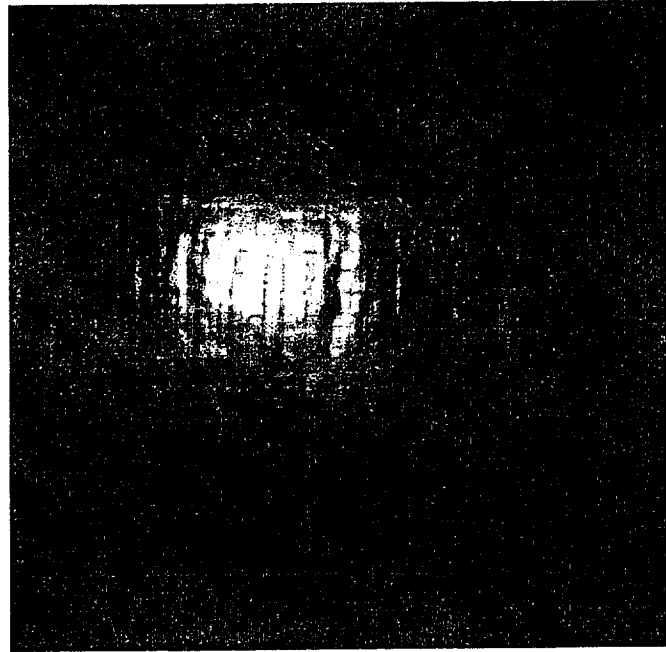
Figure 4.5. A typical specimen after two coats of Corothane I Aliphatic Finish.

Corothane I MIO-Aluminum is similar to the previous coating in that it is also a single component urethane. Achieving a uniform coating thickness was found to be nearly impossible with this particular coating, and after the first application the results were much worse than with the Aliphatic Finish. Again it was determined that a smoother more uniform application was achieved when the coating was reduced by the maximum allowable 10 percent with R7K15.[52] It is also important to note that this coating tended to separate in the can and thus thorough mixing was crucial. After a second coat, the specimens coated with the Corothane I MIO-Aluminum were not as smooth as the Aliphatic Finish, which may be an effect of the micaceous iron oxide and aluminum dispersed in the coating. Figure 4.6 shows a typical specimen after two coats of Corothane I MIO-Aluminum.
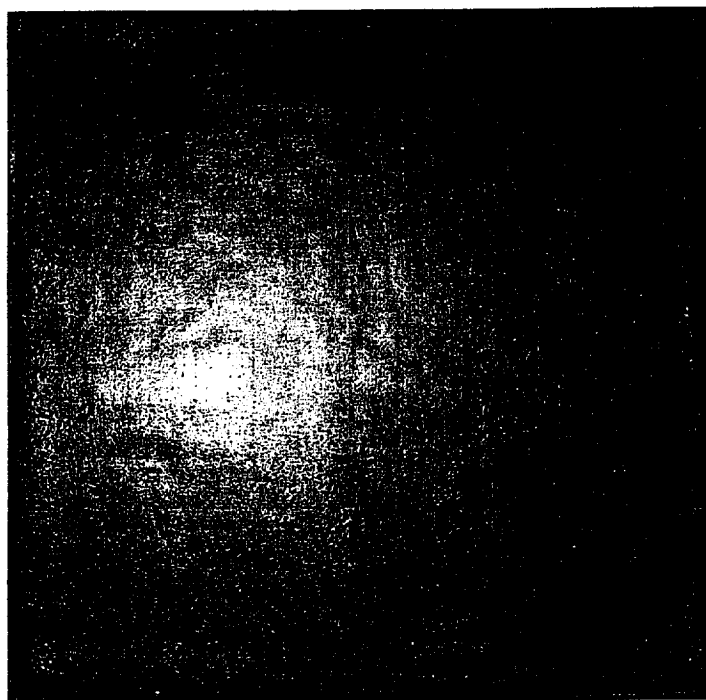
Figure 4.6. A typical specimen coated with two coats of Corothane I MIO-Aluminum.

Poly-Lon 1900 is a two-component polyester based urethane. This particular urethane must be mixed at a ratio of 3 parts component A to 1 part component B (the hardener). Reduction was not recommended,[53] so no reduction was used despite the fact that one coating provided poor coverage as shown in Figure 4.7. It was determined from the practice specimens that two coats provided complete coverage with a coating of fairly uniform thickness. Thus, all of the test specimens coated with Poly-Lon 1900 received two coats of the urethane. Figure 4.8 shows a typical specimen after two coats of Poly-Lon 1900.
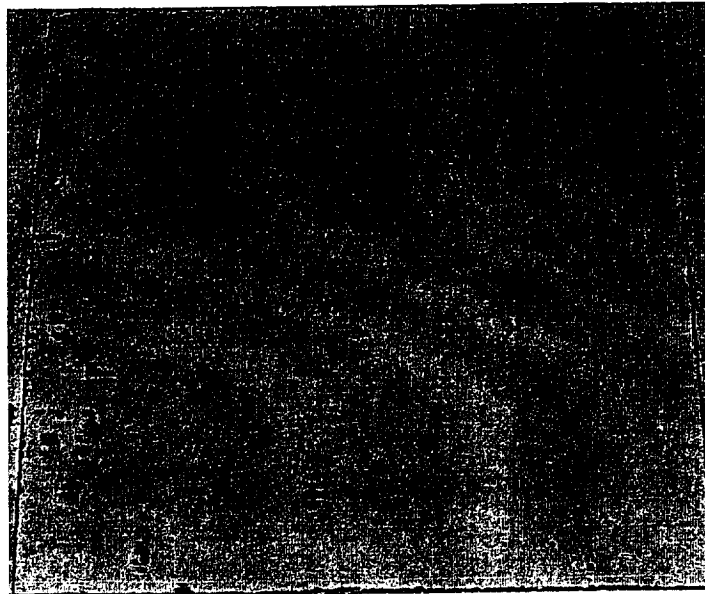
Figure 4.7. Specimen after one coat of Poly-Lon 1900 polyurethane.



Figure 4.8. Typical specimen after two coats of Poly-Lon 1900.

It should be noted that 1 day of curing/set-up time was always provided between subsequent polyurethane coatings. Also, no specimens were tested for at least a week to allow for the full manufacturer's recommended cure period.

Thermaflex IIC is a single component water based thermoplastic coating. This coating was applied via brush in a similar manner to the polyurethane materials. After one coat the Thermaflex provided a very thin coating, and after a second coating uniform coverage could not be achieved. It was found that three thin coatings provided the best possible coverage while minimizing the thickness as much as possible. Figure 4.9 shows a specimen after one coat of Thermaflex IIC.
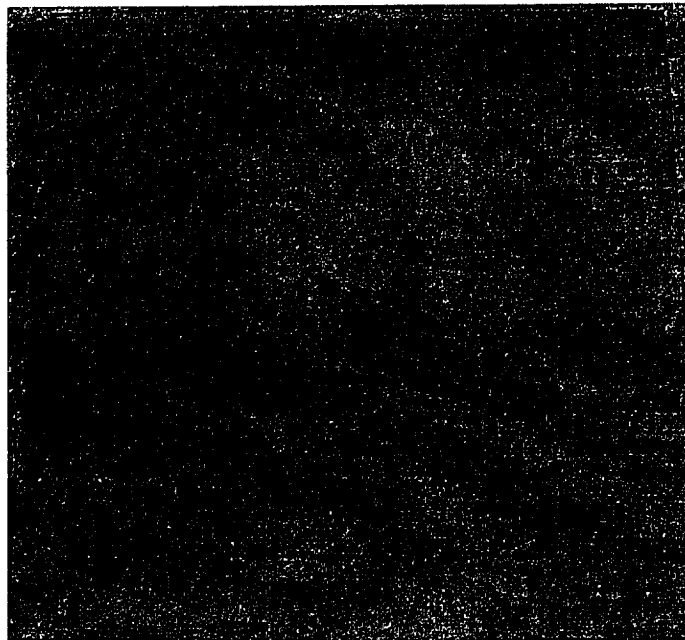


Figure 4.9. A specimen after one coat of Thermaflex IIC.

Because three coats of Thermaflex IIC were required to achieve a uniform coating the average coating thickness was noticeably greater than that of any of the polyurethane coatings. Figure 4.10 shows a specimen after three coats of Thermaflex IIC.
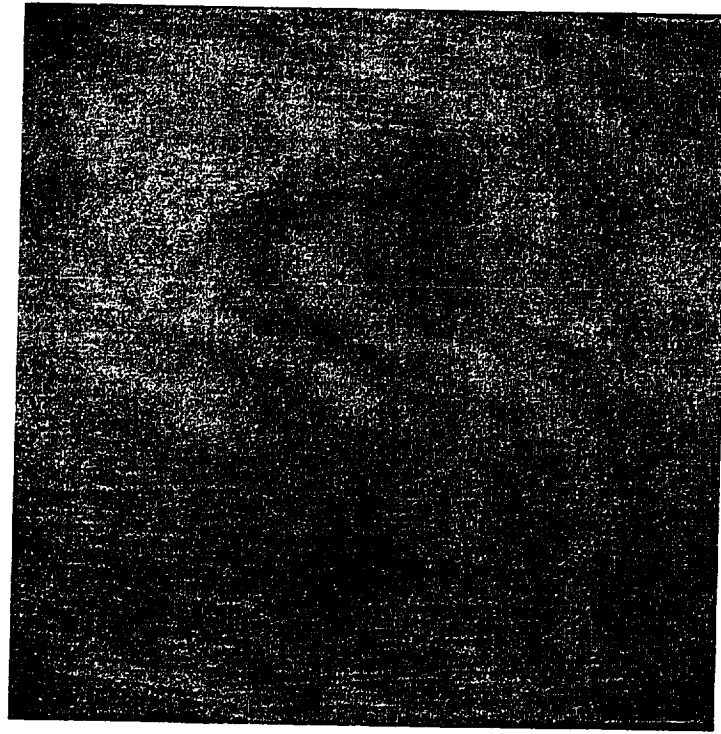


Figure 4.10. A typical specimen coated with three coats of Thermaflex IIC.

Thermashield is also a single component thermoplastic coating, but instead of being water based it is solvent based. As was the case with Thermaflex IIC it was not possible to achieve a uniform smooth coating with only two applications, thus again a third coat was required. After the first application the specimens appeared very similar to the Thermaflex IIC specimen shown in Figure 4.9. The final results are shown in Figure 4.11.
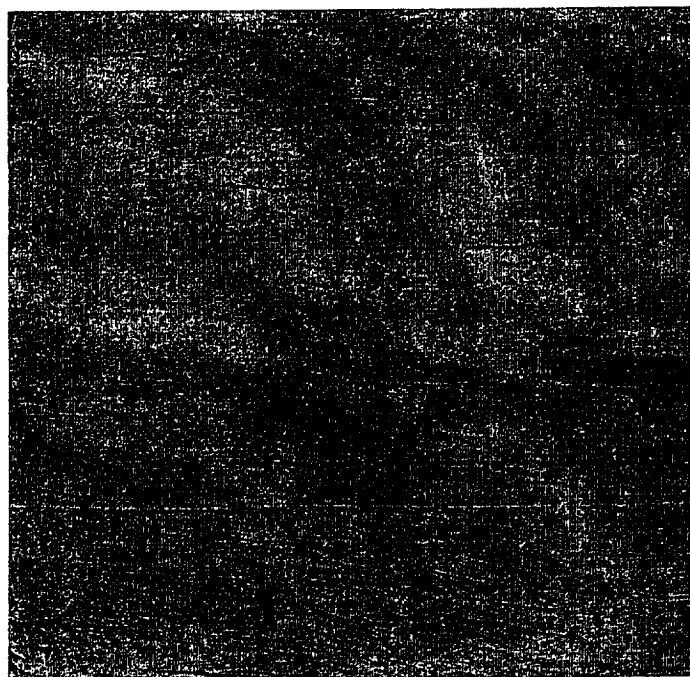
Figure 4.11. A typical specimen after three coats of Thermashield.

## 4.2.4 Procedure for Coatings Applied at NASA GRC

The specimens coated at NASA GRC with the polyimide neat resin and the polyimide nanocomposites were done in the following manner. The coating, be it nanocomposite or neat resin, was brushed onto the specimens after the mixing process outlined in Chapter III was completed. The solvent was then allowed to evaporate overnight. After around 24 hours, all of the coated specimens were B-staged at 400 °F (204 °C) for 1 hour and then at 450 °F (232 °C) for 30 minutes to ensure complete imidization of the polyimide. To remove any air bubbles from the coating, the specimens were then pressed at 465 °F (241 °C). The final neat resin has a $T_g$ of 394 °F (201 °C). Figure 4.12 shows a typical specimen coated in this manner, it is worth noting that only

one specimen is shown because it is very difficult to differentiate between the nanocomposite coated specimens and those coated with the neat resin.
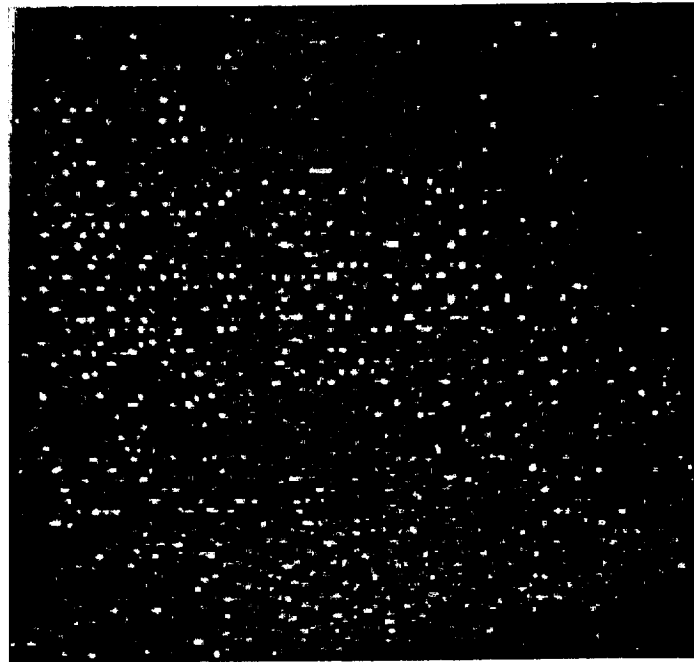


Figure 4.12. A typical polyimide/polyimide nanocomposite coated specimen.

## 4.3 Impact Testing

### 4.3.1 Impact Equipment

All of the impact testing done in this research was done to simulate either an impact caused by a dropped tool or an impact that might occur if the composite feedline were to be bumped into something during installation. A drop weight impact machine was used because as was discussed in Chapter II this is the best method of simulating

these types of impact. The impact machine used was a Dynatup 8250 as is shown in Figure 4.13.
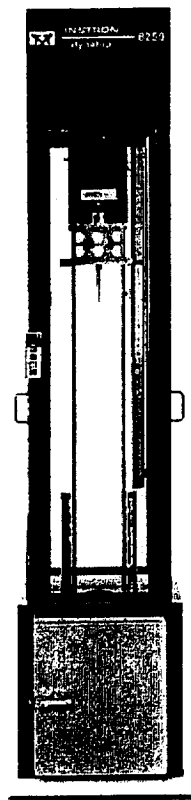


Figure 4.13. Dynatup 8250 drop weight impact test machine.

A half-inch diameter hemispherical tup was used on the 8250 for all impacts because this was found to provide a high level of matrix damage without penetrating the composite at low impact energies. The tup insert on the 8250 is connected to a load cell and computer data acquisition system that allows one to determine the impact energy, energy absorbed by the composite, velocity at impact, maximum impact load, maximum deflection, and much more. The 8250 comes with a pneumatic clamp ideally suited for a

4" by 4" (10 cm by 10 cm) specimen, and this was used for all testing to ensure that the boundary conditions for all the specimens were identical.

### 4.3.2 Impact Procedure

The Dynatup 8250 is designed to have one of its sets of weights attached to the dropping mechanism to provide the mass needed to generate the desired impact energies. For this research the 5.27 lb (23.4 N) weights were used (the lightest available for this test machine), when the weight of the tup and attachments are factored in this brings the total weight of the dropping mechanism to 8.10 lb (36.0 N). A sensor near one of the guide polls for the dropping mechanism was then adjusted so that the impact occurred from the desired height, thus resulting in an impact of the desired energy.

Before impacting any specimens, the computer read out and pneumatic catch breaks were always tested by running a couple of velocity tests. The 8250 determines the velocity of the impactor, using equation (4.1), when a flag attached to the dropping mechanism passes through a laser sensor that is adjusted to such that the flag passes through the sensor just as a specimen is impacted.

$$V = w_{flag}/t_{flag} + g*(t_{imp})$$ (4.1)

In the above equation $w_{flag}$ is the width of the spacing between the leading edge of the velocity flag and the second leading edge (1 cm), $t_{flag}$ is the time taken between the flags leading edge and second leading edge clearing the sensor, and $t_{imp}$ is the time between the second leading edge clearing the sensor and the point just before impact initiation. The

58

Dynatup software determines the energy at impact using equation (4.2), where m is the mass of the crosshead and tup, and V is the velocity of the crosshead and tup.

$$I.E. = \frac{1}{2}*m*V^2 \qquad (4.2)$$

The energy absorbed by the specimen was determined from finding the rebound velocity of the crosshead and tup, $V_r$, in the same manner that the initial velocity was found. The rebound velocity is then fed into equation (4.3).

$$Ea = \frac{1}{2}*m*[V-V_r]^2 \qquad (4.3)$$

The pneumatic rebound breaks are designed to fire when the flag reenters the velocity sensor so that no secondary impacts occur. As long as the velocities calculated by the system are consistent on multiple drops, and the rebound breaks fire each time the system is ready for testing.

With the height sensor adjusted so that the impacts occur from the desired height, a specimen is then centered in the pneumatic clamp over the 3" (7.62 cm) diameter openings that allow for deflections caused by the impacts. Figure 4.14 shows both the pneumatic clamp and the rebound breaks in the 8250.
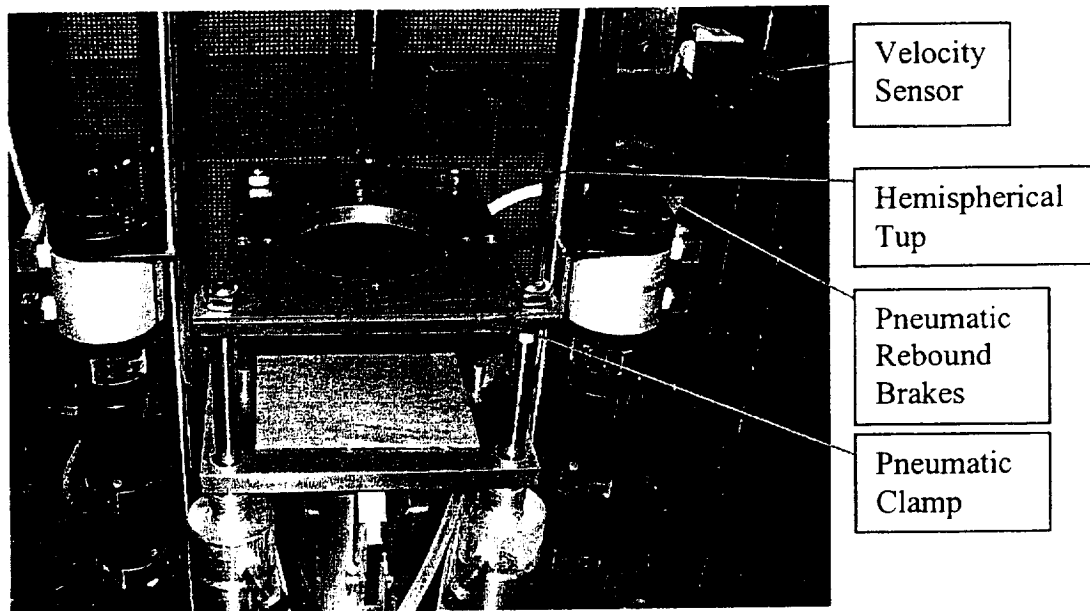
Figure 4.14. Pneumatic clamp and rebound breaks of the Dynatup 8250.

Following the impact the specimen is removed from the clamp and notes are taken regarding any damage evident on both the front and back faces. Then the machine is prepared for the next specimen and the process is repeated.

### 4.4 Permeability Testing

#### 4.4.1 Permeability Test Equipment

The equipment used to measure the permeability, or more accurately the rate of permeation, of the specimens is based off of the equipment outlined in ASTM D1434 and the apparatus that was used at NASA MSFC. This standard provides two different methods for finding the permeability of plastic films and sheeting. The first method involves measuring the increase in pressure in a fixed volume when the only way the

permeant can enter the volume is through the specimen. The other method measures the permeability by measuring the increase in volume caused by the permeating gas.[62] The permeability apparatus used at NASA MSFC was derived from latter approach. In this method all of the gas that permeates through the specimen is trapped and funneled into a tube that contains a slug of alcohol.

The equipment designed for this test incorporates the bottom plate from the leak detection apparatus already shown. The top plate in this case is identical to the bottom plate, but its hose connects to an inclined glass tube that is open to the air on the other side. Figure 4.15 shows a CAD rendering of the apparatus (minus the hose connecting the bottom plate to the helium cylinder).
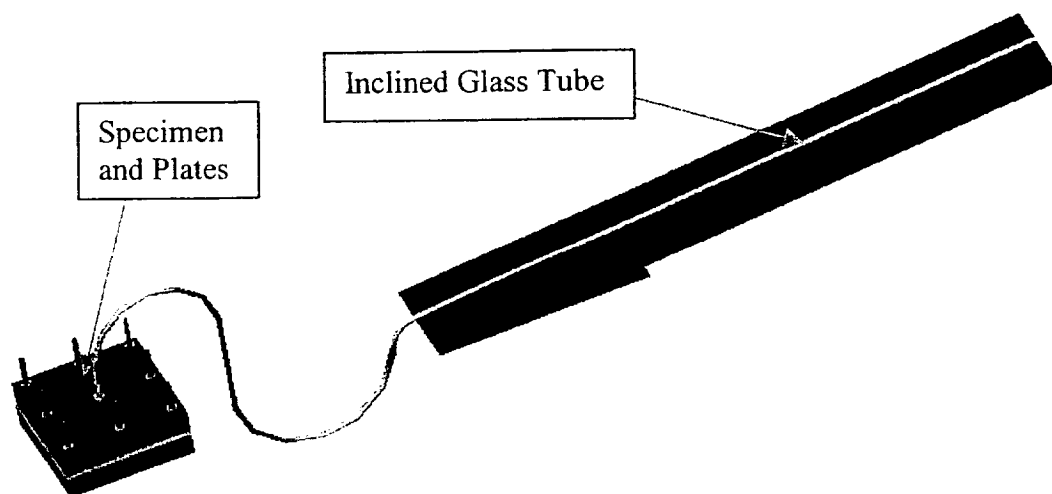


Figure 4.15. CAD rendering of the permeability test apparatus.

## 4.4.2 Permeability Test Procedure

To test a specimen for permeability is similar to the leak testing in that a specimen is placed between to 6" by 6" by 1" (15.25 x 16.25 x 2.54 cm) plates (with gaskets that have been smeared with vacuum grease on the side that bears on the composite). Again the bolts are tightened as much as can be done with a ratchet (around 100 in*lb). Next a slug of isopropyl alcohol is introduced into the system through the glass tube that is attached to the hose connected to the top plate. The glass tube is inclined at five-degrees, this was found to be an optimal angle by NASA MSFC.[60] Next the gas is applied to the specimen. The pressure is slowly increased until the slug moves at a speed such that a reading can be taken. This is an approximate science, too much leakage makes it impossible to get a reading and if the leak is extremely slow the measurement can be very slow. A stopwatch is used to determine the length of the reading, and the distance the slug moves is read off of a ruler that is next to the glass tube. Figure 4.16 shows the inclined glass tube and ruler used for the permeability readings.
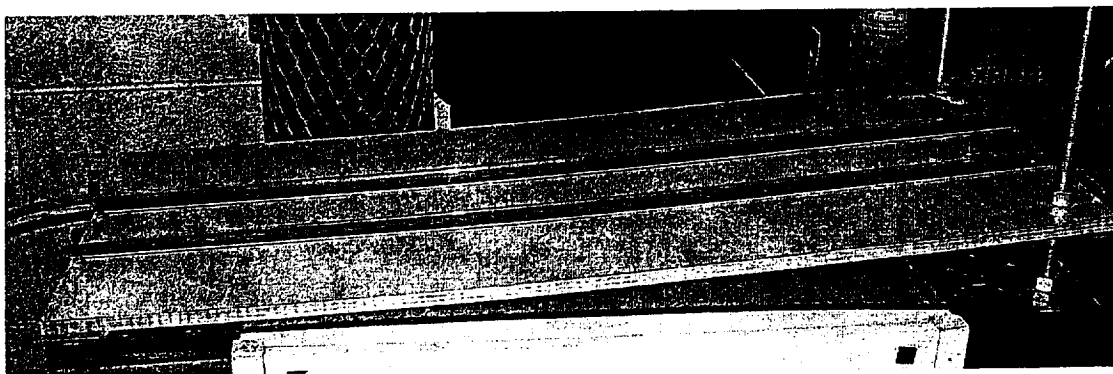


Figure 4.16. The glass tubes used to get volume measurements for the permeability tests.

62

## 4.5 Thermal Cycling of Coated Specimens

One of the problems with composite materials at very low cryogenic temperatures is that the constituent materials have significantly different CTEs. This is also a potential problem for the coating materials. While impacts are not considered likely at cryogenic temperatures, delaminations of the coating from the composite would result in a system failure. As was mentioned in Chapter II, polymeric coatings on composite structures tend to delaminate at cryogenic temperatures,[34] thus it is essential to verify that the coatings considered will not delaminate otherwise they are not suitable for this application.

The thermal cycling performed for this project consisted of taking two specimens from each coating and putting them through 5 thermal cycles. From the background research that was done, it was found that polymers reach their maximum damage densities quickly when thermally cycled so it was believed that 5 cycles would be sufficient to achieve the maximum level of damage that would occur. Also, despite the fact that one must take composites below 60K (-352 °F) in order to start getting microcracking of the matrix, it was found that it was not necessary to go below 77K (-321 °F) to get coatings to delaminate.[34] Thus, liquid nitrogen was used for the cryogenic phase of the cycling.

Each individual thermal cycle consisted of the same routine, 20 minutes immersed in $LN_2$, 20 minutes at room temperature, 20 minutes in the oven at 250 °F (121 °C), then 20 minutes are room temperature again. The specimens were all placed in racks so that

they were kept vertical and separated from each other during the testing. After each thermal cycle notes were taken regarding the state of each specimen.

## 4.6 Aging of Coated Specimens

Many polymeric materials continue to cure and embrittle with time. Thus, two specimens per coating were allowed to age for several months and then were impacted. Specimens were aged by setting them aside following the coating application in atmospheric conditions for several months. After finding the critical impact energy of the specimens with three or more leaks, the aged specimens were impacted at the critical energy (highest energy that does not cause leakage for a given coating). Following impact the specimens were tested for leakage.

# CHAPTER V

# RESULTS AND DISCUSSION

Several distinct types of tests had to be run as a part of this research, thus this section shall be broken down accordingly. The testing performed in this research had to be done in the following order: specimens had to be screened as soon as they were received, next the critical impact energy of the impermeable uncoated specimen had to be found, then the specimens had to be coated and tested for leakage, next the specimens were impacted to find the critical impact energies of the coated specimens, then tested for leakage again and, if necessary, permeability testing was performed. Also, aging and thermal cycling of the coated specimens was performed.

## 5.1 Specimen Screening

Early on in this project it was found that many of the specimens that were received actually had leaks prior to any impact events, thus it became apparent that the specimens needed to be sorted by their initial quality. In order to do this, all of the specimens were visually inspected to eliminate any obviously flawed specimens. Next, all of the specimens had to be leak tested as was outlined in section 4.1.2. While screening the specimens it was noticed that some specimen's had no leaks while others had too many to count. In order to effectively test a coating's ability to seal preexisting leaks, specimens with significant leakage were required. There was no easy way to

decide what defined significant leakage, some specimens had one large leak, while others had many smaller leaks. One large leak did not seem to be sufficient to accurately assess a coatings ability to consistently seal leaks though, so it was decided that specimens with three or more leaks would be used.

The specimens with only 1 or 2 leaks would be used as practice specimens to work out the appropriate methods of coating application and also to help close in on the critical impact energy of the leaking specimens. These practice specimens were invaluable because the total number of specimens with 3 or more leaks was only sufficient to provide 9 specimens per coating, and from these 9 specimens 2 had to be used for thermal cycling and 2 others had to be set aside to test the effects of aging the coatings. The specimens that had no leaks were used to find the critical impact energy of the uncoated impermeable specimens and also the critical impact energies of the coated impermeable specimens. Table 5.1 shows the test matrix that was used for this project; the numbers in the table represent the number of specimens used for each test.

Out of the specimens received 24 percent had no leaks, 36 percent had 1 or 2 leaks, and 30 percent had 3 or more leaks.

Table 5.1. Test matrix.

| Test | None | Corothane I Alipatic Finish | Corothane I MIO-Aluminum | Poly-Lon 1900 | Thermaflex IIC | Thermashield | Neat Polyimide | Polyimide 2% Bentolite | Polyimide 5% Bentolite |
|---|---|---|---|---|---|---|---|---|---|
| Sealing 3+ leaks | 0 | 9 | 9 | 9 | 9 | 9 | 9 | 9 | 9 |
| Finding approximate impact E | 0 | 3 | 3 | 3 | 3 | 3 | 3 | 3 | 3 |
| Finding critical impact energy | 8 | 0 | 0 | 0 | 0 | 0 | 0 | 0 | 0 |
| Coated initially impermeable | 0 | 4 | 4 | 4 | 4 | 4 | 4 | 4 | 4 |

## 5.2 Critical Impact Energy of the Impermeable Uncoated Specimens

In order to quantify the improvement achieved in impact resistance of the composite it was essential to find the critical impact energy for the uncoated initially impermeable specimens. In terms of this research, critical impact energy is defined as being the most impact energy that a specimen can withstand without leaking when tested. To this end, seven specimens were impacted and then tested for leakage. While the test matrix presented above calls for eight specimens to be tested only seven were tested because the lower limit of the machine was reached and at this point the impacted specimen did not leak (the 8250 cannot take readings with less impact energy than 0.79 ft*lbs because the velocity flag starts too close to the velocity sensor for the machine to get an accurate reading). All of the impact testing was done according via the procedure outlined in section 4.3.2 of this thesis. Table 5.2 presents the data for the impacts run on the uncoated initially impermeable specimens.

Table 5.2. Impact and leak test results for uncoated initially impermeable specimens.

| Specimen | Impact Energy, J (ft*lb) | Maximum Load, N (lb) | Maximum Deflection, cm (in) | Leakage |
|---|---|---|---|---|
| G-5 | 2.07 (1.53) | 1001 (225.14) | 0.38 (0.15) | At 68.9 kPa (10 psi) |
| H-4 | 2.55 (1.88) | 1164 (261.58) | 0.41 (0.16) | At 34.4 kPa (5 psi) |
| H-3 | 1.59 (1.17) | 882 (198.29) | 0.36 (0.14) | At 68.9 kPa (10 psi) |
| H-1 | 1.14 (0.84) | 725 (163.01) | 0.30 (0.12) | At 68.9 kPa (10 psi) |
| I-10 | 1.07 (0.79) | 699 (157.13) | 0.30 (0.12) | None |
| X-3 | 1.11 (0.82) | 664 (149.19) | 0.36 (0.14) | At 103.4 kPa (15 psi) |
| X-11 | 1.23 (0.91) | 729 (163.84) | 0.36 (0.14) | At 68.9 kPa (10 psi) |

The critical impact energy could not be clearly determined because of the lower

limit of the Dynatup 8250, but it can be seen that it is right around 0.80 ft*lb (1.08 J)

from the results shown above. Furthermore, specimens X-11, X-3, and H-1 all had only

pinhole leaks after they were impacted which suggests that the impact energies for these

tests were very close to the critical value.

## 5.3 Leak Detection Results

Early in the project while trying to find the critical impact energy of the uncoated

specimens, it was noticed that leakage was occurring from many locations away from the

impact cite. It quickly became clear that many of the specimens received had leaks prior

to impact and that the specimens would all have to be leak tested and sorted before any

coatings could be applied.

### 5.3.1 Specimens Coated to Seal Preexisting Leaks

*5.3.1.1 Results*

All of the specimens that were coated had to be leak tested prior to any impact

testing. All leak testing was done according to the procedure outlined in section 4.1.2 of

this thesis. Table 5.3 shows the results of this leak testing.

Table 5.3. Results of leak testing on coated previously leaking specimens.

| Coating | Total Specimens | Specimens with Leaks |
|---|---|---|
| Corothane I Aliphatic Finish | 12 | 0 |
| Corothane I MIO-Aluminum | 13 | 5 |
| Poly-Lon 1900 | 12 | 0 |
| Thermaflex IIC | 12 | 0 |
| Thermashield | 12 | 12 |
| GRC Neat Polyimide | 12 | 11 |
| GRC 2% Nanocomposite | 9 | 7 |
| GRC 5% Nanocomposite | 12 | 7 |

*5.3.1.1 Discussion*

From Table 5.3, it can be seen that none of the Corothane I Aliphatic Finish specimens leaked after the coating was applied. The same is true of the Poly-Lon 1900 and the Thermaflex IIC coated specimens.

Unlike the Poly-Lon 1900 and Corothane I Aliphatic Finish specimens, the Thermashield coated specimens were found to be quite permeable when tested. Furthermore, instead of having a few leaks around the composite surface, many leaks appeared through the coating, meaning that the coating was itself quite permeable. Due to these results, Thermashield had to be eliminated from further testing.

Some of the specimens coated with the Corothane I MIO-Aluminum were also found to leak prior to any impact. Out of the initial batch of twelve specimens coated 3 leaked. This seems like an alarming number of specimens on which the coating failed, but while testing one of the specimens it was noticed that there was a flaw in the coating that led to crack forming right around the edge of the leak detection apparatus top plate.

This flaw appeared to be the result of a poor degreasing of the specimen prior to the coating application. Thus the bond between the coating and the specimen was weak and a small delamination formed, which quickly cracked because of the flaw's proximity to the edge of the hole in the top plate of the leak detection apparatus. Since all of these specimens were degreased in the same manner one had to consider human error as a probable cause for many, if not all, of the specimens that leaked. As a result, a few extra specimens were prepared (all with 1 or 2 leaks). Even with the extra specimens, after setting aside two specimens for thermal cycling and two for aging, only four specimens were left to find the critical impact energy. Figure 5.1 shows the specimen with the flaw in the coating where the leak occurred.

Of the 12 specimens that were coated with the GRC polyimide neat resin, all but one had some leakage, ranging from 1 leak to too many to count. The 9 specimens coated with the 2% nanocomposite had similar leak detection results. In this case all but two leaked. Out of the 12 specimens coated with 5% nanocomposite, 5 did not leak.

Several reasons exist for the poor leak sealing capability shown by these materials. First, there were voids evident in some of the coated specimens (entrapped air). Secondly, some of the coatings appeared to be coated a little unevenly, and all of the coatings were very thin (around 0.002 inches, 0.051 mm). Finally, in order to consolidate the polyimide



Figure 5.1. Flaws in Corothane I MIO-Aluminum specimen that lead to leakage.

Cracks in coating where leakage occurred
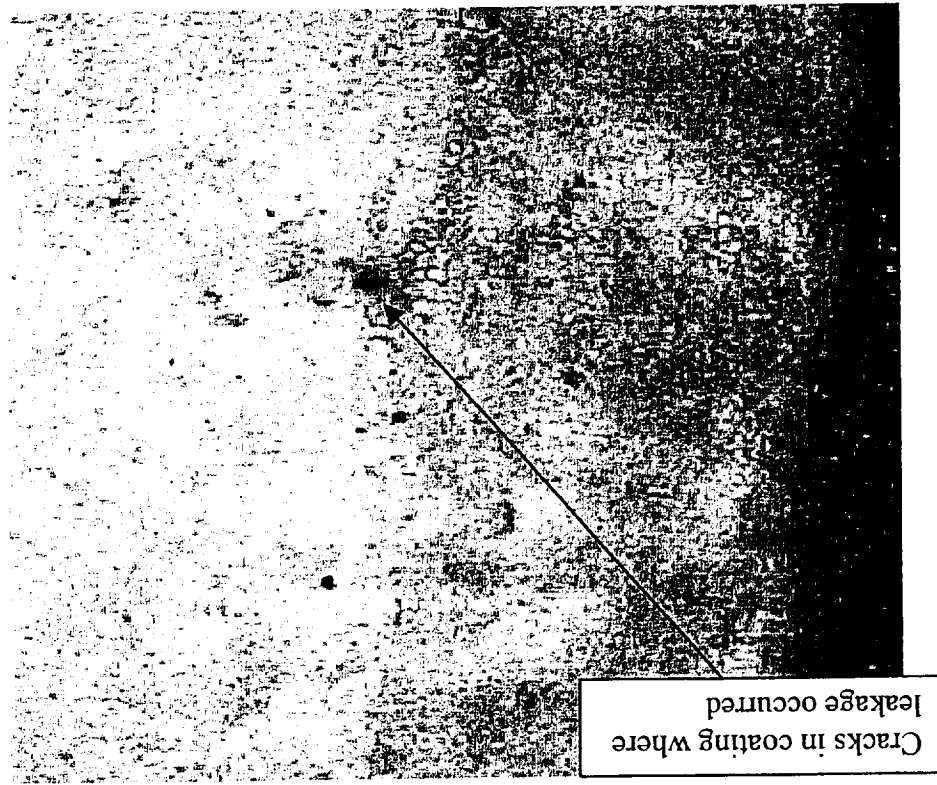
resin the specimens had to be heated to 465 °F (241 °C) and pressed. This temperature is much higher than the $T_g$ of the EX 1552 matrix, 390 °F (200 °C), and thus the properties of the matrix were altered. Normally, the polyimide material that was applied to the specimens would be consolidated at 575 °F (302 °C), but when this was tried with the composite specimens they deteriorated, which is why there are only 9 specimens coated with 2% nanocomposite. From a visual inspection of the specimens received, it appeared that in some cases the matrix material actually had begun to char. It is believed that the matrix had deteriorated enough for new leak paths to develop in the specimens.

## 5.3.2 Initially Impermeable Specimens

### 5.3.2.1 Results

Leak testing the initially impermeable coated specimens also had to be done in order to eliminate the chance that the coating process might cause leakage. The results of these tests are presented in Table 5.4.

Table 5.4. Results of leak testing on the coated initially impermeable specimens.

| Coating | Total Specimens | Specimens with Leaks |
|---|---|---|
| Corothane I Aliphatic Finish | 4 | 0 |
| Corothane I MIO-Aluminum | 4 | 0 |
| Poly-Lon 1900 | 4 | 0 |
| Thermaflex IIC | 4 | 0 |
| GRC Neat Polyimide | 4 | 1 |
| GRC 2% Nanocomposite | 4 | 2 |
| GRC 5% Nanocomposite | 4 | 0 |

*5.3.2.2 Discussion*

From Table 5.4, it can be seen that none of the specimens coated with the Corothane I Aliphatic Finish, Corothane I MIO-Al, Poly-Lon 1900, or Thermaflex IIC leaked. The results for the specimens coated at NASA GRC were again different though.

Out of the sets of four initially impermeable specimens coated with each material, one coated with the neat resin leaked, two with the 2% nanocomposite leaked, and none leaked with the 5% nanocomposite. It is not surprising that the 5% nanocomposite consistently had the fewest leaks (it has the most tortuous leakage path for a gaseous permeant), but the 2% nanocomposite having more leaking specimens than the neat resin is confusing. The neat resin and 2% nanocomposite both have a similar appearance, but upon closer inspection there appear to be more flaws in the 2% nanocomposite, which may account for the greater leakage. The reasons that leaks developed in specimens that were impermeable at the time of coating are the same 3 reasons discussed in the previous section of this document.

## 5.4 Impact Test Results (Critical Impact Energies)

The research discussed within this document strives to show two things: that coatings can improve the impact resistance and impermeability of a composite, and that composites that have sealed leaks perform as well as coated initially impermeable composites. To this end, the critical impact energies have been found for specimens both with sealed leaks and without for a variety of different coatings.

### 5.4.1 Impact of the Coated Specimens with Preexisting Leaks

*5.4.1.1 Results*

The coated previously leaking specimens were impacted at various energies and then leak tested to find the critical impact energies. Tables 5.5 through 5.9 show the results of the impact and leak testing of the individual specimens broken down by the coating. The maximum load during impact is reported in the tables as well as the impact energy so that this work can be compared to the work of some other authors who report in terms of load rather than impact energy. That said, in this thesis impacts will be described in terms of the energy. Table 5.10 shows the critical impact energies for each individual coating. There is no data for the GRC neat polyimide resin or 2% nanocomposite coated specimens because there were not enough impermeable specimens of these types to test.

Table 5.5. Impact results for the Corothane I Aliphatic Finish coated specimens (3 or more leaks prior to coating).

| Specimen | Impact Energy, J (ft*lb) | Absorbed Energy, J (ft*lb) | Maximum Load, N (lb) | Maximum Deflection, cm (in) | Leakage |
|---|---|---|---|---|---|
| C-1 | 6.11 (4.51) | 2.85 (2.10) | 1816 (408.17) | 0.56 (0.22) | @ 34.4 kPa (5 psi) |
| D-6 | 4.72 (3.48) | 1.60 (1.18) | 1667 (374.84) | 0.51 (0.20) | @ 34.4 kPa (5 psi) |
| X-59 | 5.71 (4.21) | 2.16 (1.59) | 1884 (423.45) | 0.56 (0.22) | None |
| X-19 | 5.90 (4.35) | 2.07 (1.53) | 1940 (436.02) | 0.61 (0.24) | None |
| X-6 | 6.21 (4.58) | 3.55 (2.62) | 1925 (432.82) | 0.56 (0.22) | @ 0 kPa (0 psi) |

Table 5.6. Impact results for Corothane I MIO-Aluminum coated specimens (3 or more

leaks prior to coating).

| Specimen | Impact Energy, J (ft*lb) | Absorbed Energy, J (ft*lb) | Maximum Load, N (lb) | Maximum Deflection, cm (in) | Leakage |
|---|---|---|---|---|---|
| X-21 | 5.26 (3.88) | 1.87 (1.38) | 1838 (413.20) | 0.56 (0.22) | @ 34.4 kPa (5 psi) |
| X-67 | 4.79 (3.53) | 1.46 (1.08) | 1763 (396.38) | 0.56 (0.22) | @ 34.4 kPa (5 psi) |
| X-9 | 4.27 (3.15) | 1.08 (0.80) | 1691 (380.12) | 0.53 (0.21) | None |
| W-34 | 4.31 (3.18) | 1.13 (0.83) | 1661 (373.70) | 0.56 (0.22) | None |

Table 5.7. Impact results for Poly-Lon 1900 coated specimens (3 or more leaks prior to

coating).

| Specimen | Impact Energy, J (ft*lb) | Absorbed Energy, J (ft*lb) | Maximum Load, N (lb) | Maximum Deflection, cm (in) | Leakage |
|---|---|---|---|---|---|
| G-1 | 6.09 (4.49) | 1.80 (1.33) | 2046 (459.96) | 0.56 (0.22) | None [a] |
| G-6 | 6.10 (4.50) | 2.89 (2.13) | 1829 (411.27) | 0.53 (0.21) | @ 34.4 kPa (5 psi) |
| X-66 | 5.74 (4.23) | 2.89 (2.13) | 1824 (410.13) | 0.53 (0.21) | @ 34.4 kPa (5 psi) |
| X-64 | 5.25 (3.87) | 1.69 (1.25) | 1858 (417.65) | 0.58 (0.23) | None |
| X-34 | 5.68 (4.19) | 2.26 (1.67) | 1937 (435.39) | 0.58 (0.23) | None |

[a] A delamination formed at 30 psi

Table 5.8. Impact results for Thermaflex IIC coated specimens (3 or more leaks prior to

coating).

| Specimen | Impact Energy, J (ft*lb) | Absorbed Energy, J (ft*lb) | Maximum Load, N (lb) | Maximum Deflection, cm (in) | Leakage |
|---|---|---|---|---|---|
| F-5 | 3.86 (2.85) | 1.06 (0.78) | 1502 (337.69) | 0.48 (0.19) | @ 206.9 kPa (30 psi) |
| F-8 | 3.36 (2.48) | 0.87 (0.64) | 1388 (312.14) | 0.46 (0.18) | @ 206.9 kPa (30 psi) |
| X-63 | 2.93 (2.16) | 0.72 (0.53) | 1287 (289.24) | 0.46 (0.18) | None |
| X-14 | 3.12 (2.30) | 0.75 (0.55) | 1353 (304.10) | 0.48 (0.19) | None |
| X-5 | 3.42 (2.52) | 0.89 (0.66) | 1719 (318.36) | 0.51 (0.20) | None |

Table 5.9. Impact results for 5% nanocomposite coated specimens (3 or more leaks prior to coating).

| Specimen | Impact Energy, J (ft*lb) | Absorbed Energy, J (ft*lb) | Maximum Load, N (lb) | Maximum Deflection, cm (in) | Leakage |
|---|---|---|---|---|---|
| W-50 | 1.71 (1.26) | 0.24 (0.18) | 892 (200.42) | 0.41 (0.16) | @ 0 kPa (0 psi) |
| W-32 | 1.44 (1.06) | 0.28 (0.21) | 796 (179.02) | 0.38 (0.15) | @ 0 kPa (0 psi) |
| W-47 | 1.19 (0.88) | 0.22 (0.16) | 704 (158.22) | 0.36 (0.14) | @ 0 kPa (0 psi) |
| W-51 | 1.11 (0.82) | Error | 688 (154.75) | 0.36 (0.14) | @ 34.4 kPa (5 psi) |

Table 5.10. Critical impact energies of specimens with three or more leaks prior to coating.

| Coating | Critical Impact Energy, J (ft*lb) | Multiple of uncoated specimens |
|---|---|---|
| None | 1.07 (0.79) | NA |
| Corothane I Aliphatic Finish | 5.90 (4.35) | 5.51 |
| Corothane MiO-Al | 4.31 (3.18) | 4.03 |
| Polylon 1900 | 5.25 (3.87) | 4.90 |
| Thermaflex IIC | 3.12 (2.30) | 2.91 |
| GRC 5% Nanocomposite | <1.07 (<0.79) | <1.00 |

*5.4.1.2 Discussion*

The practice specimens that have been mentioned previously, coated specimens that had only one or two leaks, were impacted repeatedly to try to zero in on the critical impact energy for a given coating. These specimens were impacted and then leak tested, if the specimens had no leaks they were impacted again. This process provided a conservative method of closing in on the critical impact energy without wasting any of

the specimens that initially had three or more leaks. This process is conservative because damage that occurs from impact is cumulative, so any specimen impacted multiple times will actually have more damage for a given impact energy than a specimen that is only impacted once at that energy. That is to say that a specimen that is impacted three times with at 3, then 3.5, then 4 ft*lb may leak while a specimen that is impacted for the first and only time at 4 ft*lb does not leak.

After finding the approximate range for the critical impact energy for a given coating, test specimens are impacted (only once per specimen) and leak tested. Specimens were impacted at an energy and then immediately leak tested so that the energy could be adjusted as needed to close in on the critical energy. Generally, the drop height of the tester was adjusted by a half inch to increase or decrease the impact energy unless the energy was very low, in which case quarter inch adjustments were usually made to the drop height.

In all cases when finding the critical impact energies efforts were made to verify the highest impact energy at which a specimen, with a given coating, would not leak through repetition. Unfortunately, with only four or five specimens to work with this was not always possible.

As one can see in Table 5.10 all of the coatings except for the 5% nanocomposite improved the impact resistance of the uncoated composite. Although, the 5% nanocomposite specimens tested were found to be impermeable prior to impact they still had been heated to well above the $T_g$ of the epoxy matrix and thus the matrix material had degraded. It is believed that this is part of the reason why all of the 5%

78

nanocomposite specimens that were impacted leaked even at energies below the critical impact energy of the uncoated composite. Furthermore, had uncoated specimens been heated in the same fashion as the 5% nanocomposite specimens they would have a lower critical impact energy than 0.79 ft*lb (1.07 J). Another contributing factor to why all of the 5% nanocomposite specimens leaked is that the coating was extremely thin, as can be seen in Table 5.11.

Table 5.11. Thickness and additional weight for coatings of specimens with 3+ leaks.

| Coating | Coating Weight, N/m$^2$ (lb/ft$^2$) | Average Coating Thickness, cm (in) | Additional Weight (%) |
|---|---|---|---|
| Corothane I Aliphatic Finish | 3.45 (0.072) | 0.023 (0.009) | 1.20 |
| Corothane MiO-Al | 2.58 (0.054) | 0.015 (0.006) | 0.84 |
| Polylon 1900 | 3.78 (0.079) | 0.025 (0.010) | 1.34 |
| Thermaflex IIC | 6.70 (0.140) | 0.051 (0.020) | 2.82 |
| GRC Neat Polyimide | 0.38 (0.008) | 0.005 (0.002) | 0.24 |
| GRC 2% Nanocomposite | 0.48 (0.010) | 0.005 (0.002) | 0.26 |
| GRC 5% Nanocomposite | 0.53 (0.011) | 0.003 (0.001) | 0.14 |

As you can see, the coatings provided by NASA GRC are at most a third as thick as the next thinnest coating. This is significant because greater thickness helps to resist impact damage and also makes the coating more impermeable to gaseous permeants.

The Dynatup 8250 determines the energy absorbed during the impact tests. These values represent the energy that was absorbed by the specimens through the creation of damage and also the energy dissipated by the test machine itself. Generally, the relative amount of energy absorbed by specimens with the same coating corresponds to the level of visible damage present. There were a couple of exceptions to this though, the most

obvious was that specimen D-6 appeared to have more damage than both X-59 and X-19 (all coated with Corothane I Aliphatic Finish) although D-6 was impacted with much less energy, and therefore absorbed less energy. This should emphasize the tremendous variability present in the composite substrate.

One of the interesting discoveries made in this research was that the amount of visible damage in the coated composite specimens was less than in uncoated specimens impacted with the same energies. While some improvement should be expected, because the moment of inertia of the specimens was increased due to the greater thickness, the amount of improvement was surprising. Figures 5.2 through 5.10 show both coated specimens impacted with the critical impact energy (for that particular coating) and also, for the sake of comparison, uncoated specimens impacted at the same energies as the coated specimens (except that there is no comparison specimen for the 5% nanocomposite specimen since an uncoated specimen would show no damage).

(a)



Indentation from impact
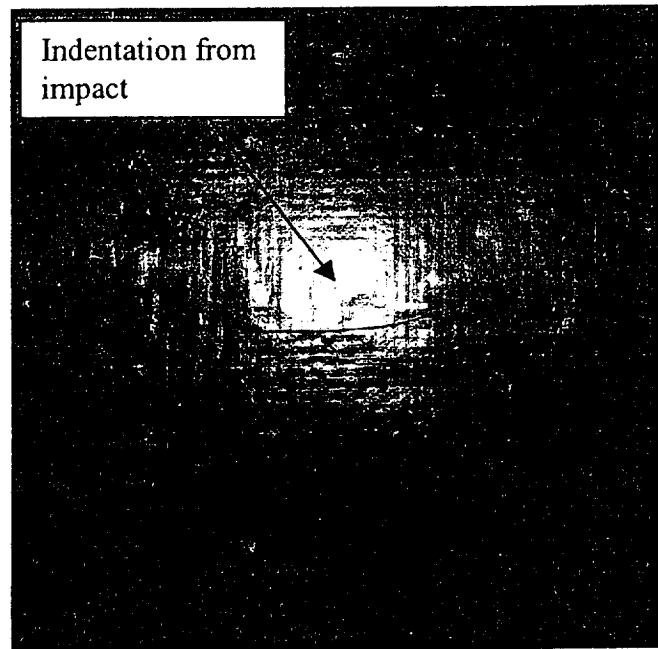
(b)
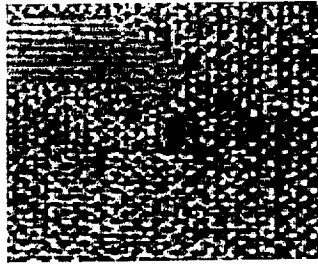
(c)

Figure 5.2. Corothane I Aliphatic Finish specimen impacted at 4.35 ft*lb (5.90 J), (a)

back of specimen, (b) front of specimen, (c) close-up of damage on back.



(a)

Indentation from impact
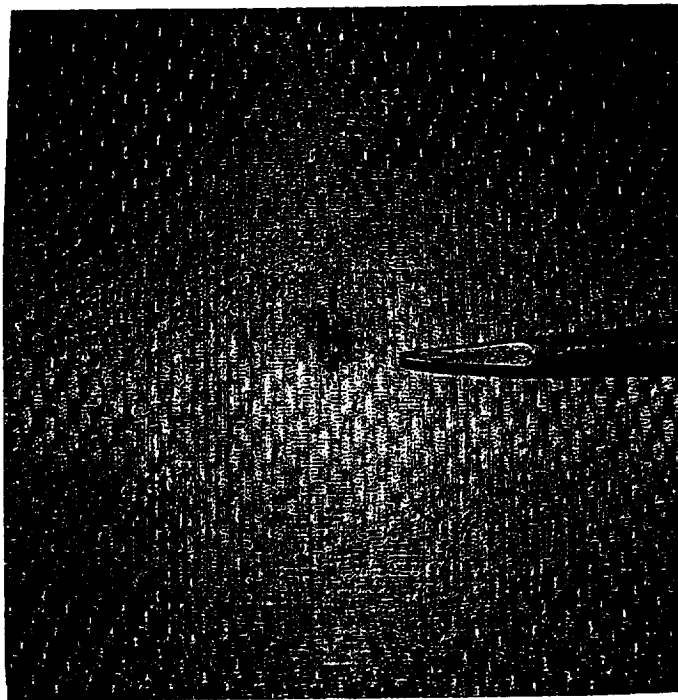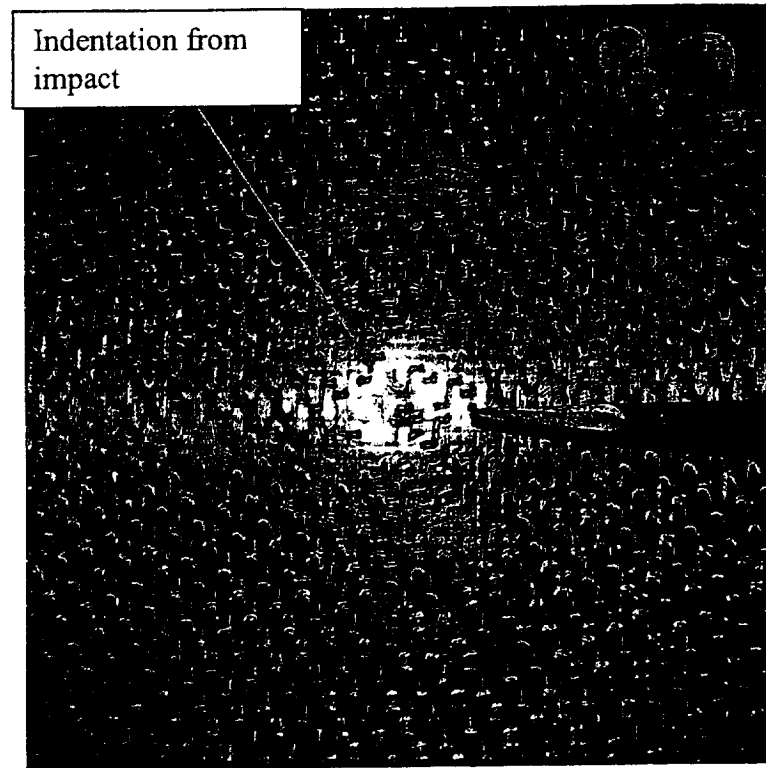
(b)



(c)

Figure 5.3. Uncoated specimen impacted at 4.35 ft*lb (5.90 J), (a) back of specimen, (b) front of specimen, (c) close-up of damage on backside.
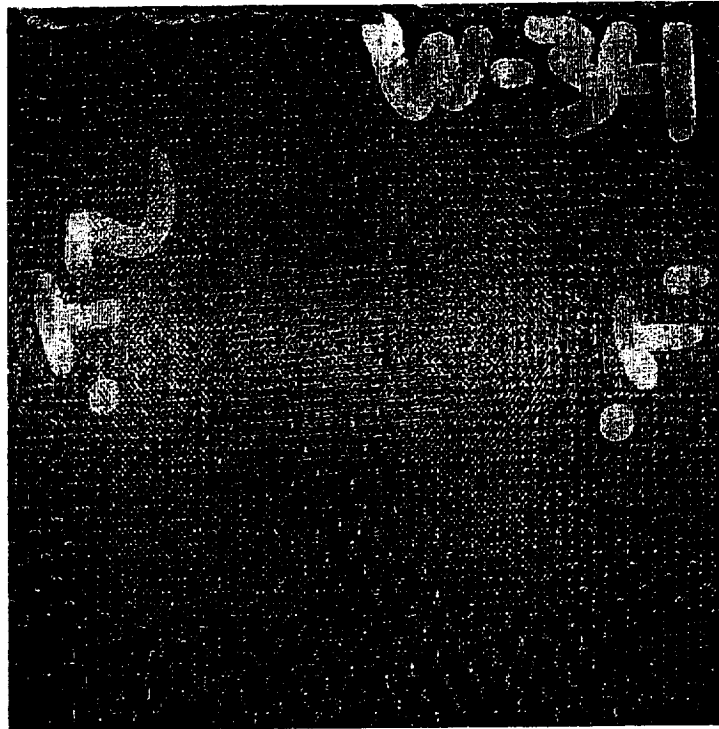
(a)
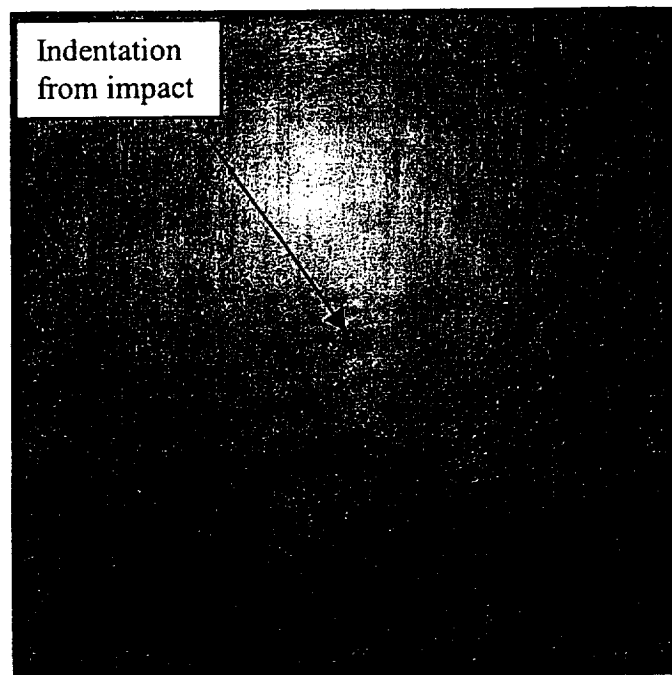


(b)
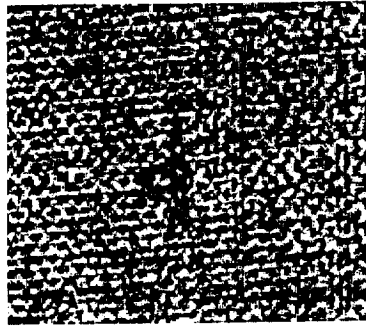
(c)

Figure 5.4. Corothane I MIO-Aluminum coated specimen after 3.18 ft*lb (4.31 J) impact, (a) back of specimen, (b) front of specimen, (c) close up of matrix crack on back.



(a)

Indentation
from impact
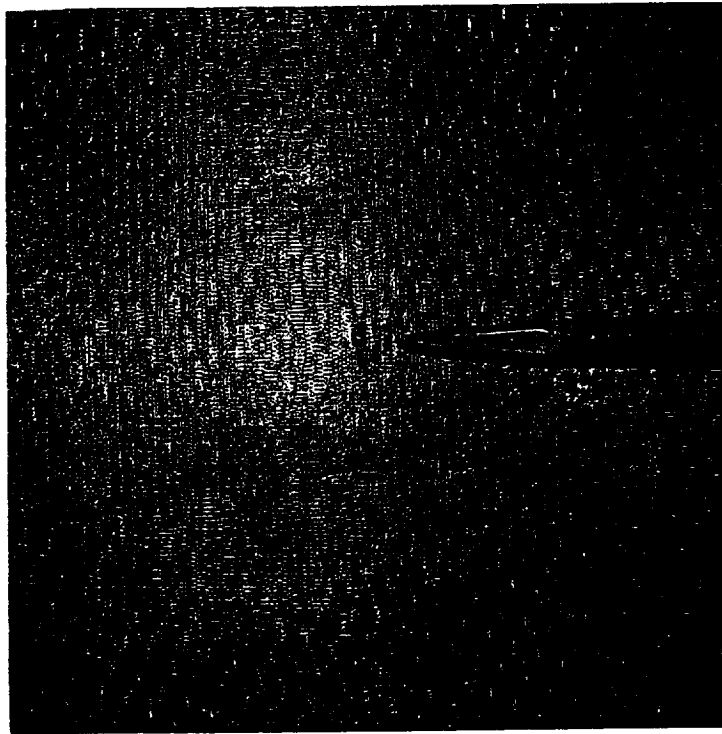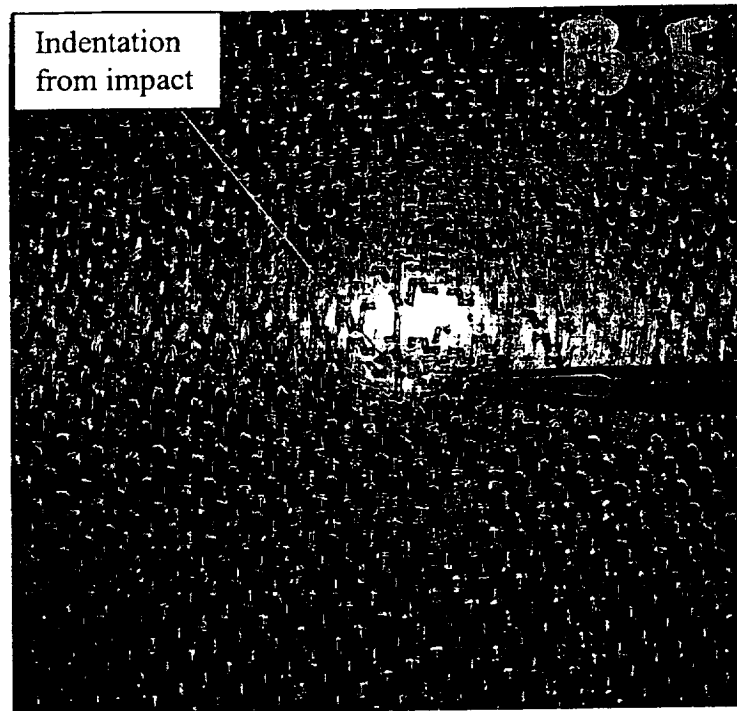
(b)



(c)

Figure 5.5. Uncoated specimen impacted at 3.18 ft*lb (4.31 J), (a) back of specimen, (b)

front of specimen, (c) close-up of damage on backside.

(a)



Indentation
from impact
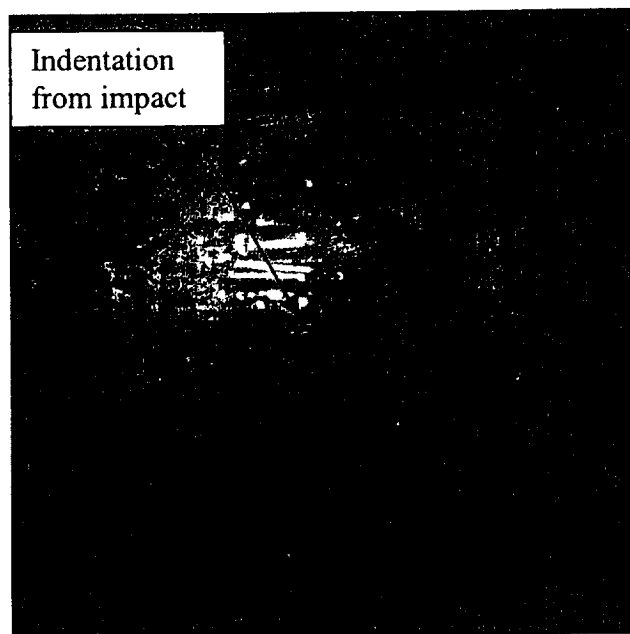
(b)
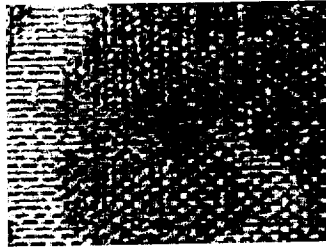
(c)

Figure 5.6. Poly-Lon 1900 coated specimen impacted at 3.87 ft*lb (5.25 J), (a) back of

specimen, (b) front of specimen, (c) close-up of damage on backside.



(a)

Indentation
from impact
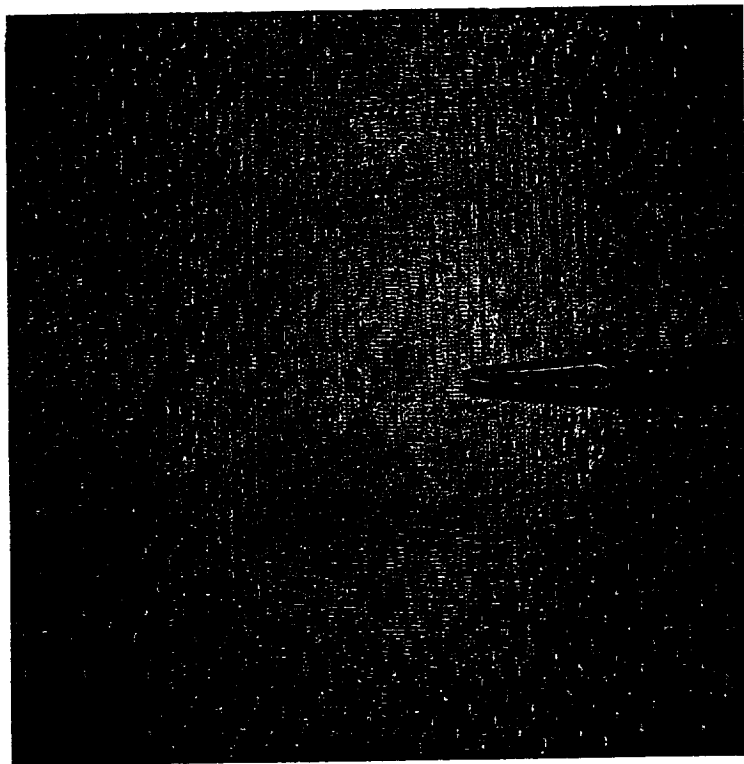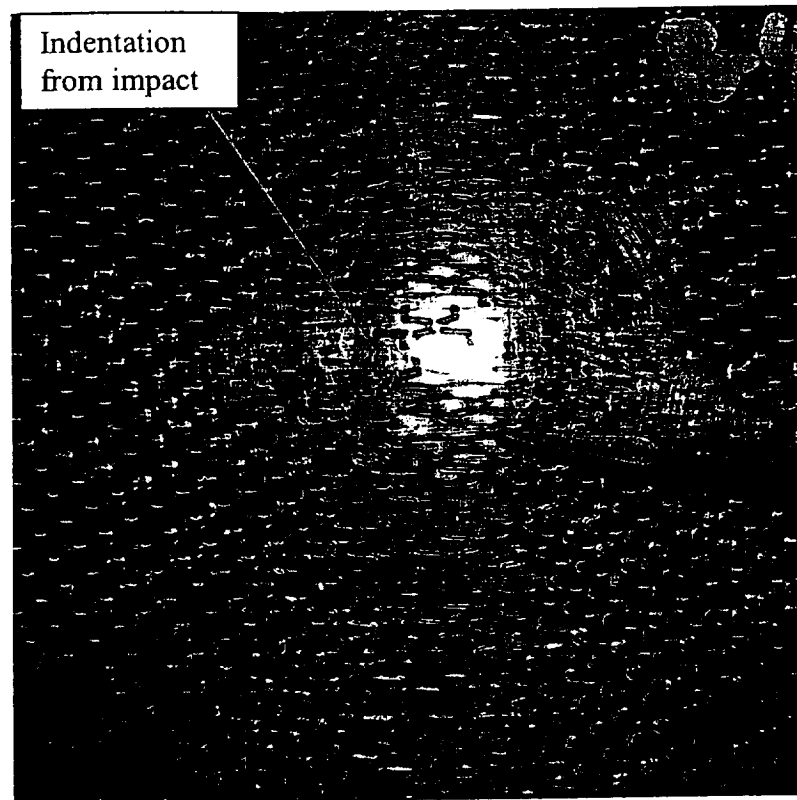
(b)
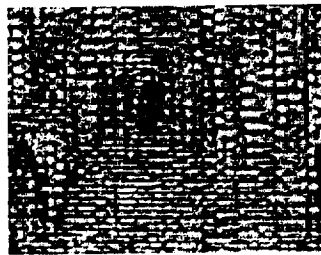


(c)

Figure 5.7. Uncoated specimen impacted at 3.87 ft*lb (5.25 J), (a) back of specimen, (b)

front of specimen, (c) close-up of damage on backside.
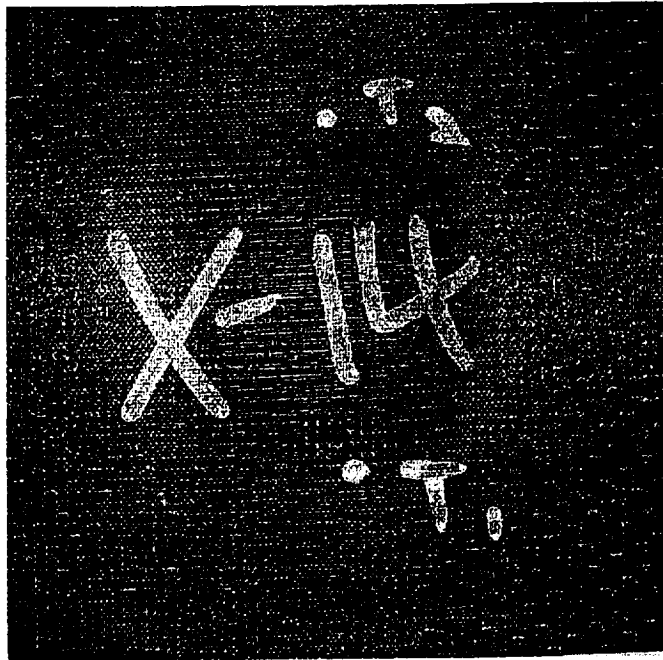
(a)
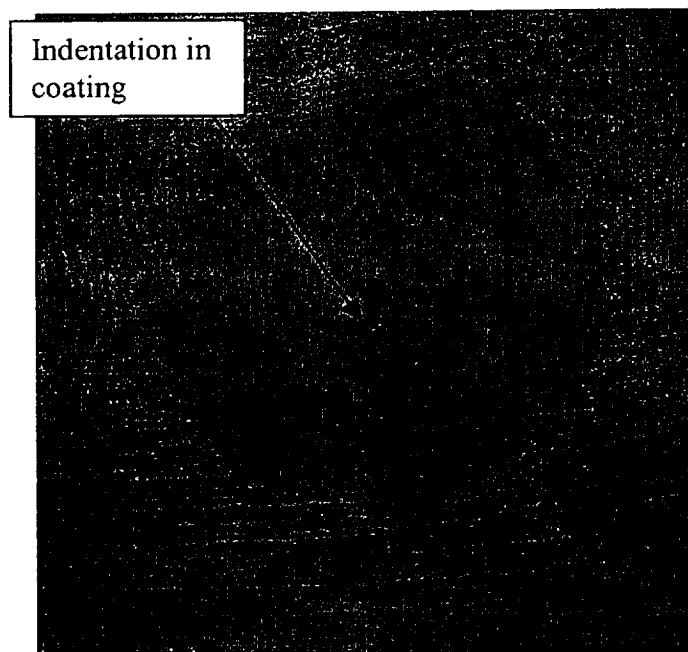


(b)

Figure 5.8. Thermaflex IIC specimen impacted at 2.30 ft*lb (3.12 J), (a) back of

specimen, (b) front of specimen (note there is no visible damage on this specimen).

(a)



Indentation
from impact
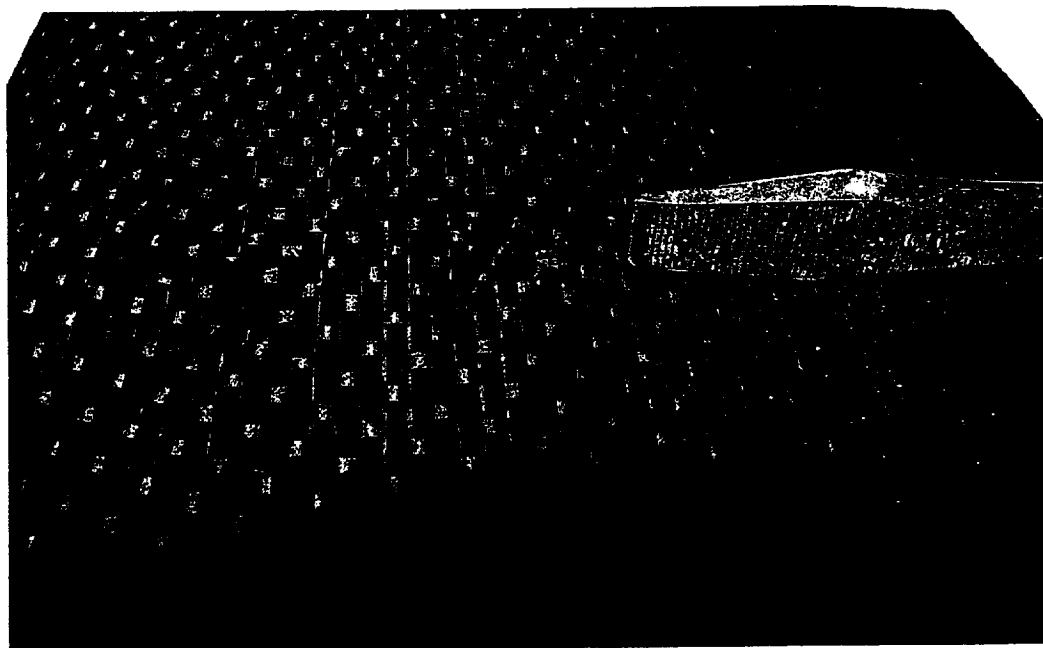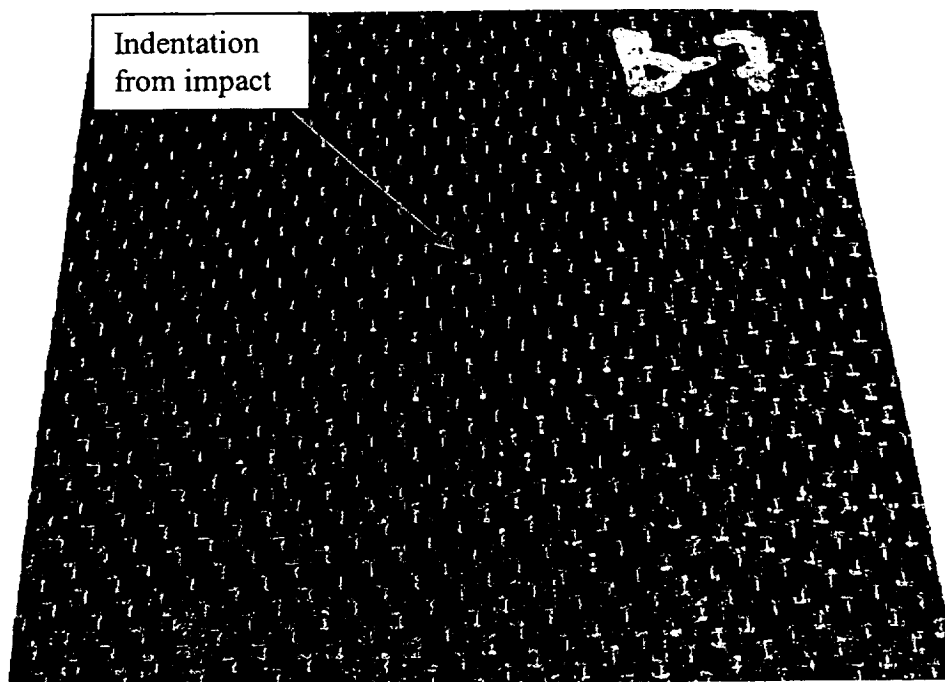
(b)

(c)

Figure 5.9. Uncoated specimen impacted at 2.30 ft*lb (3.12 J), (a) back of specimen, (b) front of specimen, (c) close up of damage in back.
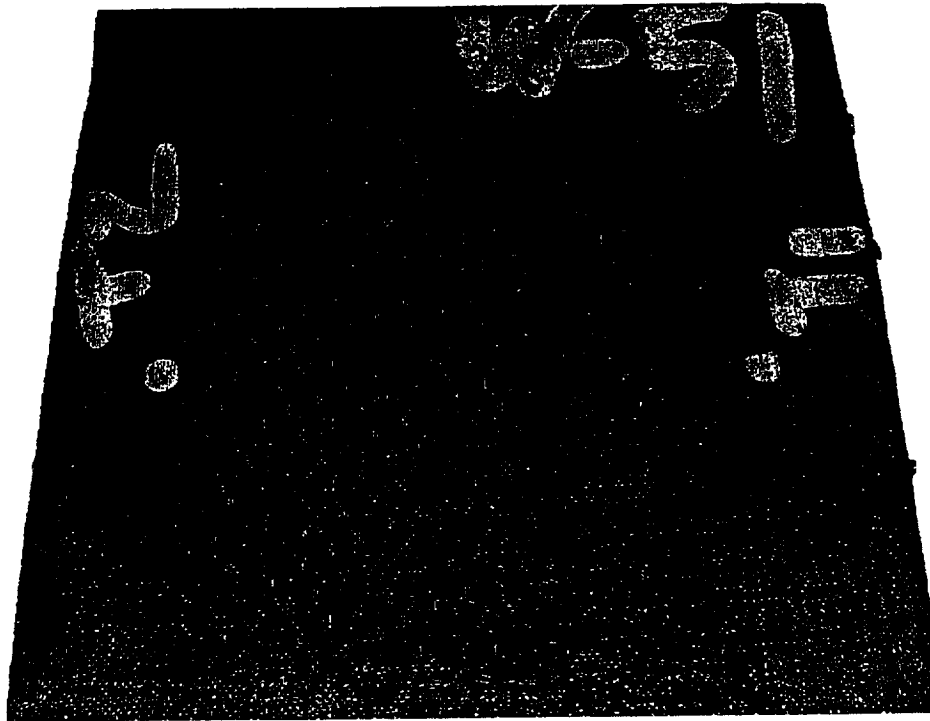


(a)
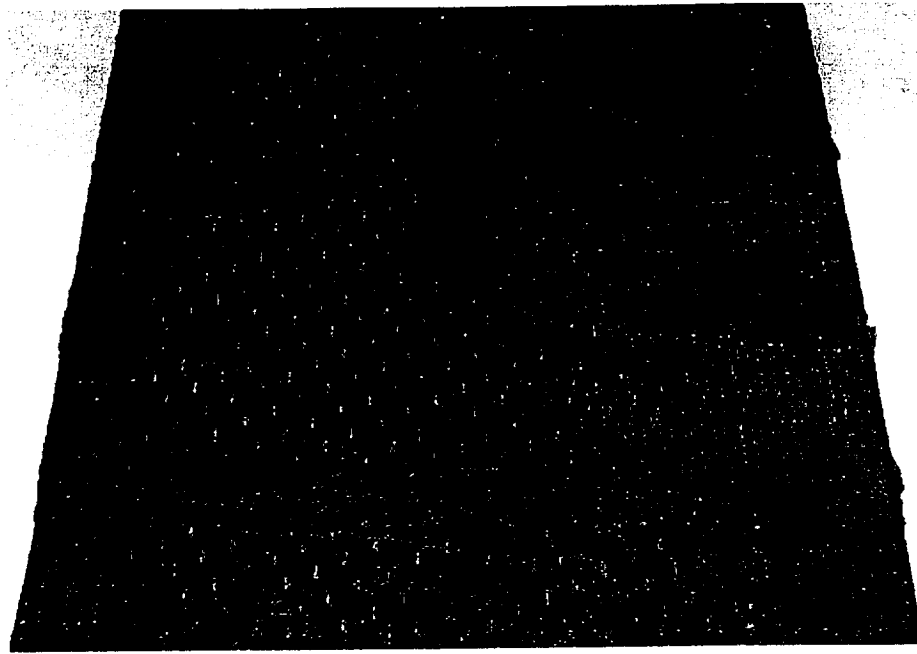
(b)

Figure 5.10. Five percent nanocomposite impacted at 0.82 ft*lb (1.11 J), (a) back of

specimen, (b) front of specimen.

As was mentioned in the caption for Figure 5.8, there is no visible damage on the back of the Thermaflex IIC coated specimen. This is even true of some of the specimens that were impacted with sufficient energy to cause leakage through the coating. In addition, when there was a leak path present in the composite substrate the Thermaflex IIC tended to delaminate around the location of damage until the coating finally failed, as shown in Figure 5.11.
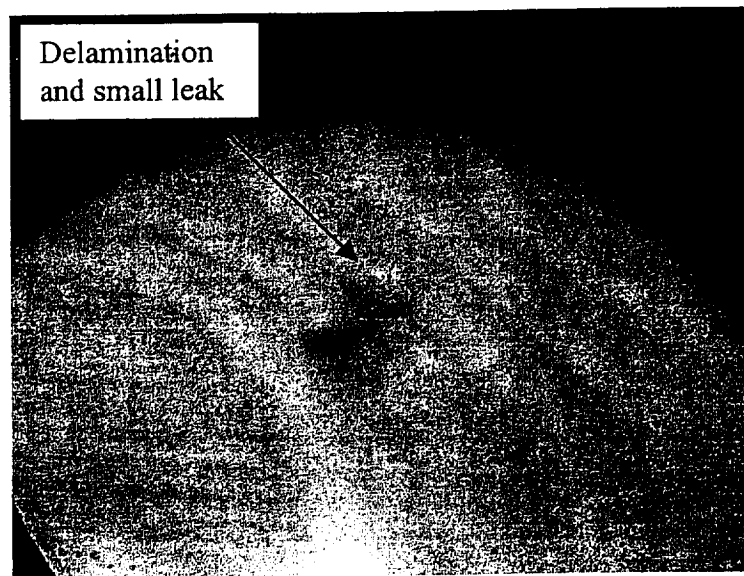
Figure 5.11. Thermaflex IIC specimen delaminating during leak test.

The Thermaflex IIC specimens were not the only ones that tended to fail by delamination when helium was applied at pressure to the backside. Several of the Poly-Lon 1900 specimens also delaminated during leak testing, in one case the delamination was able to grow enough that it actually arrested prior to the development of a leak (with helium applied at 30 psi, 206.9 kPa).

The Corothane I Aliphatic Finish coated specimens that were impacted with sufficient energy to cause leakage all featured visible cracking on the surface of the coating, which would be a desirable feature for a coating used on RLV feedlines. If a coating shows visible damage prior to its failure then during a preflight inspection any potential problems could be found and repaired.

The Corothane I MIO-Aluminum coatings tended to develop leaks through tiny pinholes that are extremely difficult to find. Further complicating locating a leak prior to

gas application is the fact that air bubbles tended to be trapped in the surface of this coating.

The GRC 5% nanocomposite coating showed no visible signs of impact damage, but always had small leaks at the impact site. With impact energies as low as 0.8 ft*lb (1.08 J) no visible damage can be expected.

### 5.4.1.3 Summary

All of the coatings were able to improve the impact resistance of the composite substrate with the exception of the GRC 5% nanocomposite. But, the Corothane I Aliphatic Finish was able to increase the impact resistance much more than the other coatings and also had the advantage of not leaking until there was visible damage on the coatings surface. The Corothane I MIO-Aluminum coating showed no visible signs of damage prior to leak initiation because air bubbles trapped in the coating surface obscured the pinhole leaks. Finally, the Poly-Lon 1900 and the Thermaflex IIC both tended to fail by delamination.

## 5.4.2 Impact of Initially Impermeable then Coated Specimens

### 5.4.2.1 Results

The initially impermeable then coated specimens were tested in same manner as the initially leaking then coated specimens. Tables 5.12 through 5.18 show the results of the impact testing on the individual specimens broken down by the coating. Table 5.19

shows the critical impact energies that were found for the initially impermeable coated specimens. In some cases the absorbed energy is listed as error, this is because the velocity flag did not have enough energy to reenter the velocity sensor and thus no data could be taken regarding the rebound energy.

Table 5.12. Impact results for Corothane I Aliphatic Finish coated initially impermeable specimens.

| Specimen | Impact Energy, J (ft*lb) | Absorbed Energy, J (ft*lb) | Maximum Load, N (lb) | Maximum Deflection, cm (in) | Leakage |
|---|---|---|---|---|---|
| W-2 | 5.98 (4.41) | 4.01 (2.96) | 1922 (432.05) | 0.56 (0.22) | @ 0kPa (0 psi) |
| X-47 | 5.26 (3.88) | 2.41 (1.78) | 1787 (401.71) | 0.53 (0.21) | @ 34.4 kPa (5 psi) |
| A-10 | 5.26 (3.88) | 1.76 (1.30) | 1816 (408.17) | 0.56 (0.22) | None |
| W-3 | 5.31 (3.92) | 1.86 (1.37) | 1905 (428.24) | 0.58 (0.23) | None |

Table 5.13. Impact results for Corothane I MIO-Aluminum coated initially impermeable specimens.

| Specimen | Impact Energy, J (ft*lb) | Absorbed Energy, J (ft*lb) | Maximum Load, N (lb) | Maximum Deflection, cm (in) | Leakage |
|---|---|---|---|---|---|
| W-12 | 4.33 (3.19) | 1.26 (0.93) | 1712 (384.97) | 0.53 (0.21) | @ 68.9 kPa (10 psi) |
| X-22 | 4.11 (3.03) | 1.02 (0.75) | 1711 (384.63) | 0.53 (0.21) | @ 34.4 kPa (5 psi) |
| C-10 | 3.92 (2.89) | 1.06 (0.78) | 1532 (344.32) | 0.48 (0.19) | None |
| W-16 | 3.96 (2.92) | 1.02 (0.75) | 1666 (374.46) | 0.51 (0.20) | @ 34.4 kPa (5 psi) |

96

Table 5.14. Impact results for Poly-Lon 1900 coated initially impermeable specimens.

| Specimen | Impact Energy, J (ft*lb) | Absorbed Energy, J (ft*lb) | Maximum Load, N (lb) | Maximum Deflection, cm (in) | Leakage |
|---|---|---|---|---|---|
| W-20 | 5.29 (3.90) | 1.68 (1.24) | 1931 (434.18) | 0.58 (0.23) | @ 103.4 kPa (15 psi) |
| X-56 | 5.11 (3.77) | 1.64 (1.21) | 1889 (424.57) | 0.56 (0.22) | None |
| B-9 | 5.30 (3.91) | 1.71 (1.26) | 1855 (417.04) | 0.53 (0.21) | @ 137.9 kPa (20 psi) |
| W-9 | 5.06 (3.73) | 1.64 (1.21) | 1873 (421.07) | 0.56 (0.22) | None |

Table 5.15. Impact results for Thermaflex IIC coated initially impermeable specimens.

| Specimen | Impact Energy, J (ft*lb) | Absorbed Energy, J (ft*lb) | Maximum Load, N (lb) | Maximum Deflection, cm (in) | Leakage |
|---|---|---|---|---|---|
| W-15 | 3.20 (2.36) | 0.69 (0.59) | 1418 (318.84) | 0.48 (0.19) | None |
| X-31 | 3.40 (2.51) | 1.10 (0.81) | 1383 (310.89) | 0.53 (0.21) | @ 34.4 kPa (5 psi) |
| W-26 | 3.42 (2.52) | 0.85 (0.63) | 1508 (339.05) | 0.48 (0.19) | None |
| B-1 | 3.44 (2.54) | 0.73 (0.54) | 1444 (324.55) | 0.46 (0.18) | None |

Table 5.16. Impact results for GRC neat polyimide coated initially impermeable specimens.

| Specimen | Impact Energy, J (ft*lb) | Absorbed Energy, J (ft*lb) | Maximum Load, N (lb) | Maximum Deflection, cm (in) | Leakage |
|---|---|---|---|---|---|
| X-53 | 1.21 (0.89) | Error | 712 (160.16) | 0.36 (0.14) | @ 103.4 kPa (15 psi) |
| W-41 | 1.13 (0.83) | Error | 688 (154.68) | 0.36 (0.14) | @ 34.4 kPa (5 psi) |
| W-52 | 1.14 (0.84) | Error | 695 (156.23) | 0.36 (0.14) | @ 137.9 kPa (20 psi) |

Table 5.17. Impact results for GRC 2% nanocomposite coated initially impermeable
specimens.

| Specimen | Impact Energy, J (ft*lb) | Absorbed Energy, J (ft*lb) | Maximum Load, N (lb) | Maximum Deflection, cm (in) | Leakage |
|---|---|---|---|---|---|
| X-76 | 1.19 (0.88) | Error | 709 (159.45) | 0.36 (0.14) | @ 68.9 kPa (10 psi) |
| X-75 | 1.18 (0.87) | Error | 712 (160.03) | 0.36 (0.14) | @ 34.4 kPa (5 psi) |

Table 5.18. Impact results for GRC 5% nanocomposite coated initially impermeable
specimens.

| Specimen | Impact Energy, J (ft*lb) | Absorbed Energy, J (ft*lb) | Maximum Load, N (lb) | Maximum Deflection, cm (in) | Leakage |
|---|---|---|---|---|---|
| X-73 | 1.23 (0.91) | Error | 725 (162.99) | 0.36 (0.14) | @ 68.9 kPa (10 psi) |
| X-72 | 1.14 (0.84) | Error | 691 (155.39) | 0.36 (0.14) | @ 68.9 kPa (10 psi) |
| W-40 | 1.11 (0.82) | Error | 698 (156.94) | 0.33 (0.13) | @ 68.9 kPa (10 psi) |

Table 5.19. Critical impact energies for the coated initially impermeable specimens.

| Coating | Critical Impact Energy, J (ft*lb) | Multiple of uncoated specimens |
|---|---|---|
| None | 1.07 (0.79) | NA |
| Corothane I Aliphatic Finish | 5.15 (3.80) | 4.81 |
| Corothane MiO-Al | 3.80 (2.80) | 3.54 |
| Polylon 1900 | 5.11 (3.77) | 4.77 |
| Thermaflex IIC | 3.20 (2.36) | 2.99 |
| GRC Neat Polyimide | <1.07 (<0.79) | <1.00 |
| GRC 2% Nanocomposite | <1.07 (<0.79) | <1.00 |
| GRC 5% Nanocomposite | <1.07 (<0.79) | <1.00 |

### 5.4.2.2 Discussion

Please note that the reason that only 3 specimens were tested of the NASA GRC neat polyimide coated and only 2 specimens of the 2% nanocomposite coated was because the other specimens in the set of four leaked prior to impact. The last of the 5% nanocomposite coated specimens was not impacted because it was determined that all of these specimens would leak after impacts at the lowest possible impact energy (around 0.79 ft*lb, 1.07 J, using the 8250).

Again, the damage caused by heating the polyimide and polyimide nanocomposite specimens to 465 °F (241 °C) caused sufficient degradation of the composite substrate that the material was able to even sustain impacts as significant as those of the uncoated initially impermeable specimens. The thickness values taken for these specimens at NASA GRC show that the specimens gained little or no thickness with the coatings. Undoubtedly, the lack of thickness is also in part responsible for the failure of the coatings to improve the impact resistance of the composite. Table 5.20 shows the average thickness and weights added for each of the coatings on the impermeable specimens.

The energy absorbed by the test specimens was again found to be a good measure of the level of visible damage present. This is exactly as one would expect, since the primary mode of energy loss should be through the formation of cracking and the breaking of fibers in the composite substrate.

Table 5.20. Average thickness and additional weight of coating for initially impermeable

coated specimens.

| Coating | Coating Weight N/m² (lb/ft²) | Average Coating Thickness cm (in) | Additional Weight (%) |
|---|---|---|---|
| Corothane I Aliphatic Finish | 3.59 (0.075) | 0.023 (0.0089) | 1.28 |
| Corothane MiO-Al | 2.54 (0.053) | 0.017 (0.0066) | 0.95 |
| Polylon 1900 | 2.87 (0.060) | 0.018 (0.0071) | 1.02 |
| Thermaflex IIC | 5.79 (0.121) | 0.047 (0.0187) | 2.70 |
| GRC Neat Polyimide | 0.24 (0.005) | 0.001 (0.0004) | 0.06 |
| GRC 2% Nanocomposite | 0.24 (0.005) | 0.003 (0.0010) | 0.15 |
| GRC 5% Nanocomposite | 0.29 (0.006) | 0.000 (0.0001) | 0.02 |

*5.4.2.3 Summary*

Again all of the coatings provided some measure of improvement in the impact

resistance of the composite with the exceptions of the NASA GRC coatings. The most

improvement was still provided by Corothane I Aliphatic Finish, and the Poly-Lon 1900

and Thermaflex IIC coatings still tended to delaminate during failure.

## 5.4.3 Comparison of Initially Impermeable and Initially Leaking Specimens

From the data in Tables 5.10 and 5.19 it can be seen that the critical impact

energies of the coated specimens with three or more leaks were actually greater than or

equal to the corresponding values for the initially impermeable coated specimens. This

means that the coatings are capable of sealing leaking composite feedlines such that they

are at least as impact resistant as initially impermeable specimens. It was expected that

there would be no difference between the initially impermeable specimens and specimens with leaks after each had been coated. The only reasons that may account for the lower critical impact energies of the initially impermeable specimens are that the coatings were generally a little thinner, and also the composite material used for this testing was highly variable.

## 5.5 Permeability Results and Discussion

The specimens that were impacted and found to leak were then tested to quantify the rate of permeation through the damage. All permeability testing was done following the procedure described in section 4.4.2 of this thesis. It was expected that the rate of permeation would increase as the impact energy above the critical value was increased.

### 5.5.1 Permeability of Coated Previously Leaking Specimens

*5.5.1.1 Results*

Table 5.21 shows the results of the permeability testing for all of the specimens that leaked following impact testing.

Table 5.21. Permeability results for previously leaking then coated specimens.

| Specimen | Coating | Permeability, $cm^3$/min-kPa ($in^3$/min-psi) | Impact Energy, J (ft*lb) |
|---|---|---|---|
| C-1 | Corothane I Aliphatic Finish | 0.126 (0.053) | 6.11 (4.51) |
| X-6 | Corothane I Aliphatic Finish | 0.904 (0.380) | 6.21 (4.58) |
| X-21 | Corothane MiO-Al | 0.017 (0.007) | 5.26 (3.88) |
| X-67 | Corothane MiO-Al | 0.002 (0.001) | 4.79 (3.53) |
| G-6 | Polylon 1900 | 0.050 (0.021) | 6.10 (4.50) |
| X-66 | Polylon 1900 | 0.240 (0.101) | 5.74 (4.23) |
| F-5 | Thermaflex IIC | 0.769 (0.323) | 3.86 (2.85) |
| F-8 | Thermaflex IIC | 0.074 (0.031) | 3.36 (2.48) |
| W-51 | GRC 5% Nanocomposite | 0.002 (0.001) | 1.11 (0.82) |
| W-47 | GRC 5% Nanocomposite | 0.002 (0.001) | 1.19 (0.88) |
| W-50 | GRC 5% Nanocomposite | 0.026 (0.011) | 1.71 (1.26) |
| W-32 | GRC 5% Nanocomposite | 0.002 (0.001) | 1.44 (1.06) |

The trend of rate of permeation versus impact energy is shown in Figure 5.12.
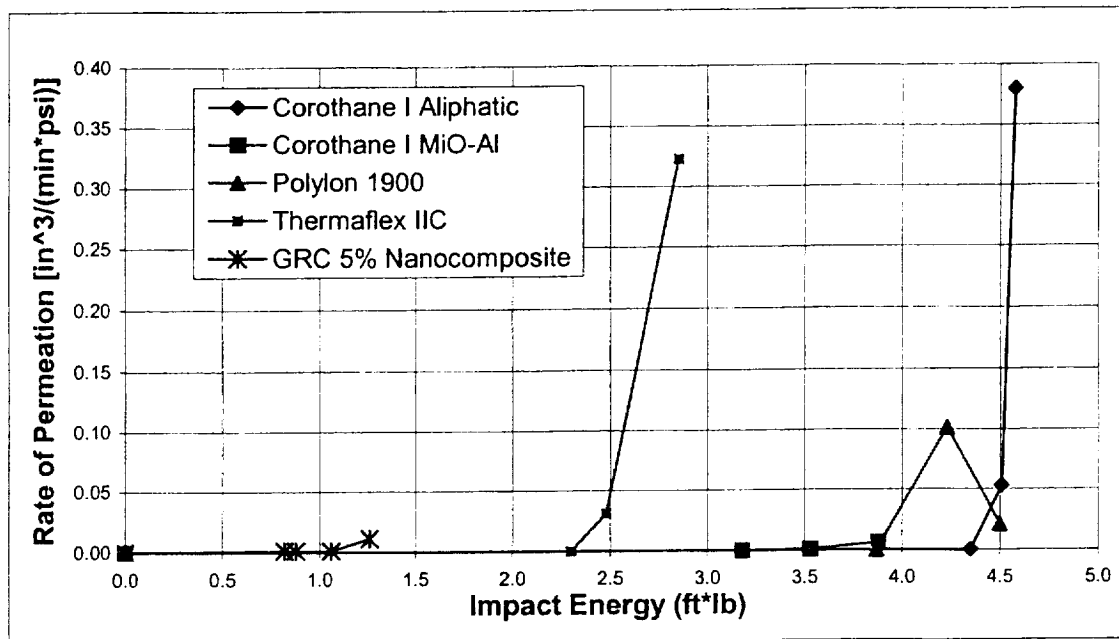
Figure 5.12. Impact energy vs. rate of permeation for coated specimens with 3 or more leaks.

### 5.5.1.2 Discussion

The general trend found from the permeability testing was that once the critical impact energy of the coating/composite system is exceeded the rate of permeability increases rapidly for impacts of increasing energy. The permeability data is presented here in terms of $in^3/(psi*min)$ because the permeability tests cannot all be performed at a given pressure in order for readings to be taken, and thus to get data that can easily be compared this is the appropriate unit.

The only material that does not follow the general trend of increasing permeability for impacts of greater energy is the Poly-Lon 1900 coated composite. While

103

the results of this testing show this odd trend, it is believed that this is attributable to the variable nature of the composite substrate. The two specimens that were used to generate the permeability data points for the Poly-Lon 1900 are from different batches, one from the first batch received which was typically about 50% thicker than the other specimens (it had what appeared to be a resin rich layer on the tooling side). The thicker specimen is the one that was impacted with greater energy, and since greater thickness leads to greater impact resistance this may help to account for the drop in permeability from the previous data point.

It is also important to note that the slopes of the trends for permeation vs. impact energy are very steep. This means that should a coating be used to seal feedlines it will be vital not to allow any impacts that may approach these critical values because failure is extremely sudden, and as was mentioned previously any leak that can be detected with the bubble leak detection set-up is not permissible.

### 5.5.2 Permeability of Initially Impermeable Coated Specimens

#### 5.5.2.1 Results

The initially impermeable specimens that were impacted beyond the critical impact energies were again tested for permeability. Table 5.22 shows the results of this permeability testing, while Figure 5.13 presents this data in chart form (note since the critical impact energy could not be found for the GRC polyimide and polyimide nanocomposite coated specimens a value of 0.70 ft*lb was used to make Figure 5.13).

Table 5.22. Permeability of impacted initially impermeable coated specimens

| Specimen | Coating | Permeability, $cm^3$/min-kPa ($in^3$/min-psi) | Impact Energy, J (ft*lb) |
|---|---|---|---|
| W-2 | Corothane I Aliphatic Finish | 4.55484 (1.91380) | 5.98 (4.41) |
| X-47 | Corothane I Aliphatic Finish | 0.02992 (0.01257) | 5.26 (3.88) |
| W-12 | Corothane I MIO-Aluminum | 0.00009 (0.00004) | 4.33 (3.19) |
| X-22 | Corothane I MIO-Aluminum | 0.00060 (0.00025) | 4.11 (3.03) |
| W-16 | Corothane I MIO-Aluminum | 0.00119 (0.00050) | 3.96 (2.92) |
| W-20 | Poly-Lon 1900 | 0.00112 (0.00047) | 5.29 (3.90) |
| B-9 | Poly-Lon 1900 | 0.00459 (0.00193) | 5.30 (3.91) |
| X-31 | Thermaflex IIC | 0.00109 (0.00046) | 3.40 (2.51) |
| X-53 | GRC Neat Polyimide | 0.00083 (0.00035) | 1.21 (0.89) |
| W-41 | GRC Neat Polyimide | 0.00419 (0.00176) | 1.13 (0.83) |
| W-52 | GRC Neat Polyimide | 0.00254 (0.00107) | 1.14 (0.84) |
| X-76 | GRC 2% Nanocomposite | 0.00183 (0.00077) | 1.19 (0.88) |
| X-75 | GRC 2% Nanocomposite | 0.00138 (0.00058) | 1.18 (0.87) |
| X-73 | GRC 5% Nanocomposite | 0.00190 (0.00080) | 1.23 (0.91) |
| X-72 | GRC 5% Nanocomposite | 0.00029 (0.00012) | 1.14 (0.84) |
| W-40 | GRC 5% Nanocomposite | 0.00062 (0.00026) | 1.11 (0.82) |
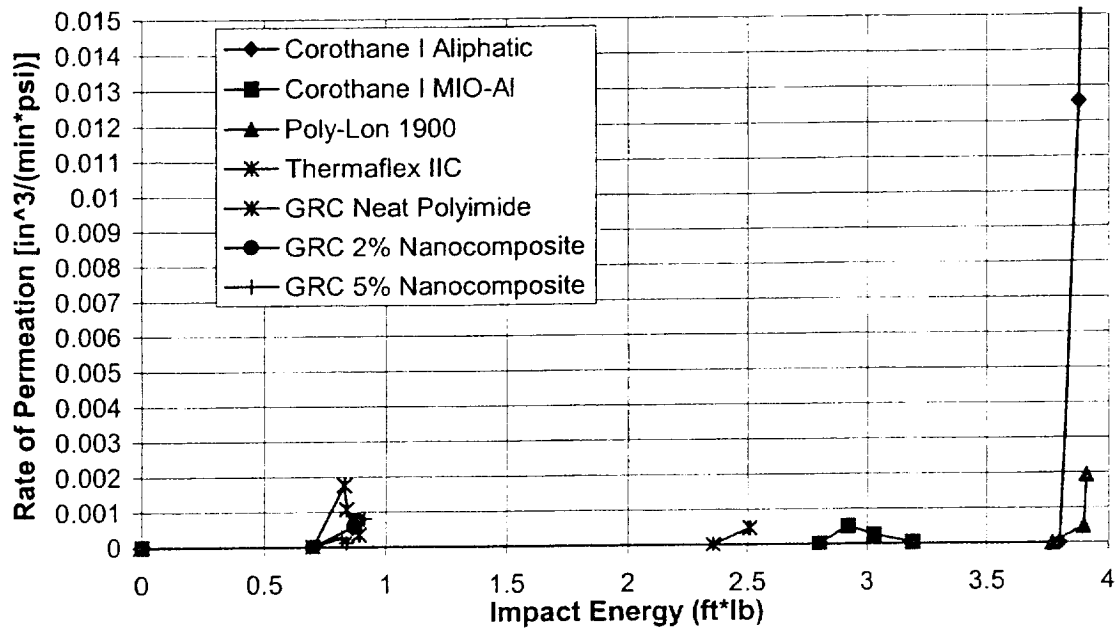
Figure 5.13. Impact energy vs. rate of permeation for coated initially impermeable specimens.

### 5.5.2.2 Discussion

The general trend for increasing permeability with increasing impact energy above the critical values is not quite as clear in Figure 5.13, but this is due to a couple of factors. The permeability rates reported here are very low and were taken from a few different specimens that were all impacted at similar energies. When the material variability of the composite is considered, along with the variation in the coating thickness, one cannot expect specimens impacted within a couple tenths of a foot-pound to show a clear trend. When the variation in impact energy is larger, as with the Corothane I Aliphatic Finish, the trend is quite clear. It is expected that had specimens

106

been impacted over a wider range of energies, instead of all around the critical values of the initially leaking specimens, that the permeability trends would be identical to those presented in section 5.5.1.1.

## 5.6 Effects of Aging on the Coatings

Two of each of the specimens coated at Georgia Tech were set-aside for aging. The GRC polyimide and polyimide nanocomposite specimens were to be aged aswell, but unfortunately, the specimens were not coated in time to perform any aging (and there were not any spare impermeable specimens). All of the specimens were aged at room temperature and at the ambient humidity for four months (approximately 75 °F at between 50 and 80% relative humidity). Table 5.23 shows the results of the leak testing performed on the aged specimens after they were impacted at the critical impact energies (for coated specimens that previously had 3 or more leaks).

Table 5.23. Results of leak testing of impacted aged coated specimens.

| Specimen | Coating | Leakage Notes |
|---|---|---|
| X-24 | Corothane I Aliphatic Finish | 1 Leak @ 172.4 kPa (25psi) |
| G-9 | Corothane I Aliphatic Finish | No Leaks |
| X-57 | Corothane I MIO-Aluminum | No Leaks |
| X-26 | Corothane I MIO-Aluminum | No Leaks |
| X-70 | Poly-Lon 1900 | Delamination formed @ 137.9 kPa (20psi) |
| H-7 | Poly-Lon 1900 | No Leaks |
| F-10 | Thermaflex IIC | No Leaks |
| X-80 | Thermaflex IIC | No Leaks |

Little or no embrittlement appears to have occurred in the coatings over the course of four months. Two of the specimens did leak (the delamination arrested prior to forming a leak, but this is still a coating failure), but both were small failures that did not occur until high pressure was applied. This could indicate that the Corothane I Aliphatic Finish and Poly-Lon 1900 become more brittle with age or it could be due to variation in the quality of the coating or composite substrate. Variation in the coating or composite seems likely since the second specimen for both of these coatings did not leak.

## 5.7 Thermal Cycling

### 5.7.1 Results

One of the larger concerns regarding the use of coatings on cryogenic feedlines and fuel tanks is that the coating must be thermally compatible with the composite substrate. Thus, it was necessary to assess if the coatings tested in impact were viable for use in cryogenic environments. Two of each of type of coated specimen were put through 5 thermal cycles with the exception of the GRC neat polyimide and 5% nanocomposite, each had only one specimen cycled, per the procedure outlined in section 4.5 of this document. Following thermal cycling each of the surviving specimens was leak tested. Table 5.24 shows the results of the thermal cycling and leak testing.

Table 5.24. Results of thermal cycling and leak testing of coated specimens.

| Specimen | Coating | Leakage Notes |
|---|---|---|
| X-46 | Corothane I Aliphatic Finish | 1 Leak @ 103.4 kPa (15 psi) |
| W-18 | Corothane I Aliphatic Finish | 1 Leak @ 68.9 kPa (10psi) |
| E-6 | Corothane I MIO-Aluminum | Leaks Everywhere @ 34.4 kPa (5psi) |
| D-1 | Corothane I MIO-Aluminum | Leaks Everywhere @ 34.4 kPa (5psi) |
| W-29 | Poly-Lon 1900 | Failed During Cycling |
| X-78 | Poly-Lon 1900 | Failed During Cycling |
| W-30 | Thermaflex IIC | Failed During Cycling |
| X-23 | Thermaflex IIC | Failed During Cycling |
| W-45 | GRC Neat Polyimide | 2 Leaks @ 172.4 kPa (25psi) |
| W-31 | GRC 2% Nanocomposite | 2 Leaks @ 34.4 kPa (5psi) |
| X-71 | GRC 2% Nanocomposite | Leaks Everywhere @ 34.4 kPa (5psi) |
| W-49 | GRC 5% Nanocomposite | 4 Leaks @ 34.4 kPa (5psi) |

## 5.7.2 Discussion

Each of the coatings tested in thermal cycling failed in some manner or other. The Thermaflex IIC and the Poly-Lon 1900 cannot withstand liquid nitrogen temperatures. The Thermaflex IIC specimens suffered severe cracking over the entire surface of the specimen, while the top coat of Poly-Lon 1900 tended to delaminate from the base coat. The only other coating to show any visible signs of degradation from the thermal cycling was the Corothane I Aliphatic Finish. After the second cycle, some very fine cracking was visible near the edge of specimen W-18. Following the third cycle, this cracking had spread to around 50 percent of the specimen, and also the other Corothane I Aliphatic Finish specimen began to have some visible cracking near an edge. The level of cracking did not change during the fourth or fifth cycle. All of the damage that was

observed in the specimens was noticed after the cold portion of the cycle, so it is believed that the elevated temperatures inflicted no damage on the coatings or specimens. Figure 5.14 shows a Thermaflex IIC specimen after two cycles. Figure 5.15 shows a Poly-Lon 1900 specimen after three thermal cycles. The cracking in the Corothane I Aliphatic Finish was too fine to appear in a photograph.
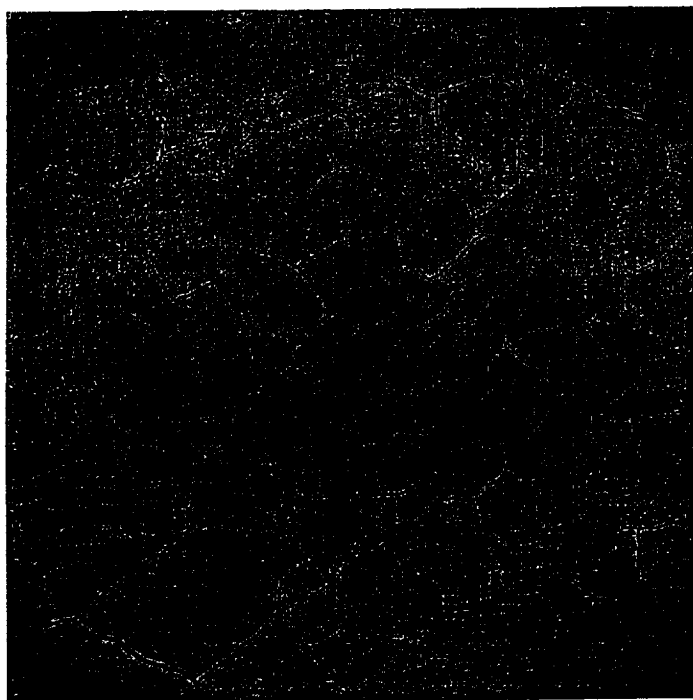


Figure 5.14. Thermaflex IIC specimen after two thermal cycles.
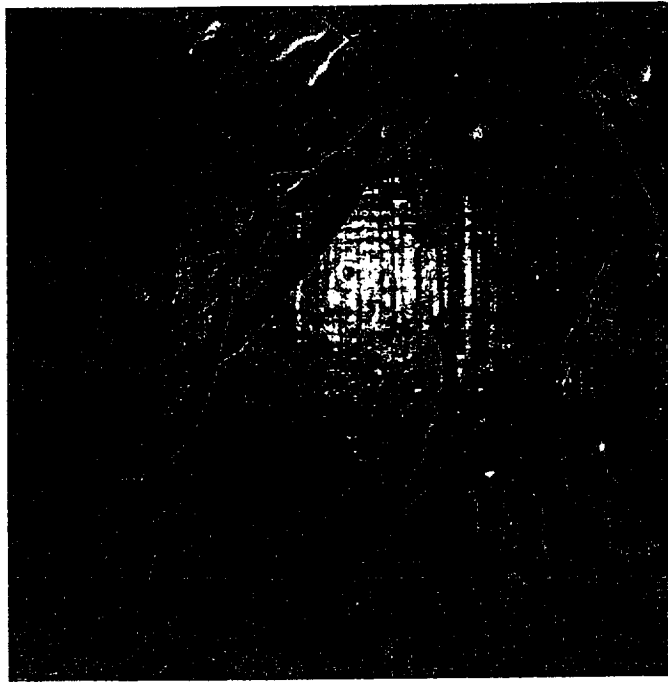
Figure 5.15. Poly-Lon 1900 specimen after three thermal cycles.

Despite what had been reported about carbon/epoxy composites not degrading due to thermal cycling until 60K[24] it was evident from the results of this testing that degradation of the matrix occurred. The Corothane I MIO-Aluminum specimens each had only three leaks prior to thermal cycling, yet when leak tested afterwards there were too many leaks to count on both of these specimens. Figure 5.16 shows one of the Corothane I MIO-Aluminum specimens being leak tested after five complete cycles.
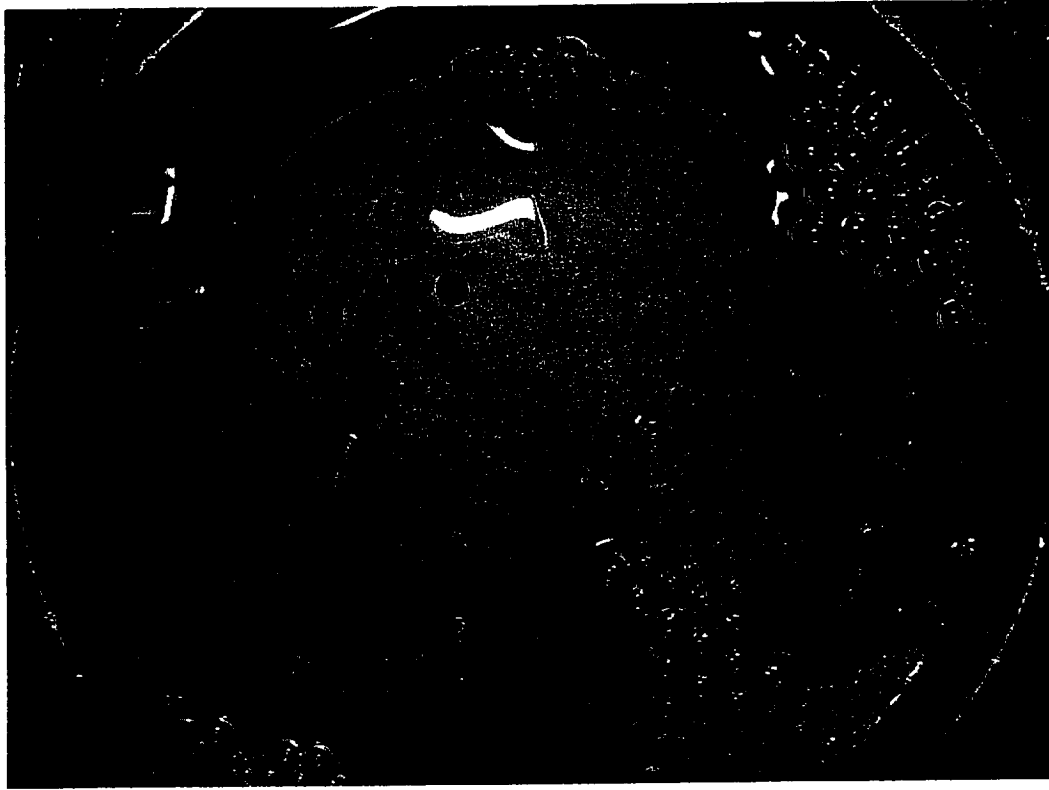
Figure 5.16. Corothane I MIO-Aluminum specimen being leak tested following thermal cycling.

The Corothane I MIO-Aluminum coated specimens both had no visible signs of damage after thermal cycling, yet leaked like sieves. This would tend to indicate that the polyurethane must have been breaking away from the aluminum and micaceous iron oxide particles creating leak paths. In light of the poor performance of the other polyurethane coatings tested, simply not delaminating makes this coating seem more promising provided that the formula could be altered enough to change the CTE slightly.

The NASA GRC polyimide and polyimide nanocomposites failed in thermal cycling as well, but according to work done by Humpenoder indicates that the

nanocomposites with silicates as the reinforcement can be adjusted so that the CTE of the nanocomposite matches that of the material it is applied to. [34] Thus, these coatings may still be promising candidates for coating cryogenic composite feedlines but the formula will have to be refined.

# CHAPTER VI

## CONCLUSIONS

The research described in this thesis explored the possibility of improving the impact resistance of a composite material, which is to be used for fuel feedlines in future generations of RLVs, through the application of a coating. In particular, this research focused on increasing the impact resistance of the composite, sealing preexisting leaks in the composite, and preventing fuel permeation through regions damaged by impact events.

The material tested was a woven carbon fiber epoxy matrix composite, IM7 fibers in an EX 1552 epoxy matrix, which is typical of the materials that are being considered for feedline applications (carbon fibers in toughened epoxy matrices). All of the impact testing was done with a drop weight impact machine, while the leak testing and permeability was done using helium gas in place of the liquid hydrogen and liquid oxygen that will be used to fuel the vehicles.

The specimens received were all tested for leaks and then divided into three categories: non-leaking specimens, specimens with one or two leaks, and specimens with three or more leaks. Initially, this research was to deal exclusively with improving the impact resistance of impermeable (non-leaking) composite fuel feedlines, but some of the feedlines made and tested at NASA MSFC leaked prior to impact and most of the specimens received also leaked prior to impact. Thus, the project was restructured to

114

determine how effectively coatings could be used to seal preexisting damage (specimens with three or more leaks) and simultaneously improve the composite materials resistance to impact. The non-leaking specimens were used to find the baseline critical impact energy, the maximum impact energy that the material could withstand without becoming permeable, and also to determine if the sealed composite was as impact resistant as coated initially impermeable composite.

Fuel feedlines in RLVs will be exposed to extreme temperatures, from Liquid hydrogen at 20K (-423 °F) all the way up to 250 °F (121 °C) during reentry. Due to the wide range of service temperatures, thermal cycling of the coated specimens was necessary. The thermal cycling performed for this project could not use liquid hydrogen for safety reasons, so liquid nitrogen was substituted (77K, -321 °F).

The results from this project definitely indicate that the overall impact resistance of the composite feedlines can be improved significantly through the application of a coating. This coating does come at a cost in weight though; the significance of the additional weight depends on how much additional weight can be tolerated to still make the use of composites preferable over more traditional metal materials. Additionally, it was found during our limited testing that specimens that leaked prior to being coated performed as well if not better than specimens the did not leak prior to the coating. So it certainly appears that coatings are a valid method of repairing/redeeming leaking feedlines.

In contrast to the results of the impact testing, the results of the thermal cycling were generally not favorable; all of the coatings considered in this research failed, but

there were a couple of small positives. The expected mode of coating failure during thermal cycling was for the coating to delaminate from the substrate, or to have significant cracking. The Corothane I MIO-Aluminum did not have either of these problems, but numerous leaks did develop. This suggests that the polymer bonding the aluminum and micaceous iron oxide particles may have broken down some, but perhaps a similar type of coating containing small-scale reinforcement might be able to withstand the thermal stresses.

In addition to thermal cycling the coated specimens, some were set-aside for aging. Of these specimens little or no degradation was found in their impact resistance. It therefore appears that the coatings will not become appreciably more brittle over time.

The three coatings provided by NASA GRC performed poorly in the tests performed. It is difficult to say that this testing provided an accurate reflection of these materials however. The coatings were extremely thin when compared to all of the other coatings tested. Also, as has been mentioned throughout Chapter 5 in order to imidize and consolidate the coatings they had to be heated well above the $T_g$ of the composite's epoxy matrix, which actually caused the majority of the specimens received to leak prior to impact. Thus, comparisons between these coatings and the others, applied to composite material that had not been heated above the $T_g$, are not valid. While this particular coating might not be well suited to a composite with a matrix with a low $T_g$, there may be other nanocomposites that are. Finally, the application of these coatings also had numerous voids and did not appear to be even.

One cannot overlook the variability in the composite tested in this research. The material was found to be highly variable between separate batches received, and also, as was shown in the C-scans performed by NASA LaRC, the material does not have consistent density and curing throughout the entirety of even one panel. The variability of the material makes comparing impacts from one batch to another difficult, especially due to the thickness variations. It is believed that the variability of the composite combined with the variation in the thickness of the coatings accounts for the drop in critical impact energies found between the previously leaking specimens and the initially impermeable specimens. The variation found in the material also emphasizes the importance of maintaining a consistent methodology for the lay-up and curing of the composite.

# CHAPTER VII

# LESSONS LEARNED AND RECOMMENDATIONS

## 7.1 Lessons Learned

In any research project many lessons are learned, and this project was no different. Some of the lessons learned would simply help to smooth the testing process while others would help to avoid the pit-falls, of which there were several in this project. It is hoped that by noting the lessons learned during this project some problems can be circumnavigated when the problem of low-energy impacts in composite fuel feedlines is revisited in the future.

### 7.1.1 Specimen Fabrication.

NASA MSFC made all of the composites used in this research from prepreg material supplied by Bryte Technologies. It is understood that when making more than 250 specimens variability is unavoidable, but there was a great deal of variability in the thickness of the specimens, the specimens appearance, and even the consistency of the cure. This may be typical of full scale parts produced for the actual vehicles, especially some of the large cryogenic tanks, but for research the variability in the quality of the specimens introduces an extra variable. Comparing some of the results in this research was made more difficult because it was not possible to test more than a couple of specimens for each coating from any given batch of specimens. Also, it is important that

specimens are nominally the same size to ensure that the boundary conditions in the impact test machine are similar. Some of the specimens received were considerably smaller on one side than the 4" (10 cm) length the pneumatic clamp on the impact test machine was designed for.

## 7.1.2 Experimental Procedures

Several of the Corothane I MIO-Aluminum specimens leaked after being coated and prior to being impacted, and at least one of the specimens leaked because of poor degreasing prior to the coating application. Obviously, the importance of removing all vacuum grease from the specimens cannot be overstated.

The test matrix used for this research also was too small. With all of the variation presented by the coating process, it is really necessary to have more redundancy in the impact testing to be sure that the results accurately represent the behavior of the coated specimens. Impacting two or three specimens at each impact energy right around the critical value would help to define this value more clearly.

The specimens that were aged for this research were only aged for four months. While this provided some insight into how the coatings will age, the trends would have been more obvious had the specimens been coated earlier and aged longer.

## 7.2 Recommendations

While this project provided a good starting point for analyzing the potential of coatings to improve the impact resistance of composite materials, a lot of work remains to be done, which is obvious since the coatings all failed during thermal cycling. Furthermore, while conducting this research several observations have been made that may help future researchers avoid some of the difficulties that were encountered.

One of the biggest difficulties encountered in this research was that there were too many variables. Two that could be eliminated, or at least improved upon, were the variability within the composite itself and the thickness of the coatings. As was shown in Figure 3.2, the composites received were vastly different in terms of their cure alone, but also there were significant differences in the thickness of the specimens. In future work, it would be wise to use a material that is understood well enough to get a consistent specimen every time. Also, some potential coatings, in this case the polyimides supplied by NASA GRC, require heating to temperatures in excess of the $T_g$ of the epoxy that was used here, thus it might be wise to use a composite with a higher $T_g$. One material that might be suitable for this application, and has been researched thoroughly at Georgia Tech, is IM7/PETI-5.

The coatings that were applied both at Georgia Tech and at NASA GRC were as consistent in thickness as they could be when applied with a brush. The use of a professional grade spray gun would probably yield a much better coating, especially if

someone with significant experience could be found to apply the coatings. Also, several of the coatings applied at Georgia Tech had some entrapped air bubbles. A spray gun might also help to eliminate these flaws, which would make it easier to see damage in the coatings following impacts.

While several different coatings were used, many were polyurethane, and it would be desirable to test a wider variety of coatings. Efforts were made to consider different types of coatings, but it was discovered that many of the commercial suppliers are reluctant to supply experimental samples and that the products themselves are not available in reasonable quantities and/or are prohibitively expensive. Two of the coatings that were considered for this research that could not be acquired due to cost were an aerospace epoxy-based coating, and Parylene. Both of these materials seem well suited to this project, so if the problem of impact resistance of composite feedlines is revisited both of these types of coatings warrant being revisited.

Despite the results of this testing, it is believed that nanocomposites may actually be some of the most promising coating candidates available. This statement is based on both the work discussed in Chapter II[32-34], and also the fact that the Corothane I MIO-Aluminum coating (this may not be a nano-scale composite but it is a micro-scale composite) did not delaminate or have visible cracking. Had a different composite substrate been used, and the coatings been applied thicker, it is suspected that the nanocomposites provided by NASA GRC may have yielded totally different results, and thus more research is needed on these materials.

This project was structured from the start to consider whether or not the impact resistance of a composite material could be improved through the use of coatings. But after completing the testing it has become clear that while this may be the ultimate goal it is not the appropriate starting point for the research. Instead, it is suggested that the first problem that must be explored further is simply to find what types of coatings will actually remain both intact and adhered to the composite after extensive thermal cycling. Only after finding materials that survive thermal cycling does it make since to determine if they actually help make the composite more impact resistant. To this end, it is suggested that thermal cycling be used as a method of screening all potential coatings considered in the future.

The final suggestion stems from the background reading. Humpenoder[34] found that placing a thin layer of tin sheeting in the center of the lay-up prevented permeation. It is believed that the tin may also improve the impact resistance, and depending on the thickness of the foil the weight may not be too significant. In addition to considering a layer of tin in the composite, it would be interesting to study the effects of an adhesive layer in the center of the composite.

# REFERENCES

[1] Rogacki, "Row", "The Coming Revolution in Space Transportation," <u>Georgia Institute of Technology Structural Mechanics Seminar Series</u>, Atlanta, GA, February 1, 2001.

[2] Kessler, S. S., T. Matuxzeeski, and H. McManus, "Cryocycling and Mechanical Testing of CFRP for the X-33 Liquid $H_2$ Fuel Tank Structure," <u>ASC 16th Technical Conference Proceedings</u>, Blacksburg, VA, September 9-12, 2001.

[3] Freeman, D., and T. Talay, "Reusable Launch Vehicle Technology Program," *Acta Astronautica*, Vol. 41, No. 11, 1998, pp. 777-790.

[4] Nettles, A., "Impact Damage Resistance of Carbon/Epoxy Composite Tubes for the DC-XA Liquid Hydrogen Feedline," *NASA Technical Paper 3583*, September 1995.

[5] Sinclair, T., Personal Communication, NASA LaRC, Langley, VA, December 2000.

[6] Cantwell, W. J., and J. Morton, "The Impact Resistance of Composite Materials—A Review," *Composites*, Vol. 22, No. 5, September 1991, pp. 347-362.

[7] Choi, H. Y., R. J. Downs, and F.-K. Chang, "New Approach Toward Understanding Damage Mechanisms and Mechanics of Laminated Composites due to Low-Velocity Impact," *Journal of Composite Materials*, Vol. 25, No. 8, August 1991, pp. 992-1011.

[8] Wang, H., and T. Vu-Kanh, "Low-Velocity Impact Damage in Laminated Composite Materials," *Impact Response and Dynamic Failure of Composites and Laminate Materials*, Key Engineering Materials, Vols. 141-143, Part 1, 1998, pp. 277-304.

[9] Hsieh, C. Y., A. Mount, B. Z. Jang, and R. H. Zee. "Response of Polymer Composites to High and Low Velocity Impact," <u>22nd International SAMPE Technical Conference</u>, Boston, MA, November 6-8, 1990, pp. 14-27.

[10] De Freitas, M., A. Silva, L. Reis, "Numerical Evaluation of Failure Mechanisms on Composite Specimens Subjected to Impact Loading," *Composites: Part B*, Vol. 31, 2000, pp. 199-207.

[11] Schoeppner, G.A., and S. Abrate, "Delamination Threshold Loads for Low Velocity Impact on Composite Laminates," *Composites: Part A*, Vol. 31, 2000, pp. 903-915.

[12] Zhong, W. and B. Z. Jang, "Material Design Approaches for Improving Impact Resistance of Composites," *Impact Response and Dynamic Failure of Composites and Laminate Materials*, Key Engineering Materials, Vols. 141-143, Part 1, 1998, pp. 169-186.

[13] Bibo, G. A. and P. J. Hogg, "Damage Tolerance of Continuous Fiber Composites: Material and Environmental Effects," *Impact Response and Dynamic Failure of Composites and Laminate Materials*, Key Engineering Materials, Vols. 141-143, Part 1, 1998, pp. 93-125.

[14] Choi, H. Y., H.-Y. T. Wu, and F.-K. Chang, "A New Approach to Understanding Damage Mechanisms and Mechanics of Laminated Composites Due to Low-Velocity Impact: Part I I– Experiments," *Journal of Composite Materials*, August 1991, pp. 1012-1038.

[15] Papanicolaou, G. C., A. M. Blanas, A. V. Pournaras, and C. D. Stavropoulos, "Impact Damage and Residual Strength of FRP Composites," *Impact Response and Dynamic Failure of Composites and Laminate Materials*, Key Engineering Materials, Vols. 141-143, Part 1, 1998, pp. 127-147.

[16] Xu, L. R., "Sequence and Nature of Matrix Cracking and Delaminations in Composite and Sandwich Structures Subjected to Low-Speed Impact," ASC 16th Technical Conference Proceedings, Blacksburg, VA, September 9-12, 2001.

[17] de Moura, M. F. S. F., and A. T. Marques, "Prediction of Low Veolocity Impact Damage in Carbon-Epoxy Laminates," *Composites:Part A*, Vol. 33, 2000, pp. 361-368.

[18] Finn, S. R. and S. Springer, Composite Plates Impact Damage: an Atlas. Technomic Publishing Co., Lancaster, PA, 1991.

[19] Mahfuz, H., M. Saha, R. Biggs, and S. Jeelani, "Damage Tolerance of Resin Infiltrated Composites Under Low Velocity Impact — Experiment and Numerical Studies," *Impact Response and Dynamic Failure of Composites and Laminate Materials*, Key Engineering Materials, Vols. 141-143, Part 1, 1998, pp. 209-234.

[20] Abrate, S. "The Dynamics of Impact on Composite Structures," *Impact Response and Dynamic Failure of Composites and Laminate Materials*, Key Engineering Materials, Vols. 141-143, Part 2, 1998, pp. 671-694.

[21] Kim, J.-K., "Methods for Improving Impact Damage Resistance of CFRPs," *Impact Response and Dynamic Failure of Composites and Laminate Materials*, Key Engineering Materials, Vols. 141-143, Part 1, 1998, pp. 149-168.

[22] Riess, G. and Y. Jolivet, "Rubber-Modified Polymers. Location of Block Copolymers in Two-Phase Materials," Chapter 22, <u>Copolymers, Polyblends, and Composites</u>. Advances in Chemistry Series, American Chemical Society, Washington D.C., 1975, pp. 243-256.

[23] Rivers, H. K., J. G. Sikora, and S. N. Sankaran, "Detection of Micro-Leaks through Complex Geometries Under Mechanical Load and at Cryogenic Temperature," <u>42nd AIAA/ASME/ASCE/AHS/ASC Structures, Structural Dynamics, and Materials Conference and Exhibit</u>, Seattle, WA, April 16-19, 2001.

[24] McManus, H. L., A. Faust, and S. Uebelhart, "Gas Permeability of Thermally Cycled Graphite-Epoxy Composites," <u>ASC 16th Technical Conference Proceedings</u>, Blacksburg, VA, September 9-12, 2001.

[25] Kumazawa, H., T Aoki, T. Ishikawa, and I. Susuki, "Modeling of Propellant Leakage Through Matrix Cracks in Composite Laminates," <u>42nd AIAA/ASME/ASCE/AHS/ASC Structures, Structural Dynamics, and Materials Conference and Exhibit</u>, Seattle, WA, April 16-19, 2001.

[26] Roy, S., W. Xu, S. Patel, and S. Case, "Modeling of Moisture Diffusion in the Presence of Bi-Axial Damage in Polymer Matrix Composite Laminates," *International Journal of Solids and Structures*, Vol. 38, 2001, pp. 7627-7641.

[27] Evans, D., and J. T. Morgan, "The Permeability of Composite Materials to Hydrogen and Helium Gas," *Advances in Cryogenic Engineering*, Vol. 34, 1987, pp. 11-16.

[28] Comyn, J., *Polymer Permeability*, Elsevier Applied Science Publishers, New York, 1985.

[29] He, G., X. Huang, R. Xu, and B. Zhu, "An Improved Model for Gas Permeation in Composite Membranes," *Journal of Membrane Science*, Vol. 1, No. 18, 1996, pp. 1-7.

[30] Melchiors, M., M. Sonntag, C. Kobusch, and E. Jürgens, "Recent Developments in Aqueous Two-Component Polyurethane (2K-PUR) Coatings," *Progress in Organic Coatings*, Vol. 40, 2000, pp. 99-109.

[31] Evans, D., and R. P. Reed, "The Permeability of Resin Based Composite Materials to Radiolytic Gases," *Cryogenics*, Vol. 38, No. 1, 1998, pp. 149-154.

[32] Lincoln, D. M., R. A. Vaia, J. M. Brown, and T. H. Benson Tolle, "Revolutionary Nanocomposite Materials to Enable Space Systems in the 21st Century," <u>IEEE Aerospace Conference Proceedings</u>, Vol. 4, 2000, pp. 183-192.

[33] LeBaron, P. C., Z. Wang, and T. J. Pinnavaia, "Polymer-Layered Silicate Nanocomposites: an Overview," *Applied Clay Science*, Vol. 15, 1999, pp. 11-29.

[34] Humpenoder, J., "Gas Permeation of Fiber Reinforced Plastics," *Cryogenics*, Vol. 38, No. 1, 1998, pp. 143-147.

[35] Disdier, S., J. M. Rey, P. Pailler, and A. R. Bunsell, "Helium Permeation in Composite Materials for Cryogenic Applications," *Cryogenics*, Vol. 38, No. 1, 1998, pp. 135-142.

[36] Okada, T., and S. Nishijima, "Gas Permeation and Performance of an FRP Cryostat," *Advances in Cryogenic Engineering*, Vol. 34, 1987, pp. 17-24.

[37] Qu, X., S. Venkataraman, and R. T. Haftka, "Reliability, Weight, and Cost Tradeoffs in the Design of Composite Laminates for Cryogenic Environments," 42nd AIAA/ASME/ASCE/AHS/ASC Structures, Structural Dynamics, and Materials Conference and Exhibit, Seattle, WA, April 16-19, 2001.

[38] Curtis, P. T., and S. M. Bishop, "An Assessment of the Potential of Woven Carbon Fiber-Reinforced Plastics for High Performance Applications," *Composites*, Vol. 15, No. 4, October 1989, pp. 259-265.

[39] Hosur, M. V., J. Alexander, U. K. Vaidya, and S. Jeelani, "Impact Response of Affordable Graphite/Epoxy Woven Fabric Composites," 42nd AIAA/ASME/ASCE/AHS/ASC Structures, Structural Dynamics, and Materials Conference and Exhibit, Seattle, WA, April 16-19, 2001.

[40] Nettles, A., Personal Communications, NASA MSFC, Huntsville, AL, February 2002.

[41] Nettles, A. T., "Permeabiltiy of Composite Materials and Adhesive Bonds of the DC-XA Composite Feedline Program," NASA Technical Memorandum 108483, NASA MSFC, Huntsville, AL, March 1995.

[42] Gudaitis, C. N., "High Pressure Cryogenic Composite Tank Qualification," 32nd International SAMPE Technical Conference, Nov 5-9, 2000, pp. 342-351.

[43] Wright, R. J., and G. M. Roule, "Large Scale Composite Liquid Oxygen Feedlines for Launch Vehicles," 32nd International SAMPE Technical Conference, Nov 5-9, 2000, pp. 352-359.

[44] Burgess, J. W., B. S. Hayes, J. C. Seferis, "Second Phase Toughening of Electron Beam Cured Epoxies," 32nd International SAMPE Technical Conference, Nov 5-9, 2000, pp. 744-756.

[45] Magnamite IM7 (5000) Product Data Sheet, Hexcel Fibers, http://www.hexcelfibers.com, March 2002.

[46] Magnamite IM7 (6000) Product Data Sheet, Hexcel Fibers, http://www.hexcelfibers.com, March 2002.

[47] EX-1552 Resin System Product Data Sheet, Bryte Technologies, Inc., Morgan Hill, CA, February 1999.

[48] Nettles, A., Personal Communications, NASA MSFC, Huntsville, AL, July 2002.

[49] ASTM D3039, "Standard Test Method for Tensile Properties of Polymer Matrix Composite Materials," Annual Book of ASTM Standards, American Society for Testing and Materials, West Conshohocken, PA, 2000.

[50] Centurion Water Based Urethane Product Data Sheet, The Sherwin Williams Company, http://www.sherwinwilliams.com, March 2001.

[51] Corothane I Aliphatic Finish Coat Product Data Sheet, The Sherwin Williams Company, http://www.sherwinwilliams.com, March 2001.

[52] Corothane I MIO-Aluminum Product Data Sheet, The Sherwin Williams Company, http://www.sherwinwilliams.com, March 2001.

[53] Poly-Lon 1900 Polyester Polyurethane Product Data Sheet, The Sherwin Williams Company, http://www.sherwinwilliams.com, March 2001.

[54] ASTM D2794, "Standard Test Method for Resistance of Organic Coatings to the Effects of Rapid Deformation (Impact)," Annual Book of ASTM Standards, American Society for Testing and Materials, West Conshohocken, PA, 1999.

[55] ASTM D522, "Standard Test Methods for Mandrel Bend Test of Attached Organic Coatings," Annual Book of ASTM Standards, American Society for Testing and Materials, West Conshohocken, PA, 1993

[56] Rowen, J. Personal Communications, Avtec Industries, Hudson, MA, February 2001.

[57] Thermaflex II-C Product Bulletin, Avtec Industries, Inc., Hudson, MA, May, 2001.

[58] Bentolite H Product Bulletin, Southern Clay Products, Inc., http://www.scprod.com, 2002.

[59] Campbell, S., Personal Communications, NASA GRC, Cleveland, OH, July 2002.

[60] Nettles, A., "Permeability Testing of Impacted Composite Laminates for Use on Reusable Launch Vehicles," Technical Publication, NASA MSFC, Huntsville, AL, 2001.

[61] ASTM D 1005, "Standard Test Method for Measurement of Dry-Film Thickness of Organic Coatings Using Micrometers," American Society for Testing and Materials, West Conshohocken, PA, 1995.

[62] ASTM D 1434, "Standard Test Method for Determining Gas Permeability Characteristics of Plastic Film and Sheeting," American Society for Testing and Materials, West Conshohocken, PA, 1982.